UNIVERSITY OF NAIROBI

Green Synthesis, Characterization and Antimicrobial Evaluation of Silver and Zinc Oxide Nanoparticles from Extracts of Bidens pilosa

KYOMUHIMBO HILDA DINAH

I56/83188/2015

A Thesis Submitted in Partial Fulfillment for the Degree of Master of Science in Chemistry, University of Nairobi

2019

DECLARATION

I declare that this thesis is my original work and has not been submitted elsewhere for examination. Where other people's work has been cited and properly referenced in accordance with the University of Nairobi's requirements.

Signature……. Date 25/04/2019

KYOMUHIMBO Hilda Dinah

This thesis is submitted for examination with our approval as University supervisors:

Signature…….. Date……..
Date 26/04/19

Dr. Solomon Derese

Department of Chemistry

Sciences

University of Nairobi

sderese@uonbi.ac.ke

Signature…….. Date 26/4/2019

Prof. Francis B. Mwaura

School of Biological

University of Nairobi

fbmwaura@uonbi.ac.ke

Signature…….. Date 29/04/2019

Dr. Immaculate N. Michira

Department of Chemistry

University of Nairobi

imichira@uonbi.ac.ke

DEDICATION

I dedicate this work to my beloved husband, Mr. Daniel Omaya, My parents Mr. Isingoma Festus and Ms. Businge Deborah plus all my siblings.

ACKNOWLEDGEMENTS

I appreciate my supervisors, Dr. Immaculate Michira, Prof. Kamau Geoffrey (RIP), Dr. Solomon Derese and Prof. Francis B. Mwaura for all their support and guidance during my research work.

I thank University of Nairobi for granting me an opportunity to study and carry out my research. Special thanks go to the Chemistry Department, Department of Physics, School of Biological Sciences (Microbiology section) and Department of Biochemistry. I thank Mr. Boniface Muthoka from the Department of Physics for the assistance he accorded to me during the characterization of the nanoparticles using UV-Vis spectroscopy and Ms. Tereza from Microbiology section in the school of Biological Sciences, for helping me with the antimicrobial activity.

I thank Prof. Emmanuel I. Iwouha for granting me the opportunity to carry out research in the Sensor Lab of University of Western Cape and for your support and guidance during my stay in the sensor lab. I also thank the entire sensor lab group, Dr. Maskini Milua, Dr. Usisipho Feleni, Dr. Unathi Sidwaba and postgraduate students for the good working atmosphere and assistance you accorded me.

Above all I thank the almighty God for his guidance, love and providence during this research study. I also wish to extend my gratitude to DAAD-NAPRECA for sponsoring my MSc program at University of Nairobi.

I extend my gratitude to the Department of Chemistry University of Nairobi and the Kenya/South Africa collaborative grant REF: NCST/5/003/2/53, for the project titled, 'Nanobiosensor Chips for Anti-Tuberclosis', that facilitated my research visit in University of Western Cape.

I appreciate my family at University of Nairobi and at home for all the support they gave me during this research. Special thanks go to my husband Mr. Omaya Daniel for his love, care and support during this study.

LIST OF ABBREVIATIONS

AFM:	Atomic Force Microscopy
AgNPs:	Silver nanoparticles
FTIR:	Fourier Transmission Infrared
GDP:	Gross Domestic Product
MERS:	Middle East respiratory syndrome
ROS:	Reactive Oxygen Species
SARS:	Severe acute respiratory syndrome
SEM:	Scanning Electron Microscope
TEM:	Transmission Electron Microscope
UV-Vis:	Ultraviolet visible
WHO:	World Health Organization
XRD:	X-ray Diffraction
ZnO-AgNPs:	Zinc oxide – Silver nanocomposite
ZnONPs:	Zinc oxide nanoparticles

ABSTRACT

There has been rampant outbreak of infectious diseases and various antibiotics have been introduced to treat these infections; however, they are turning out to be less effective due to their abuse leading to emergence of antimicrobial resistant infections. Various antiseptics have been used but their active ingredients are becoming ineffective to most resistant strains of bacteria. However, nanotization of antimicrobial agents has shown improvement of their disinfecting efficacy since nanoparticles have proved to have effective antimicrobial activity, even to resistant strains of microbes. In this study, nanotization of chemical constituents of *Bidens pilosa* was carried out because traditionally this plant is proven to have antimicrobial activity. In this study, biosynthesis of silver nanoparticles (AgNPs), zinc oxide-silver nanoparticles (ZnO-AgNPs) and zinc oxide nanoparticles (ZnONPs) using the seed, leaf and root extracts of *Bidens pilosa* with Silver nitrate and Zinc nitrate solutions, is reported. Extracts of *Bidens pilosa* contain a variety of bio-molecules such as polyphenols and water soluble heterocyclic compounds which reduce metal ions and stabilize nanoparticles. The plant (*Bidens pilosa*) was harvested; its seeds, leaves and roots were plucked, washed, dried under shed and crushed. The powders were dissolved in water to form extracts. The extracts were used to make AgNPs, ZnONPs and ZnO-AgNPs. The nanoparticles were characterized using UV-Vis spectroscopy, Fourier Transform Infrared, Raman spectroscopy, Scanning Electron Microscopy, Transmission Electron Microscopy, X-ray Diffraction and Atomic Force Microscopy. The antimicrobial activity of the nanoparticles was determined using agar well diffusion method. The most active nanoparticles were used as active ingredients in the formulation an antiseptic. The antimicrobial activity of the antiseptic was determined. The UV-Visible spectra showed a complete reduction of Ag^{+} ions to Ag^{0} with Plasmon resonance bands at around 410nm which is characteristic of AgNPs and formation of ZnONPs with a Plasmon resonance bands around 370nm. The synthesized nanoparticles had an average size of 2-20nm and were sphere-shaped without significant agglomeration as revealed from the SEM and TEM analysis. The synthesized AgNPs, ZnONPs and ZnO-AgNPs exhibited face–centered cubic crystals as demonstrated from XRD studies. FT-IR and Raman spectra of the seed, leaf and root extracts of *Bidens pilosa,* AgNPs, ZnONPs and ZnO-AgNPs revealed presence of

functional groups C-O, O-H, =C–H, aromatic C-H bending, O-H, C=O, C=C aromatic and thiol groups attached to them. This indicated that these functional groups capped and stabilized the nanoparticles. Anti-Microbial activity of synthesized AgNPs, ZnONPs and ZnO-AgNPs against *Escherichia coli*, *Staphylococcus aureus* and a fungus *Candida albicans* were studied. Clear zones of inhibition were observed for the nanoparticles against the microorganisms. The ZnO-AgNPs obtained from the root extract of composition 0.8 Ag/0.2 ZnO had the highest antimicrobial activity. The ZnO-AgNPs obtained using root extracts of composition 0.8 Ag/0.2 ZnO were found to be effective as an active ingredient to make a hand sanitizing antiseptic against *E. coli*, and *S. aureus* bacteria and the fungus *C. albicans.*

LIST OF FIGURES

LIST OF TABLES

TABLE OF CONTENTS

CHAPTER ONE: INTRODUCTION

1.1 Background of the Study

There has been rampant outbreak of infectious diseases all over the world, particularly in East Africa which is a significant burden to our health systems since most of our health facilities are poorly financed, have limited equipment and human resource (World Health Organization, 2015; Tran *et al*., 2013). This is evidenced in the high patient to doctor ratio and poor service delivery in our health care facilities. Governments are also burdened with these infections by diverting the resources from more productive ventures to constructing health facilities, training more health workers, and buying antimicrobial drugs (Bloomfield *et al*., 2009). The economic burden brought about by these infectious diseases cannot be overlooked because of the great impact they have caused on the Gross Domestic Products (GDPs) of various countries. There are always direct and indirect costs met by the infected and non-infected individuals respectively, for example hospital admission, payment of hospital bills, time spent by healthy people to care for the patients in hospitals, missing work and school (Wamalwa *et al*., 2013). More so, the infectious diseases which have not been effectively treated have led to development of chronic diseases such as cancers and allergies which is a big threat to the human species (Bloomfield *et al*., 2009).

Most infectious diseases today are caused by poor hygiene such as poor disposal of garbage, dumping of children's faeces in the compound and poor hand hygiene. Another major cause of these infections is poor sanitation leading to overflowing trenches, use of unsafe or contaminated water and contact with unclean surfaces that are highly populated with pathogens (Tumwine *et al*., 2002). More so the rampant spread of these diseases has been facilitated by human behavior or cultural practices such as shaking hands while greeting and free movement or travel (Morse, 1995).

The main approach that has been used to treat these infectious diseases is through administering antimicrobials to infected people (Gibson and Toscano, 2012). Most of these antimicrobials have been extracted from plants such as berberine from *Berberis vulgaris* L (Farnsworth *et al*., 1985) and penicillin from *Penicillium chrysogeum* (Gaynes, 2017). Many antimicrobial drugs have been introduced into the community which in a way has resulted in their misuse through over dosage, wrong prescriptions

and using them to treat other diseases that are not necessarily microbial infections (Levy and Marshall, 2004). This has led to development of microbial strains that are resistant to antimicrobials in the community (Amábile-Cuevas *et al*., 1998) and the choice of antimicrobial drugs for treatment of these rampant infections is diminishing as the resistance increases at an alarming rate (O'Neill, 2014). World Health Organization (2014) published a general global increase in antimicrobial resistance to antimicrobials introduced on the market and the highest rates were observed in bacteria that cause common health care associated and community acquired infections.

Since misuse of antimicrobials among humans will not be easily overcome, the microbes will always develop mechanisms to resist the already existing and newly invented antimicrobial drugs. There is therefore need to for a practical tool that will prevent microbial infection in the first place and also prevent the spread of the existing infections (Gelbrand *et al*., 2015). One of the possible approaches that can be taken to prevent these infectious diseases is good hygiene practices. This entails regular washing of hands, proper handling of food and water, proper handling of infected people and contaminated surfaces (Bloomfield *et al*., 2009). One of the tools of proper hand hygiene are use of antiseptics which prevents movement of pathogenic microorganisms from infected people and contaminated surfaces (Prüss-Üstün *et al*., 2004). However for all the existing antiseptics, their active ingredients are not effective for most resistant strains of microbes (Jeffrey, 1995). This calls for nanotization of active antimicrobial agents to improve their disinfecting efficacy since nanoparticles have been proved to have effective antimicrobial activity, even to resistant strains of microbes. Even at very low concentrations, their antimicrobial activity is highly effective and their toxicity is low (Kim *et al*., 2007). More so, they need very short contact time to cause a long lasting cell growth inhibition (Tran *et al*., 2013; Gunalan *et al*., 2012; Feris *et al*., 2010). Nanoparticles have been used as antimicrobial agents in many public places such as railway stations and elevators (Prabhu and Poulose, 2012). They have also been incorporated in polymeric matrices to improve packaging properties by providing antimicrobial activity to the packaging material (Espitia *et al*., 2012). Nanotization of active antimicrobial agents can be achieved by synthesizing nanoparticles from plants that have antimicrobial property.

This method is relatively cheap and also ecofriendly (Mishra and Sharma, 2015). On this basis, nanotization of chemical constituents of *Bidens pilosa* was selected in the present research work. Globally this plant has proved to have antibiotic activity (Adedapo *et al*., 2011; Bartolome *et al*., 2013).

1.2 Statement of the Problem

There is a high rate of microbial traffic from infected human and non-human sources to non-infected human beings, facilitated by human behavior such as inadequate sanitation, use of contaminated hypodermic apparatus in health facilities and contact of an infected person or contaminated source with an uninfected person (Morse, 1995; Prüss and Weltgesundheits, 1999). This has led to increased microbial infection which is an economic burden on the government as well as our households (Ezzati and World Health Organization, 2004). In a bid to treat these infections, many antimicrobial drugs have been introduced into the environment which have misused through over dosage, wrong prescription and unnecessary use due to poor diagnosis. This has led to occurrence of microbial strains that are resistant to antimicrobials in the community (Prüss-Üstün *et al*., 2004). This implies that a new antimicrobial drug will face similar challenges making it ineffective (Bloomfield *et al*., 2009). The only likely action that can prevent the spread of these infections is to reduce microbial transfer from person to person using antiseptics (Prüss and Weltgesundheits, 1999). However the available antiseptics are not very effective since they are not active on some resistant strains of microbes (Jeffrey, 1995). Inclusion of nanoformulations containing these active ingredients of the antiseptics gives new hope by improving on their efficacy. Nanoparticles have been used to increase solubility, bioavailability, effectiveness, selectivity and safety of herbal drugs (Sachan & Gupta, 2015). On this basis, nanotization of chemical constituents of *Bidens pilosa* leaf extracts has been selected. This is because this plant has been proved to have antibiotic activity (Adedapo, *et al*., 2011; Bartolome *et al*., 2013a). Therefore the focus of this study is develop an antiseptic (hand sanitizer), using active ingredient of ZnO-AgNPs synthesized using leaf extract of *Bidens pilosa*, so as to prevent infection thus cutting on the need to use antimicrobial drugs.

1.3 Objectives

1.3.1 General Objective

To synthesize nanoparticles and formulate an effective antiseptic that can be applied to prevent the spread of pathogenic microorganisms

1.3.2 Specific Objectives

1. To synthesize silver and zinc oxide nanoparticles using leaf, seeds and root extracts of *Bidens pilosa*.
2. To characterize the nanoparticles using spectroscopic techniques of UV-Vis, Fourier Transform Infrared, X-ray Diffraction and Raman spectroscopy and Scanning Electron Microscopy, Transmission Electron Microscopy and Atomic Force Microscopy.
3. To assess the antimicrobial activity of the synthesized AgNPs, ZnONPs and ZnO-AgNPs against *E. coli, S. aureus* and *C. albicans* by measuring diameters of inhibition zones.
4. To formulate an effective antiseptic that can be applied to prevent the spread of pathogenic microorganisms.

1.4 Justification and Significance of the Study

This research aims at formulating an effective antiseptic that can be applied to prevent the spread of pathogenic microorganisms through transfer of antimicrobial-resistant microbes from individual to individual and also from contact with dirty surfaces in the environment. This will also prevent the spread of microbial infections. This as a result will reduce on consumption of antimicrobial drugs and hence reduce on the intensification of the spread of antimicrobial-resistant infections.

The plant *Bidens pilosa* was selected because it is proved to have antimicrobial activity (Adedapo *et al*., 2011; Bartolome *et al*., 2013). However, its extracts show moderate antimicrobial activity to gram positive bacteria as compared to chloramphenicol and no activity against gram negative bacteria (Geissberger & Séquin, 1991). Therefore there is need to increase the potency of the extracts against microbes. Currently nanotization of metabolites is widely used to improve their

potency (Zhang *et al.*, 2018). Therefore, nanotization of the chemical constituents of *Bidens pilosa* will improve on its antimicrobial efficacy so that it can destroy a variety of microbes, even those which had proved to be resistant to antimicrobials. since silver and zinc oxide nanoparticles inhibit growth of microbes though at very low concentrations (Tran *et al*., 2013; Mishra and Sharma, 2015). AgMPs, ZnONPs and Ag-ZnO nanocomposites have been used in water disinfecton against microbes, however, the Ag-ZnO nanocomposite exhibited higher antimicrobial activity in a short time as compared the independent AgNPs and ZnONPs (Motshekga *et al.,* 2015). Therefore in this study nanocomposite of AgaNPs and ZnONPs was applied in the formulation of an effective antiseptic.

CHAPTER TWO: LITERATURE REVIEW

2.1 Infectious Diseases

Infectious diseases are the major leading causes of death killing approximately 15 million people per annum worldwide (Abat *et al*., 2016). Examples include; ebola, influenza, monkey pox, Severe Acute Respiratory Syndrome (SARS) and Middle East Respiratory Syndrome (MERS). They are mainly caused by viruses, fungi, bacteria, helminthes and protozoa (Weber *et al*., 2016). These infectious diseases are spread through poor sanitation, inadequate vector control (Hansen and Paintsil, 2016) and unhygienic practices (Prater *et al*., 2016). Originally they were considered as diseases for developing countries but due to globalization and interconnections, they have become a threat to all economies (Hansen and Paintsil, 2016). The burden imposed by these infectious diseases is reflected in lower income per capita due to low productivity and impaired cognitive ability (Madsen, 2016; Gale *et al*., 2016), adverse outcomes in pregnancy and child development (Hansen and Paintsil, 2016) and poverty (Adhikari *et al*., 2016). Many antibiotics have been made to treat these diseases. However, the increased use of antibiotics has led to colonization with resistant organisms and new infections are emerging as a result of evolution of existing pathogens (Hopp *et al*., 2016; Weber *et al*., 2016). This has led to an outbreak of resistant infectious diseases which often result to chronic diseases (Withrock *et al*., 2015).

2.2 Ethnomedicinal uses and Phytochemistry *Bidens pilosa* L (Asteraceae)

Figure 1: A photo of *Bidens pilosa* plant.

Bidens pilosa L. (Asteraceae) (**Figure 1**) is a herbal plant which grows all over the world in both temperate and tropical regions. It can grow in agricultural areas, roadsides and disturbed sites (Grombone-Guaratini *et al*., 2005). It is considered as a weed due to its intrusive tendencies (Young *et al*., 2010; Khoza *et al*., 2016). This plant is extensively used as traditional medicine and food without obvious adverse effects (Khoza *et al*., 2016). Its shoots and roots are used as active ingredients in tea and herbal medicine to treat a number of ailments (Bartolome, *et al*., 2013). In most cases the plant leaves are administered orally and in a few cases used externally to treat snake bites and wounds in some communities (Dharmanada, 2013), toothaches, abdominal pains, sore eyes, ulcers and rheumatism (Zulueta *et al*., 1995; Khan *et al*., 2001). The plant can be prepared in different ways to treat over 40 kinds of illnesses and has proved to have anti-diabetic (Chien *et al*., 2009), anti-inflammatory, antimicrobial (Khan *et al*., 2001; El-Gawad *et al*., 2015; Chung *et al*., 2016), antioxidant (Yang *et al*., 2006), and antimalarial activities (Bartolome *et al*., 2013; Oliveira *et al*., 2004; Brandao *et al*., 1998). According to Adedapo *et al* (2011) and Khan *et al* (2001), the leaf extracts of *Bidens pilosa* have proved to have antimicrobial activity. The pharmacological activity of *Bidens pilosa* is due to the existence of large quantities of phytochemicals, namely terpenes (Zulueta *et al*., 1995), flavonoids and polyacetylenes (Cortés-Rojas *et al*., 2013; Khoza *et al*., 2016; Chien *et al*., 2009; Oliveira *et al*., 2004). In a 2013 review (Bartolome *et al.*, 2013) listed 201 compounds as reported from this plant. Among these were 70 aliphatics, 60 flavonoids (heterocyclic), 25 terpenoids, 19 phenyl propanoids, 13 aromatics, 8 porphyrins and 6 other compounds. Some of the compounds that have been isolated from the plant are listed below in **Table 1**.

Table 1: Compounds that have been extracted from *Bidens pilosa*

Compound	Reference
Aliphatics	
2-Butenedioic acid (**1**)	Wang *et al*., 1997; Zhao *et al*., 2004
2-β-D-glucopyranosyloxy-1-hydroxy-5(E)-tridecene-7,9,11-triyne (**2**)	(Ubillas *et al*., 2000)
3-β-D-glucopyranosyloxy-1-hydroxy-6(E)-tetradecene-8,10,12-triyne (**3**)	(Ubillas *et al*., 2000)
Tridecadiene-7,9-diyn-3,4,13-triol (**4**)	Wang *et al*., 2010
5-Tridecene-7,9,11-triyne-1,2-diol (**5**)	Wu *et al*., 2007; Wu *et al*., 2004; Yang *et al*., 2006
7-Phenyl-2(E)-heptene-4,6-diyn-1-ol (**6**)	Chien *et al*., 2009; Yang *et al*., 2006; Chang *et al*., 2005; Ubillas *et al*., 2000
3-β-D-Glucopyranosyl-1-hydoxy-6(E)-tetradecene-8,10,12-triyne (**7**)	Dimo *et al*., 2001
Flavonoids	
(E)-3-(3,4-dihydroxyphenyl)-1-[2,4-dihydroxy-3-[3,4,5-trihydroxy-6-(hydroxymethyl)oxan-2-yl]oxyphenyl]prop-2-en-1-one (**8**)	Hoffmann and Hölzl, 1989
2-(3,4-Dihydroxyphenyl)-2,3-dihydro-7,8-dihydroxy-4H-1-benzopyran-4-one (**9**)	Yuan *et al*., 2008
2(3,4-Dihydroxyphenyl)-3,5,7-trhydroxy-4H-1-benzopyran-4-one (**10**)	Zhao *et al*., 2004; Yuan *et al*., 2008; Xia *et al*., 2009
5,7-Dihydroxy-2-(4-hydroxyphenyl)-4H-chromen-4-one (**11**)	Bartolome *et al*., 2013
Terpenoids	
3,7,11,11-Tetramethylbicyclo[8.1.0]undeca2,6-diene (**12**)	Bartolome *et al*., 2013
Stigmast-5-en-3-ol (**13**)	(Geissberger and Séquin, 1991)

Phenyl propanoids	
3-(3,4-Dihydroxyphenyl)-2-propenoic acid, ethyl ester (**14**)	Wu *et al*., 2007; Yang *et al*., 2006; Kim *et al*., 2006
3-(4-Hydroxy-3-methoxyphenyl)-2-propenoic acid (**15**)	Deba *et al*., 2007
2-Methoxy-4-(2-propen-1-yl)-phenol (**16**)	Bartolome *et al*., 2013
Aromatics	
2-Hydroxybenzoic acid (**17)**	Deba *et al*., 2007
3,4,5-Trihydroxybenzoic acid (**18**)	Xia *et al*., 2009
Porphyrins	
Bidenphytin A (**19**)	Bartolome *et al*., 2013

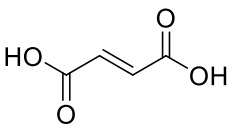

1

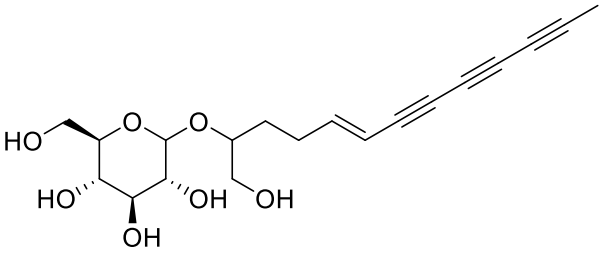

2

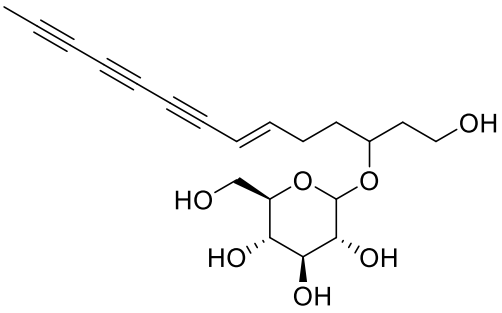

3

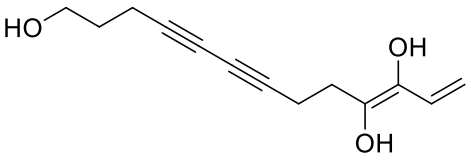

4

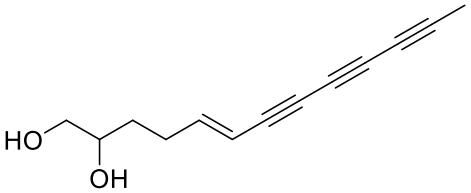

5

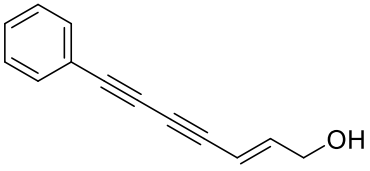

6

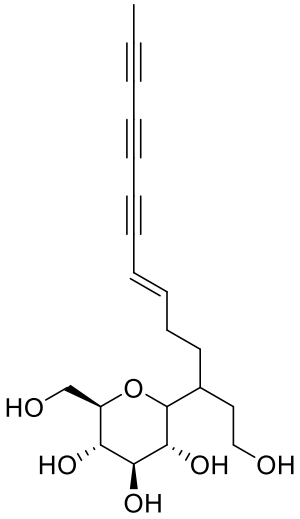

7

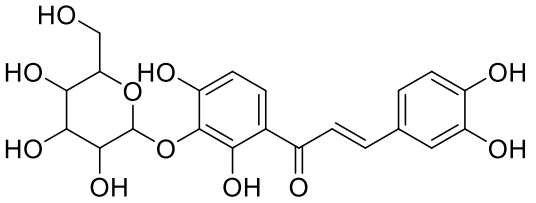

8

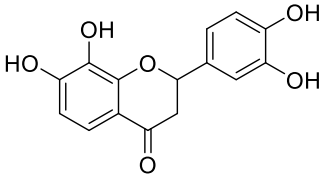

9

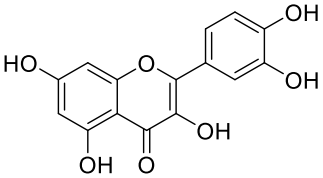

10

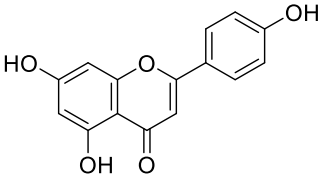

11

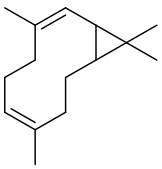

12

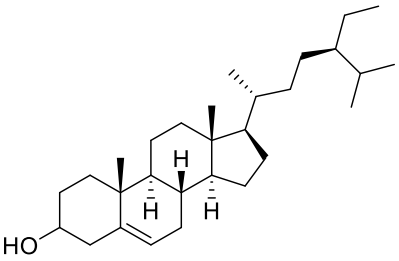

13

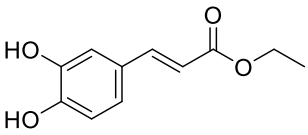

14

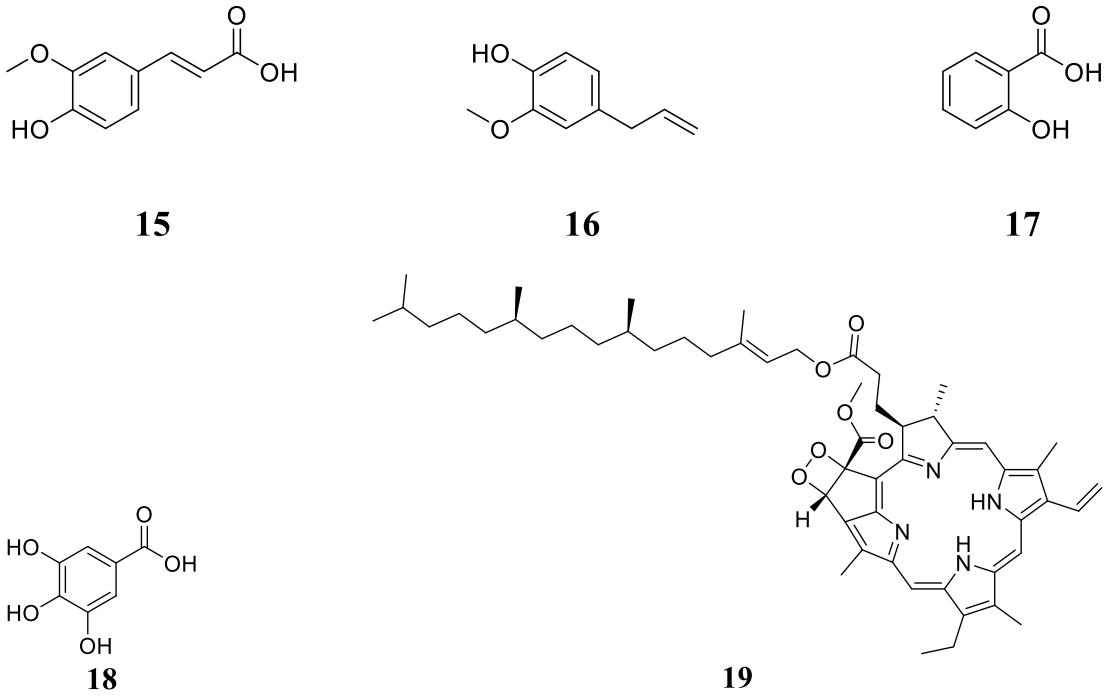

Figure 2: Molecular structures of some of the compounds found in *Bidens pilosa*

On this basis the chemical constituents of the crude water extract were nanotized with silver and zinc oxide nanoparticles to improve on its antimicrobial activity and its possible application as a hand sanitizer.

2.3 Nanoparticles

Nano particles refer to materials whose single particle has a diameter range of 1nm to 100nm (Vaseem *et al*., 2010). In most material processing techniques applied today, they involve breaking down of large size materials to desirable sizes and shapes so as to attain the desirable properties of the material (Vishwakarma, 2013). This is based on the principle that, particles with high surface area to volume ratio are highly reactive with improved physical properties (Vaseem *et al*., 2010). This is evidence that most work and devices in the future will be derived from nanomaterial. Because of their distinctive chemical, biological and physical properties, nanoparticles have found more applications compared to their large scale counterparts (Virender *et al*., 2008). This has significantly boosted the nanotechnology sector where nanoparticles with various functions have been produced (Ju-Nam and Lead, 2008; Okeke and Sosa., 2003). The distinctive properties of AgNPs and ZnONPs have been applied in various areas such as medicine, sensors, renewable energies, cosmetology,

environmental remedial and bio-therapeutic devices (De *et al*., 2008; Lu *et al*., 2007; Chaudhuri *et al*., 2012).

In this study emphasis was put on AgNPs, ZnONPs and ZnO-AgNPs. The characteristics of these nanoparticles have attracted great importance due to their special features such as ophthalmic, magnetic, electrical, antimicrobial activity and catalytic properties (Singhal *et al*., 2011). In this study emphasis was put on their synthesis, characterization and their antimicrobial properties.

2.3.1 Applications of Silver and Zinc oxide Nanoparticles

Silver Nanoparticles exhibit high chemical stability and because of this, they have been used in a number of applications such as; in washing machines, in hair straighteners, athletic clothing and socks (Krutyakov *et al*., 2008), in environmental treatments, surface disinfection and antimicrobial gel formation (Tran *et al*., 2013). Since they show antimicrobial activity (Ahamed *et al*., 2010), they have gained popularity in manufacture of many products such as adhesives, foodstuff, fabrics and plastics which has led to increase in their market value (Tran *et al*., 2013).

ZnONPs have low toxicity, are environmentally friendly, have chemical stability and compatibility (Basha *et al*., 2016). Due to these qualities, the scientific and industrial fields have showed special interest in ZnONPs for various applications in sensors, paints catalysis, fibers and antimicrobial properties (Varghese and George, 2015). The antimicrobial property of AgNPs, ZnONPs and ZnO-AgNPs was utilized in this study.

2.3.2 Synthesis of AgNPs and ZnONPs

A number of synthetic routes for AgNPs and ZnONPs have been exploited. They can be classified as physical, chemical and biological synthetic routes (Tran *et al*., 2013). The methods are illustrated in **Figure 3** below (Dhand *et al*., 2015).

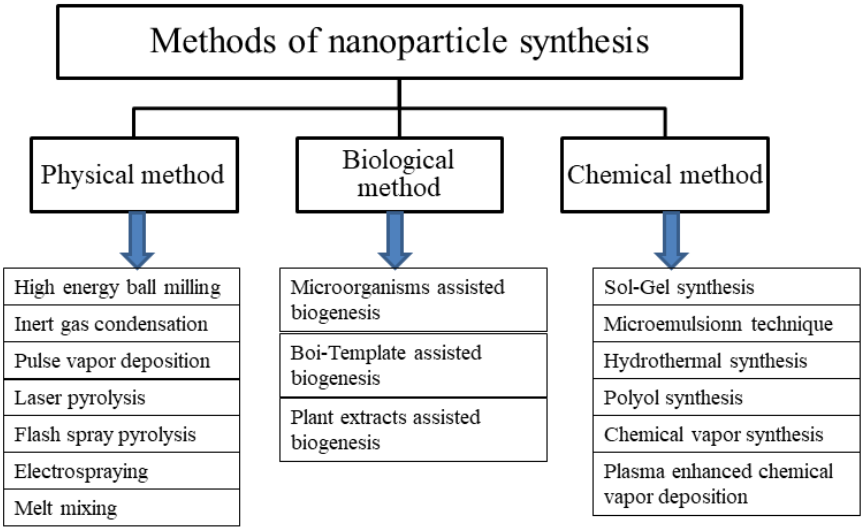

Figure 3: Methods of synthesis of nanoparticles. Adopted from (Dhand *et al*., 2015)

2.3.2.1 Chemical synthesis methods

The chemical method is mainly used to synthesize nanoparticles in solution form and it involves three major components: - the reducing agent, metal precursor and the stabilizing or capping agent (Tran *et al*., 2013). In this synthetic route, the formation of metal and metal oxide nanoparticles involves two stages; nucleation and subsequent growth (Tran *et al*., 2013). The two stages are generally controlled by variable factors such as pH, temperature, reducing agents, precursors and stabilizing agents (Patil *et al*., 2012). Both of these stages contribute to size and geometry of the nanoparticles produced (Chen and Zhang, 2012). Since all nuclei form simultaneously and have the same successive growth, they usually have uniform size distribution (Dang *et al*., 2012). The magnitude and geometry of the nanoparticles produced are governed by experimental conditions, such as pH, temperature and concentration (Sun and Xia, 2002; Chen *et al*., 2007; Yu *et al*., 2014).

The main disadvantage of this synthetic route is that it uses large amounts of harmful solvents and synthetic reactants which are later released to the environment at the end of the reaction (Rodríguez-León *et al*., 2013).

2.3.2.2 Physical synthesis methods

In this method, the nanoparticles are basically synthesized by distillation mechanism which is carried out in a tube furnace and run at atmospheric pressure. The particles are formed by thermolysis of a complex of a metal salt at fairly high temperatures. The major disadvantage of this method are; Big size of the tube furnace and high energy required to increase the temperature around the source material to achieve thermal steadiness (Tran *et al.*, 2013). The nanoparticles produced usually have narrow size distribution and are in powder form (Tien *et al*., 2008).

2.3.2.3 Biological synthesis methods

In this method, living organisms that produce stabilizers and reducing agents, such as fungi/ bacteria, yeast and plants are used instead of chemicals (Sintubin *et al*., 2012). The nanoparticles produced are usually stable, hydrophilic and have very small diameter (Alagummuthu and Kirubha, 2012). This is by far the cheapest method because it is simple and requires few chemicals and energy compared to the other synthetic routes (Tran *et al*., 2013). However use of microorganisms in synthesis of nanoparticles involves detailed processes of maintaining and controlling cell cultures, many purification steps as well as intracellular synthesis which makes the process tedious.

Green synthetic method increasingly becomes a topic of interest because it is faster and provides more stable nanoparticles compared to that from microbes (Mishra and Sharma, 2015; Mason *et al*., 2012; Devi and Gayathri, 2014). The plants used in green synthesis are plants that contain polyphenols. Polyphenols have high antioxidant activity and are strong reducing agents. This is due to the presence of many hydroxyl (OH) groups in there structural composition (Rodríguez-León *et al*., 2013). It is because of this that plants containing polyphenols are used as stabilizers and reducers in nanoparticle synthesis. The benefit associated with using plant extracts in the synthesis of nanoparticles is that they are easily accessible, have an extensive variety of active ingredients which aid in the reducing and stabilizing process, are safe to handle and the process can be easily scaled up without use of energy, high temperatures or toxic reagents (Vishwakarma, 2013; Bhainsa and Souza, 2006). The

green synthesis method gives an environmentally friendly alternative to physical and chemical syntheses (Devi and Gayathri, 2014).

Plant leaf extracts have been used as stabilizers and reducing agents for silver and zinc oxide nanoparticles-synthesis. Some of the leaf extracts that have been used include; *Camellia sinesis* (Shah *et al*., 2015), *Hibiscus Rosa-Sinesis* (Devi and Gayathri 2014), *Rumex hymenosepalus* (Rodríguez-León *et al* 2013), *Cissus quadrangularis* (Alagummuthu and Kirubha 2012), *Olea rupea* (Awwad *et al* 2014), *Octinum sanctum* (Singhal *et al* 2011), *Ocimun tenuiflorum* (Raut *et al* 2013) and *Panicum virgatum* (Mason *et al* 2012).

In this study, silver and zinc oxide nanoparticles were synthesized using the biological/ green synthetic route. *Bidens pilosa* was used as the plant to produce stabilizer and also act as the reducing agent. The plant (*Bidens pilosa*) was selected because it has proved to have antimicrobial activity (Khan *et al*., 2001; Bartolome *et al*., 2013; Deba *et al*., 2008) and contains a number of polyphenols such as flavonoids and polyacetylenes which reduce and stabilize the silver and zinc oxide nanoparticles (Wang *et al*., 1997; Wang *et al*., 2010; Yuan *et al*., 2008).

2.4 Characterization of Nanoparticles

Nanoparticles can be characterized by a number of techniques such as spectroscopic techniques of UV-Vis, Fourier Transform Infrared, X-ray Diffraction and Raman spectroscopy and microscopic techniques of Scanning Electron Microscopy, Transmission Electron Microscopy and Atomic Force Microscopy.

2.4.1 UV- VIS Spectroscopy

Ultraviolet and visible radiation are a small part of the electromagnetic spectrum that is used in the characterization of nanoparticles (Owen, 1996). Metal nanoparticles such as AgNPs and ZnONPs have conduction and valence bands lying close to each other with freely moving electrons (Joshi *et al*., 2008). These freely moving electrons lead to a surface plasmon resonance absorption band that occurs as a result of combined alternation of the electrons in resonance with the light wave. The incoming wave of electric field induces a polarization of electrons with respect to the ionic core of spherical nanoparticles. This leads to a resorting force producing a dipolar

alternation of all electrons in the same phase. The resonance flanked by the frequency of the magnetic field and the fluctuating electrons results in a resilient absorption that is in the basis of the observed color (Desai *et al*., 2012).

2.4.2 Raman Spectroscopy and Fourier Transform Infrared

Raman and Infrared spectroscopy are the most techniques used in vibrational spectroscopy. They involve the study of interaction of radiation with molecular vibrations to obtain information on molecular structures, physical forms and amount of substance in a sample (Larkin, 2011; Smith and Dent, 2005). The samples can be solid, liquid, gases, in hot or cold state, in bulk, microscopic particles or as surface layers. Certain functional groups show characteristic vibration in which only the atoms in that particular group are displaced hence the presence or absence of various functional groups can be identified. Raman spectroscopy best measures symmetric vibrations of non-polar groups while infrared best measures asymmetric vibrations of polar groups. The two techniques give different intensity patterns and should be used hand in hand to obtain complete measurement of vibrational modes of a molecule (Larkin, 2011; Bumbrah and Sharma, 2016).

2.4.2.1 Raman spectroscopy

Raman spectroscopy was discovered by Sir CV Raman who along with his colleague KS Krishnan published the first paper on this technique (Raman and Krishnan, 1928). Raman spectra are normally observed for vibrational and rotational transitions but can also be observed for electronic transitions between ground and low energy excited states (Bumbrah and Sharma, 2016). Unlike Infrared, Raman spectra are measured in the UV-Vis region where the excitation as well as Raman lines appear (Ferraro *et al*., 2003).

Raman spectroscopy is based on the principle that when light interacts with matter, the photons which make up the light interact with the molecule and scatter from it, the scattered photons can be observed by collecting light at an angle to the incident light beam (Smith and Dent, 2005).

The sample is irradiated with a single frequency of radiation in the UV-Visible region and the scattered radiation from the molecule is detected. The scattered light is observed in the direction perpendicular to the incident beam. The light interacts with

the molecules and polarizes the electron cloud around the nuclei to form a short-lived state (virtual state). When nuclear motion is induced during the scattering process, energy is transferred either from the incident photon to the molecule or from the molecule to the scattered photon. Therefore the energy of the scattered photon is different from the energy of the incident photon by one vibrational unit. A Raman spectrum is expressed as a plot of intensity against Raman shift (cm^{-1}) (Ferraro *et al*., 2003; Smith and Dent, 2005; Bumbrah and Sharma, 2016).

2.4.2.2 Fourier Transform Infrared Spectroscopy

An infrared spectrum is a graph of measured infrared light intensity against transmittance or absorbance. It is produced using an infrared spectrometer (Jaggi and Vij, 2006; Smith, 2002). Examination of an infrared spectrum can give the type and concentration of particles present in a particular sample. The spectrum is usually plotted in absorbance units (amount of light absorbed by a given sample). Absorbance is calculated from;

$$A = \log(\frac{I_0}{I}) \quad (1)$$

Where A is the absorbance, I_0 is the intensity in the background spectrum and I is the intensity in the sample spectrum (Smith, 2011) (Griffiths and DeHaseth, 2007; Smith, 1999; Alvarez-Ordóñez and Prieto, 2012; Jaggi and Vij, 2006).

The y axis can be plotted in units of percentage transmittance (%T) (percentage of light transmitted by a sample).

$$\%T = 100(\frac{I}{I_0}) \quad (2)$$

.

2.4.3 Electron Microscopy

Electron microscopy is a tool used for microstructural characterization of materials. High energy electrons are bombarded onto the sample there by causing excitation of the electrons in the sample. These excitations are then used to obtain chemical information of the sample such as concentration and structure of the different components in the sample (Fultz and Howe, 2008).

The advantages electrons have over x-rays are;

i) It is easier to focus electrons

ii) It is probable to handpick a single microcrystal for diffraction measurements

iii) Their optics are used to create images from the electron intensity evolving from the samples and the images of blemishes such as disarticulations, second phase particles and interfaces can be made from variations in the intensity from the specimen (Fultz and Howe, 2008).

The two common electron microscopes used are the Scanning Electron Microscope (SEM) and Transmission Electron Microscope (TEM). In a TEM, the basic principle is that it uses fourier transformation through a convergent lens shadowed by transitional and projector lenses that broaden the image. The TEM requires very thin specimen, uses convex lens and elastically scattered electrons and imaging is transmitted by electrons through the specimen. For a SEM, it uses scanned electron probe and subordinate electrons emitted from the specimen surface to reveal its surface features. The SEM imaging uses inelastically disseminated electrons transmitted from the specimen surface on the same side of the incident electrons and it is used to observe thick specimens (Tanaka, 2014).

2.4.3.1 Scanning Electron Microscopy

Scanning Electron Microscopy (SEM) is a technique in which an electron beam of high energy (60-100 keV) is subjected onto a sample surface, which is scanned, there by producing an image. The experiment is carried out on thick specimens, the electrons cannot be transmitted through the sample, and information is obtained only from electrons from the surface of the specimen. The signals obtained from these electrons give the characteristic of the sample (Vernon-Parry, 2000). SEM can be used to characterize large or bulk specimens up to 200mm diameter (Reimer, 1984). SEM shows detailed three dimensional images that are black and white and its magnification goes up to x300000 (Joshi *et al*., 2008). SEM provides information of crystalline structure, surface topography and chemical composition of the top specimen. The advantages of using SEM for characterization are; it allows non-destructive evaluation of the specimen and needs little time for specimen preparation

because the sample is simply placed on a special SEM stub (Reimer, 1984; Vernon-Parry, 2000).

The SEM as depicted in **Figure 4** mainly comprises of;

i) The electron gun which produces electrons

ii) Electromagnetic condenser lenses which shrink the electron beam into a fine probe that is scanned through a given area of the specimen.

iii) Detector which receives the backscattered electrons from the specimen

iv) Monitor which receives and interprets the signal from the detector (Vernon-Parry, 2000).

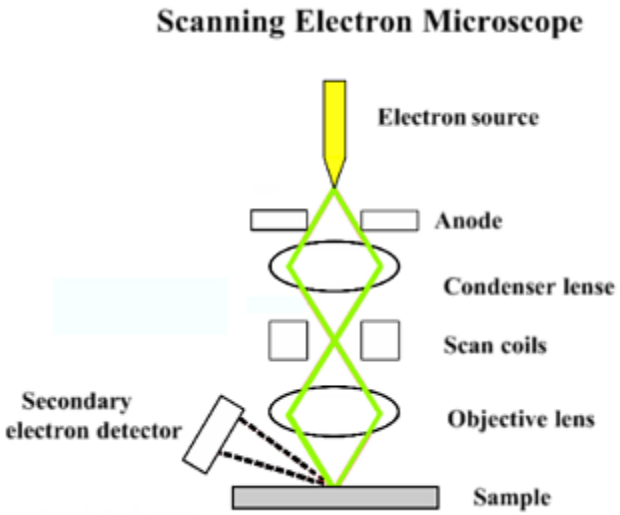

Figure 4: schematic representation of the basic SEM components ("What is SEM?," 2018)

2.4.3.2 Transmission Electron Microscopy

Transmission Electron Microcopy (TEM) is a microscopic technique in which a specimen is subjected to an electron beam of uniform current density. The energy for the electron beam ranges from 60 to 150 keV (Reimer, 1984). The high energy electrons interact with the sample by diffraction and cause microelectronic excitation of the atoms in the sample (Brent *et al*., 2008). The extent of diffraction of the electron beam is determined by the angle of orientation of the atoms of the specimen. The specimen is made thin enough to ensure that the electron beam penetrates through

it. The image formed is magnified and focused on an imaginary screen (Joshi *et al*., 2008).

TEM provides information of a specimen on material size, crystallinity, composition, shape and elemental mapping by use of a high-energy electron beam that transmits through the specimen of nanometer thickness (Kumar, 2014).

There are two imaging modes that can be attained by positioning the objective aperture, namely bright field (BF) and dark field (DF) images. When the objective aperture is positioned in such a way that only the transmitted electrons go through, a bright field (BF) image is made (Fultz and Howe, 2008). The images obtained in this case are generated by transmitted electrons. It gives the shape, size, uniformity and dispersity of the nanomaterials. It is the most commonly used imaging mode (Kumar, 2014). When the objective aperture is placed in such a way that some diffracted electrons pass through, a dark field (DF) image is formed (Fultz and Howe, 2008). The image obtained is generated by diffracted electrons from a set of crystal planes. This imaging mode is used to locate defects in crystals (Kumar, 2014).

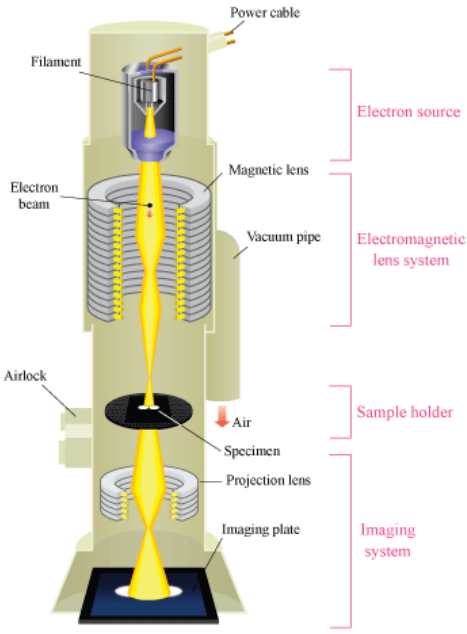

Figure 5 showing the components of TEM. Obtained from ("Atomic World - Transmission electron microscope(TEM) - Principle of TEM,")

2.4.4 X-Ray Diffraction

X-ray Diffraction (XRD) is a non-destructive technique used in analysis and characterization of crystalline and amorphous materials and determination of sample purity (Bowen and Tanner, 1998; Fultz and Howe, 2008). The technique was first discovered by Von Laue in 1912 where he revealed that crystals diffract X-rays (Bowen and Tanner, 1998). Each crystal diffracts X-rays in a unique diffraction pattern. XRD data provides information about size, orientation and phase composition of crystallites (Joshi *et al*., 2008). In the early years, XRD was dominated by two methods that is, Single crystal diffraction which was used in structure analysis for crystal molecule structures and Powder diffraction which was used for practical analysis of materials (Bowen and Tanner, 1998).

In an X-ray diffraction experiment, an incident beam of X-rays is directed onto a sample (Fultz and Howe, 2008). X-rays are produced by acceleration or deceleration of charged particles (Bowen and Tanner, 1998). The incident X-ray beam consists of an oscillating electric field which induces movement of atomic electrons of the sample and their acceleration generates an outgoing wave. The detector is adjusted so as to record the direction and intensity of the diffracted beam (Fultz and Howe, 2008). Strong diffraction occurs when the angle of incidence is identical to the angle of diffraction and the intensity of the diffracted beam depends on the strength of the scattering the sample impacts on the radiation (Bowen and Tanner, 1998).

The components of an XRD are:

i) X-ray source: This is usually a sealed tube (Fultz and Howe, 2008). For X-rays to be produced the acceleration of the particles must be sufficiently high and the particles must have sufficient energy so that the radiation is in the X-ray region. X-rays can also be produced by shift of electrons between quantum levels in an atom. The energy difference between levels in an atom gives rise to a spectrum in the X-ray region. The energy is given by:

$$E = \frac{hc}{\lambda} \tag{3}$$

Where; λ is the wavelength of emitted radiation, c is the velocity of light, h is Planck's constant and E is the energy difference between the levels (Bowen and Tanner, 1998).

ii) Monochromators/slits: These comprise of the direct beam slits and the detector slits. The direct beam slits control the divergence of the incident beam. The detector slits mend the signal-to-background ratio of the diffraction design. They cancel the detection of contaminated radiation from the X-ray tube and florescence X-rays that are released by the sample when it is excited by the incident beam (Bowen and Tanner, 1998).

iii) The detector: This accepts all the X-rays scattered off the specimen. The detector produces a pulse of current when it absorbs an x-ray. The net charge of the pulse of current is directly proportional to the energy of the x-ray photon (Bowen and Tanner, 1998; Fultz and Howe, 2008).

The general relationship between the wavelength of the incident X-rays, angle of incidence and spacing between the crystal lattice planes of atoms is known as Bragg's Law, expressed as:

$$n\lambda = 2d\sin\Theta \quad (4)$$

Where n (an integer) is the "order" of reflection, λ is the wavelength of the incident X-rays, d is the interplanar spacing of the crystal and Θ is the angle of incidence.

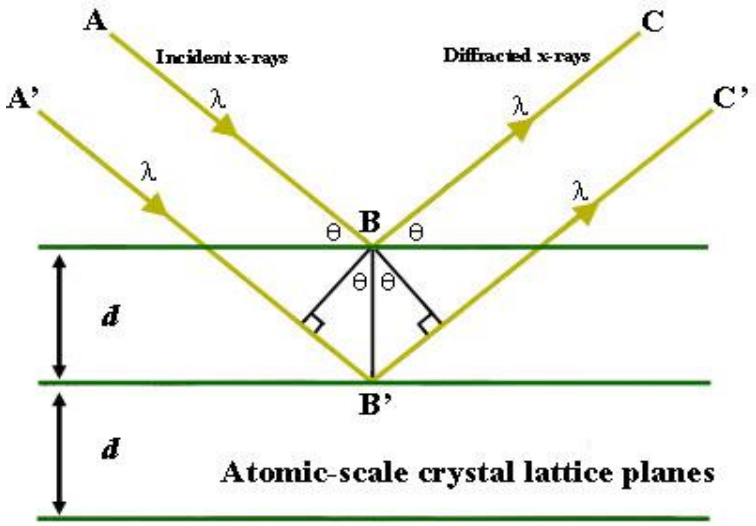

Figure 6: Bragg's Law reflection. Obtained from (Henry *et al*., 2004)

From **Figure 6** above, the diffracted X-rays exhibit constructive interference when the distance between paths ABC and A'B'C' differs by an integer number of wavelengths (λ)

2.4.5 Atomic Force Microscopy

The first idea of Atomic Force Microscopy (AFM) was observed in 1986 where an ultra-small probe tip was used at the end of a Cantilever (Binnig *et al*., 1986). In 1987, an AFM set up consisting of a vibrating cantilever technique with a light lever mechanism was developed (Martin *et al*., 1987). The AFM machine comprises of the following parts: the cantilever (spring)/probe tip which scans the sample surface, the Piozoelectric scanner which positions the sample, the photodetector which measures the bend of the cantilever, probe tip which senses surface characteristics and causes the cantilever to deflect and the computer which is the control system and is used to perform data acquisition, display and analysis. AFM is used to obtain surface profile, that is topography and properties of the surface, of the sample (Santhoshkumar *et al*., 2017; Elumalai and Velmurugan, 2015; Ferni *et al*., 2011).

2.5 Antimicrobial Activity of Synthesized Silver and Zinc Oxide Nanoparticles

The bacterial cell wall provides shape and protection from osmotic rapture and mechanical destruction to the cell (Singleton, 2004). As a result of the differences in the cell wall structures and functions, bacteria can be divided into Gram positive bacteria and Gram negative bacteria (Hajipour *et al*., 2012). The Gram positive bacterial cell wall comprises of teichoic acids attached to a thick layer of peptidoglycan (PG). The thickness of the PG layer ranges from 20-50nm (Hajipour *et al*., 2012; Scott and Barnett, 2006). For the case of Gram negative bacteria, the PG close to the surface membrane is of a thin layer. The surface membrane lies underneath an outer membrane which is resistant to hydrophobic compounds. The outer membrane is negatively charged and this is attributed to the lipopolysaccharides present in it (Hajipour *et al*., 2012; Roberts, 1996). Other than the differences in the cell walls of Gram positive and Gram negative bacteria, other factors also influence the endurance of bacteria against antimicrobial drugs; microbes with a slow growth rate are more tolerant to antimicrobial drugs than those with a fast growth rate

(Hajipour *et al*., 2012; Mah and Otoole, 2001). Some microbes have the capacity to produce biofilms to protect themselves against antimicrobial agents. Biofilms are a microbial community formed by secretion of a matrix and adhesion to a solid surface (Hajipour *et al*., 2012). The continuous abuse of antimicrobials has led to the emergence of microbes resistant to antimicrobial drugs (Hajipour *et al*., 2012). Development of new drugs alone may not be adequate in dealing with the pathogens rate of developing resistance. More so the continuous evolution of microbes threatens human health by our inability to treat emerging infections (Huh and Kwon, 2011).

Nanoparticles have proved to have antimicrobial activities even on resistant strains of microbes (Gunalan *et al*., 2012; Sheehy *et al*., 2015; Huh and Kwon, 2011). This is accredited to their large surface area to volume ratio and their characteristics are dissimilar from those of their bulk counterparts (Hajipour *et al*., 2012). The nanoparticles destroy many biological pathways in a cell and it would necessitate the microorganism to go through many concurrent transmutations so as to develop resistance (Huh and Kwon, 2011). The advantages nanoparticle antimicrobial agents have over the conventional antimicrobials are that they can withstand harsh conditions such as high temperatures and sterilization which is not the case with the conventional antimicrobials and they have a longer retention time than the small molecule antimicrobials in the body which is beneficial for obtaining sustained curative effect in the body (Huh and Kwon, 2011).

Silver has been used for centuries to treat infections, wounds and burns and whether in ionic or nanoparticle form is extremely poisonous to microbes (Rai *et al*., 2009; Hebeish *et al*., 2014; Radzig *et al*., 2013; Mirzajani *et al*., 2011). AgNPs exhibit antimicrobial activity to over 650 microbial species such as bacteria, fungi and viruses even in low doses. At these doses, the AgNPs present low toxicity towards humans and the environment (Ouay and Stellacci, 2015; Ahmed *et al*., 2016). Research on ZnO as an antimicrobial agent started in early 1950s and over the years, zinc oxide nanoparticles have proved to have high antimicrobial activity (Sharma *et al*., 2009; Espitia *et al*., 2012). ZnONPs are heat resistant, nontoxic and compatible with human skin (Dizaj *et al*., 2014; Basha *et al*., 2016; Zarrindokht Emami-Karvani, 2012; Aysaa and Salman, 2016).

2.5.1 Proposed mechanisms of antimicrobial activity of AgNPs and ZnONPs

The mechanism for antimicrobial activity for the AgNPs and ZnONPs has not been fully understood (Hajipour *et al*., 2012). Nanoparticles attach to microbial membrane by electrostatic interaction. They accumulate and aggregate on the cell membrane there by destroying its structure, stability and permeability through penetration and thus leading to cell death (Aysaa and Salman, 2016; Ouay and Stellacci, 2015; Hajipour *et al*., 2012; Li *et al*., 2008; Raghunath and Perumal, 2017; Dizaj *et al*., 2014; Durán *et al*., 2016; Thill *et al*, 2006). They therefore offer a new mechanism for dealing with multidrug resistant microbes (Leid *et al*., 2012). In the case of green synthesized nanoparticles, the antibacterial effect could be due to constituents of the plant materials that are attached to the nanoparticles. The compounds used in the preparation of the nanoparticles could possess antimicrobial activity and a synergistic effect between the nanoparticles and the antimicrobial agent can occur. This could lead to antimicrobial effects at very low concentrations where by the compound wouldn't be active if used alone (Ouay and Stellacci, 2015).

2.5.1.1 AgNPs

The AgNPs once inside the cell of the microbe, inhibit replication of the DNA by reacting with the bases in the DNA and also interfere with the transport system of the cell (Salem *et al*., 2015; Radzig *et al*., 2013; Durán *et al*., 2016). AgNPs also act as catalysts in the manufacture of Reactive Oxygen Species (ROS) which exert a high oxidative stress to the cell there by inactivating it (Ouay and Stellacci, 2015). The ROS are produced from endogenous sources such as mitochondria, peroxisomes and endoplasmic reticulum where oxygen consumption is high (Phaniendra *et al*., 2015). The AgNPs also dissolve to produce antimicrobial Ag+ (Li *et al*., 2008; Hebeish *et al*., 2014). Which reacts with peptidoglycan cell wall, plasma membrane and the cell DNA (Chaloupka *et al*., 2010). They have a high affinity for thiol groups and organic amines (Radzig *et al*., 2013). They can act as bridging agent for several thiol groups within the cell and form chains that lead to aggregation of thiol bearing molecules. This disorganizes the cell metabolism and leads to cell death (Ouay and Stellacci, 2015; Radzig *et al*., 2013). The Ag+ also form complexes with nucleic acids in the cell there by preventing replication of the cell DNA (Li *et al*., 2008; Ahmed *et al*., 2016). According to Durán *et al* (2016), the AgNPs simply act as sources for Ag+

without actively participating in antimicrobial activity. However, Chaloupka *et al* (2010) observed that in a comparative study between Ag+ and AgNPs, the AgNPs exhibited more antimicrobial activity than the free silver ions and thus ruled out the dependence of antimicrobial activity on the Ag+ entirely. Rai *et al* (2009) suggested that, when the AgNPs penetrate into the bacterial cell, a low molecular weight region is formed by the AgNPs in the center of the microbe. The microbes conglomerate around the low molecular weight region in a bid to protect the DNA for Ag+. The AgNPs then destroy the respiratory chain and cell division hence leading to cell death. The AgNPs then release the Ag+ into the cells which enhances the antimicrobial activity.

2.5.1.2 ZnONPs

ZnONPs interact with membrane lipids of the cell thereby leading to malfunction of the cell wall hence cell death (Salem *et al*., 2015). The ZnONPs once penetrated into the cell walls oxidize membrane lipids of the microbes leading to production of Reactive Oxygen Species (ROS) such as super oxide ion (O^{2-}), hydrogen peroxide (HOO·) and hydroxyl radicals (·OH) which cause damage to all organic biomolecules like lipids, proteins and DNA in the cell thus causing cell death (Raghunath and Perumal, 2017; Salem *et al*., 2015; Dutta *et al*., 2012). The ROS also interfere with biofilm formation of microbes hence making them susceptible to destruction (Hajipour *et al*., 2012). In addition the ZnONPs suppress the cell division of microbes by disrupting the replication process of DNA (Raghunath and Perumal, 2017). According to Li *et al* (2008) and Raghunath and Perumal (2017), the ZnONPs upon dissolution, produce Zn^{2+} ions which are attracted to the electronegative groups of the polymers on the microbial cell wall and prolong the lag phase of their growth cycle. The Zn^{2+} ions act as weak acids and react with soft bases such as sulphur and phosphorous in the DNA and this disrupts the helical nature of the DNA by cross linking in the DNA strands. The Zn^{2+} ions also act as catalyst for the oxidation of amino acid side chains which result in protein bound carbonyls. The carbonyls lead to loss of catalytic activity in enzymes (Xie *et al*., 2011).

2.6 Antiseptics with Nanoparticles as Active Ingredients

As already stated above, one of the easiest and most reliable way of preventing infectious diseases is proper hand hygiene, since it has shown significant reduction in infectious diseases transmission in many settings such as military, health care and schools (Mott *et al*., 2007). The common approach to proper hand hygiene is hand washing but it has its own limitations such as; insufficient time, (Mott *et al*., 2007; Dyer *et al*., 2000) and forgetfulness (Oke *et al*., 2013). More so a hand washing program cannot be maintained in high population communities like schools, military and market places since it would consume a lot of time for very individual to wash their hands (Dyer *et al*., 2000). Hence use of instant hand sanitizers is a more convenient approach to prevention of infectious diseases transmission and hand washing can only be used when the hands are visibly soiled (Mott *et al*., 2007; Oke *et al*., 2013). The advantage with hand sanitizers is that they are independent of sinks and running water, kill microbes faster, are convenient, easy to use and are time saving (Macinga *et al*., 2008). Hand sanitizers are majorly composed of the antimicrobial agent, humectant, emollients and emulsifiers.

The humectant / moisturizer helps to retain water loss from the skin by lubricating it and also soften the skin (Peters, 2008). Humectants that can be used include but are not limited to glycerin, agarose, ammonium lactate, benzyl luronate, erythritol, honey, inulin, maltose, lysine, potassium lactate, sodium aspartate and lactitol (Chiang, 2003).

Emollients / skin conditioners such as octyl isononanoate also help in reducing evaporative water loss from the skin, they also improve the skin texture and feel (Fitchmun, 2007; Peters, 2008). Examples of emollients include tea tree oil, lanolin, floral oils, jojoba, aloe-based oil and chamomile (Narula and Narula, 2003).

The emulsifiers / thickeners prevent nanoparticles from settling at the bottom thus preventing the formation of clusters. This maintains the size and properties of the nanoparticles thus making the antiseptic effective (Bouchard and Bouchard, 2011). They also help the antiseptic to wet quickly but hydrate slowly (Peters, 2008). Examples of emulsifiers used include acrylic copolymers, chitosan, hydoxypropyl methylcellulose and maleic anhydride (Peters, 2008; Chiang, 2003).

The compounds that have been used as active ingredients in instant hand sanitizers are;

i) Quaternary Ammonium Compounds such as Benzethonium chloride and Benzalkonium chloride (Chiang, 2003). These are cationic compounds and are more effective in prevention of growth of microbes than in killing them. They show more activity with Gram positive bacteria compared to Gram negative bacteria and fungi. Their activity decreases in the presence of hard water, soiling matter and soaps and detergents. More so in high concentrations, it corrodes iron (Jeffrey, 1995).

ii) Phenolic compounds such as Triclosan (Trichloro-2-hydroxydiphenylether) and Para-chloro-meta-xylenol (PCMX) (Chiang, 2003). These have an extensive range of antibacterial activity but some microbes like *E. coli*, *Salmonella typhimurium* and Mycobacterium tuberculosis have developed strains resistant to these phenolic compounds (McMurray *et al*., 1998). Also phenolic compounds have shown to be ineffective on most viruses and have poor surface activity (Harvey, 1980; Jeffrey, 1995).

iii) Chlorohexidine: These have a wide range of antimicrobial activity but are not effective on most non-enveloped viruses (Park *et al*., 2010). They also cause skin irritation and moisture loss on the skin (Leece, 2004).

iv) Alcohols: These are the most active compounds with activity retention of 10% (Jeffrey, 1995). They demonstrate effectiveness over an extensive range of bacteria, viruses and fungi but they have poor activity against bacteria spores, non-lipophilic viruses and protozoan oocysts (Oke *et al*., 2013). These alcohol based hand sanitizers cause skin irritation and drying of the skin (Chiang, 2003; Leece, 2004). Their continuous use can result to skin disorders such as contact dermatitis (Leece, 2004). In order to prevent skin drying caused by use of alcohol based sanitizers, emollients can be added but they make the hand sticky and can easily pick up and transfer microbes (Michaels *et al*., 2003). Also, alcohol based hand sanitizers have high composition of ethanol that is to say, 60-70% thus making them

highly flammable. This increases their storage and transportation costs (Chiang, 2003). Because of the high volatility of ethanol, the hand sanitizers easily evaporate off the skin few seconds after application. The hands remain free from the antimicrobial agent thus making them prone to recolonization by pathogens (Dyer *et al*., 1998).

CHAPTER THREE: METHODOLOGY

3.1 Materials and Reagents

The materials used in this study were beakers, 10ml sample bottles, test tubes, 250ml volumetric flasks, petri dishes, silver nitrate salt, zinc nitrate salt, chloramphenicol capsules, fluconazole capsules, guar gum, *Bidens pilosa* leaf, stem and root powder.

The analytical grade reagents used were distilled water, bacteria cultures of *E. coli* and *S. aureus*, fungus *C. albicans*, α-tocopherol, pure glycerin and fragrance (chantia).

The equipment used in this study were weighing balance, centrifuge, heater, magnetic stirrer, UV-Vis spectrophotometer [UV-1700 Pharma Spec (Shimadzu)], Fourier Transmission Infrared Microscope (FTIR JASCO 4100), Raman spectroscopy (Reinshaw RM1000), Transmission Electron Microscope (Philips Technai – FE 12), Scanning Electron Microscope (Hitachi S3000N), X-ray Diffraction Spectrometer (Pananalytical Xpert-Pro), Atomic Force Microscope (DI, Santa Barbra CA), oven, and temperature bath.

3.2 Methods

3.2.1 Sample collection and leaf extract preparation.

The plant (*Bidens pilosa*) was collected from Chiromo forest in Nairobi County. The plant was identified and authenticated by Mr. Patrick Mutiso from the University of Nairobi herbarium, School of Biological Sciences. The leaves, seeds and roots were plucked of the whole plant and placed in separate containers. They were separately washed using distilled water, air dried under shed for 72h and pounded to powder. The leaf powder (2g) was transferred in 250ml of distilled water and refluxed at 90^{o}C for 10 minutes, cooled and filtered using a Whatman filter paper. The residue was discarded. The filtrate was centrifuged at 14,500 rpm for 10 minutes. The above procedure was repeated at 65, 45 and 25^{o}C. The above procedure was repeated for the powdered roots and seeds (Savithramma *et al*., 2011; Niraimathi *et al*., 2013; Jyoti *et al*., 2016).

3.2.2 Preparation of 1mM metal salt solutions.

Silver nitrate salt (0.0425g or 0.25mmol) was weighed and dissolved in 100ml of deionized water. The solution was transferred to a 250ml volumetric flask and filled the volumetric flask to the mark with deionized water. The above procedure was repeated for 0.0744g (0.25mmol) of zinc nitrate hexahydrate ($Zn(NO_3)_2$. $6H_2O$) (Verma and Mehata, 2016; Raja *et al*., 2017).

3.2.3 Preparation of silver and zinc oxide nanoparticles from different parts of *Bidens pilosa*

AgNPs and ZnONPs were prepared as shown below for the three parts of *Bidens pilosa*.

1. 20 ml of the leaf extract obtained at 90°C were transferred to a beaker followed by 80ml of 1mM metal salt solution (silver nitrate solution). The mixture was allowed to stand for 12h.
2. 1ml of the mixture was removed and transferred to a cuvette for UV-Vis analysis. The rest of the mixture was centrifuged at 14,500 rpm for 10 minutes. The supernatant obtained after centrifugation was transferred to the oven where it was dried at 60°C for 8h.
3. The nanoparticles, in powder form, were removed and transferred to a closed container and kept for further analysis.
4. The above procedure was repeated for different compositions of silver nitrate and zinc nitrate as shown in **Table 2** below.

Table 2: Volume and compositions of silver nitrate and zinc nitrate used in the preparation of the silver and zinc oxide nanoparticles

Composition of $AgNO_3$	Composition of $Zn(NO_3)_2$	Volume of 1mM $AgNO_3$ (ml)	Volume of 1mM $Zn(NO_3)_2$ (ml)
0.8	0.2	64	16
0.6	0.4	48	32
0.5	0.5	40	40
0.4	0.6	32	48
0.2	0.8	16	64
0.0	1.0	0.0	80

5. Procedures 1-4 was repeated for the seed and root extracts obtained at 65, 45 and 25°C (Ren *et al*., 2016; Ibrahim, 2015; Gurunathan, 2015; Emmanuel *et al*., 2015).

3.2.4 Characterization of AgNPs and ZnONPs using UV-Vis spectrophotometry

The Surface Plasmon Resonance (SPR) properties and spectral analysis of the AgNPs were analyzed using UV–visible spectrometer [UV-1700 Pharma Spec UV-Vis spectrophotometer (Shimadzu)] from the Department of Physics, University of Nairobi. The instrument was switched on and left to initialize for about 2h. Deionized water was used as the control sample. In order to obtain the baseline, the cuvette in the reference slot and the cuvette in the sample slot were filled with deionized water. The wavelength range was set between 250 and 700nm. The cuvettes in the sample slot were replaced with each of the solution of nanoparticles. The samples were scanned, spectra recorded and data saved in a computer. The cuvettes in the sample slot were washed with deionized water whenever a new sample was to be introduced (Krishnaraj *et al*., 2010; Guzman *et al*., 2012; Agarwal *et al*., 2017).

3.2.5 Screening for antimicrobial activity

These tests were carried out in a microbiology laboratory at University of Nairobi. Nutrient agar was the culture medium used for growth of microorganisms.

3.2.5.1 Preparation of the culture medium

Nutrient agar (28.0g) was added in a 250ml beaker followed by 100ml of distilled water while stirring and transferred the medium to a 1L sterilizing bottle. The bottle was filled to the mark with distilled water. The medium was heated to boiling point and then sterilized by autoclaving at 15Psi for 15 minutes. It was allowed to cool for 2h and then 20ml of medium was poured in each of several sterile petri dishes under aseptic conditions and left to solidify for 24h. This was to ensure that no other bacteria were present in the dishes (Sharma *et al*., 2013).

3.2.5.2 Preparation of cultures of the test microorganisms

The microbial cultures used to test for antimicrobial activity of silver and zinc oxide nanoparticles prepared in **Section 3.5.1** above were two bacterial species *Escherichia coli, Staphylococcus aureus* and a yeast *Candida albicans.* Pure cultures of the microorganisms were obtained from the Microbiology laboratory in the School of Biological Sciences, University of Nairobi. Microbial cell suspensions were prepared by transferring microorganisms growing on a solid medium in petri plates to 9ml of sterile distilled water in a culture bottle using a flamed inoculating wire loop. The above procedure was repeated separately for *E. coli*, *S. aureus* and *C. albicans* (Sharma *et al*., 2013; Abdel-Fatah *et al*., 2016).

3.2.5.3 Preparation of nanoparticle solutions for antimicrobial test

The nanoparticles (0.5mg) were transferred to a sample bottle followed by 5ml of deionized water and the solution homogenized using a vortex mixer. The prepared solution had a concentration of 100µg/mL (100ppm). The solutions were then labelled for ease of identification (Vijayakumar *et al*., 2013; Ahmad *et al*., 2016).

The positive control for *E. coli* and *S. aureus* was prepared by dissolving 10mg of Chloramphenicol capsule in 10mL of water and the solution homogenized using a vortex mixer. The concentration of the positive control was 1mg/ml or 1000ppm.

The positive control for *C. albicans* was prepared by dissolving 10mg of fluconazole capsule in 10mL of water and the solution homogenized using a vortex mixer. The concentration of the control was 1mg/ml or 1000ppm (Vijayakumar *et al*., 2013; Ahmad *et al*., 2016).

3.2.5.4 Antimicrobial test for the nanoparticles

The *E. coli* microorganisms were inoculated on the surface of the nutrient agar culture medium plates using a sterile cotton wool swab. The above procedure was repeated for *S. aureus* and *C. albicans* on different nutrient agar plates using different swabs. Wells were made in the agar medium using a sterilized cork borer of diameter 6mm. Five wells were made on each plate. The middle well was for the control sample. Distilled water was used as the negative control while Chloramphenicol, an antibiotic, was used as the positive control *E. coli* and *S. aureus*. Fluconazole was used as the positive control for the yeast strain of *C. albicans*.

Using a micropipette, 45µl of the nanoparticle solution, A, was transferred into a well in the petri dish inoculated with *E. coli*. A similar amount of nanoparticle solution, A, was transferred into the neighboring well so that the test could be done in duplicate. The remaining two wells in the same petri dish were filled with nanoparticle solution B. Each petri dish contained two samples for analysis. The above procedure was repeated for plates containing *S. aureus* and *C. albicans*. The plates, containing *E. coli* and *S. aureus*, filled with nanoparticle solutions were incubated for 24h at 37^{o}C. The plates, containing *C. albicans*, filled with nanoparticle solution were left at room temperature for 48h. The above procedure was repeated for all the prepared nanoparticle solutions.

After the incubation period, the diameters of the zones of growth inhibition around the wells containing the nanoparticle solutions were measured with a Vernier caliper and recorded (Kaviya *et al*., 2011; Raja *et al*., 2017; Balouiri *et al*., 2016).

3.2.5.5 Minimum Inhibitory Concentrations (MIC)

From the results obtained from the test of antimicrobial activity, samples G1 (S90-0.8), U1 (L90-0.8) and ρ1 (R90-0.8) were selected for determination of the Minimum Inhibitory Concentration since they showed the highest activity.

In a 250ml beaker, added 13g of nutrient broth followed by 100ml of distilled water while stirring and transferred the medium to 1ltr media sterilizing bottle. The medium was heated to boiling, allowed to cool for 2h and then poured into 15ml tubes each tube receiving 9ml of the medium. The tubes, containing the broth medium, were autoclaved at a pressure of 15Psi for 15 minutes in order to kill any microorganisms

present. 1ml (100µg/ml) of G1 (S90-0.8) was drawn using a micropipette and transferred to a medium containing tube. The solution was thoroughly shaken to ensure uniform mixing. This was concentration of 10µg/ml (10ppm) ZnONP concentration. 1ml of solution was drawn using a micropipette from the solution of 10µg/ml (1 ppm) ZnONP concentration and transferred to another medium containing tube to make a solution of 1ppm ZnONP concentration. The solution was thoroughly shaken to ensure uniform mixing.

1ml was drawn from the solution of 1ppm concentration using a micropipette and transferred to the third medium tube to make 0.1µg/ml (0.1ppm) ZnONP concentration. The tube was shaken thoroughly. Drops of the broth cultures of *E. coli* medium were added to each of the samples. The above procedure was repeated for *S. aureus* and *C. albicans*.

The above procedure was repeated for the leaf extract ZnO-AgNP (0.2:0.8) and root extracts ZnO-AgNPs (0.2:0.8) at 10, 1 and 1ppm. The tubes for *E. coli* and *S. aureus* were incubated at 37°C for 24h and for *C. albicans* were incubated at room temperature for 48h (Ravichandran *et al*., 2016; Prabhu and Poulose, 2012).

3.2.6 Characterization of AgNPs and ZnONPs using FTIR

In order to remove any residue or compound that is not the capping ligand of the nanoparticles, the residual solution was centrifuged at 14000rpm for 10min and the supernatant liquid decanted. The resulting suspension was re-dispersed. The resulting residue was oven dried to obtain dry powder. The solid nanoparticles were then crushed with potassium bromide (KBr) and the mixture pressed in a mechanical press to form a thin and transparent pellet. The collar and the pellet were put onto the sample holder. While the FTIR of plant extract was obtained by dropping a sample between two plates of sodium chloride (salt) and analyzed in a liquid cell. (Santhoshkumar *et al*., 2017; Janaki *et al*., 2015; Ahmed *et al*., 2016). The FTIR analysis was carried using FTIR-JASCO 4100 spectrophotometer from the Department of Chemistry, University of Nairobi

3.2.7 Characterization of AgNPs, ZnONPs and ZnO-AgNPs using Raman Spectroscopy

A Renishaw RM1000 Raman spectrometer (from University of Western Cape) system equipped with a Leica DMLB microscope and a 785nm near-infrared diode laser source (maximum at 300mW) was used in this study to determine the functional groups of the compounds adsorbed on the surface of nanoparticles. Raman scattering signals were detected by a 578 x 385 pixels CCD array detector. Raman spectra were acquired for the AgNPs, ZnONPs and ZnO-AgNPs using a 50x objective with a detection range from 600 to 1800 cm^{-1} in the extended mode. The measurement was conducted with a 10s exposure time and a 10MW laser power (Krutyakov *et al*., 2008; Nava *et al*., 2017; Emmanuel *et al*., 2015).

3.2.8 Characterization of AgNPs and ZnONPs using SEM

For SEM analysis, images were taken using a Hitachi S3000N Scanning Electron Microscope at an acceleration voltage of 20kV at various magnifications at University of Western Cape. Gold sputtering of the SEM samples were done using a SC7640 Auto/ Manual high resolution super coater (Quorum Technology Ltd., England) at a voltage of 2kV and plasma current of 25mA for one minute (Basha *et al*., 2016; Elumalai and Velmurugan, 2015; Edison and Sethuraman, 2012).

3.2.9 Characterization of AgNPs and ZnONPs using TEM

Samples for transmission electron microscopy (TEM) analysis were prepared by drop coating biologically synthesized silver and zinc oxide nanoparticles solution on to carbon-coated copper TEM grids. The films on the TEM grid were allowed to stand for 2 minutes, following which excess solution was removed using a blotting paper and grid allowed to dry under a lamp prior to measurement. TEM images were acquired on Philips Technai-FE 12 TEM instrument (from University of Western Cape) operated at an accelerating voltage of 120 kV equipped with an Energy dispersive X-ray (EDAX) detector (Oxford LINK-ISIS 300) for elemental composition analysis and the EDAX spectra was measured at an accelerating voltage of 10 kV (Panáček *et al*., 2009; Fayaz *et al*., 2010; Bagherzade *et al*., 2017).

3.2.10 Characterization of AgNPs and ZnONPs using XRD

XRD analysis was done using Pananalytical Xpert-Pro powder diffractometer (from University of Western Cape) using Cu-Kα radiation in range 2θ. Scans were in the range 30 - 80°C at 2θ, with 0.02° step sizes held for 2 seconds each (Ravichandran *et al*., 2016; Bar *et al*., 2009; Ravichandran *et al*., 2016).

3.2.11 Characterization of AgNPs and ZnONPs using Atomic Force Microscopy

AFM measurements were performed on AgNPs, ZnONPs and ZnO-AgNPs using a digital Nanoscope III a multimode system (DI, Santa Barbara. CA) from University of Western Cape. The images were acquired in the tapping mode. Measurements were made using the Si cantilever. The force constant of the cantilever was 0.1~0.6 N/m with the scan rate at 1~2 Hz. The AFM measurements were made in air at room temperature (Jia *et al*., 2002; Lu *et al*., 2015; Aysaa and Salman, 2016).

3.2.12 Formation of a hand sanitizing antiseptic

Deionized water (77.1g) was poured into a beaker followed by 0.7g of guar gum (gelling agent). The solution was heated to 50ºC while stirring at 1,000rpm for 30 minutes. The solution was then allowed to cool to room temperature and 2g of α-tocopherol (emollient) and 0.1g of ZnO-AgNPs (active ingredient) was added while stirring at 1,000 rpm. Lastly 7g of pure glycerin (humectant) followed by 0.2g of fragrance were added to the mixture. The mixture was stirred for more 30 minutes at 1,000 rpm at room temperature. The antiseptic/ hand sanitizer was then allowed to stand for 2h and then tested for antimicrobial activity (Peters, 2008; Willard *et al*., 2005).

The antimicrobial activity of the antiseptic was evaluated against gram positive Staphylococcus aureus, gram negative Escherichia coli and fungus Candida albicans. Fresh overnight inoculums (50µL) of each culture were spread on to agar plates. Wells of 6mm diameter were made in the agar pates using a sterile coke borer. 45µL of the antiseptic was poured into the wells. The *E. coli* and *S. aureus* plates were incubated at 37°C for 24h. The plates with *C. albicans* were left to stand at room temperature for 48h. The diameters of zones of inhibitions were recorded. The above procedure was repeated for ZnONPs and ZnO-AgNPs.

CHAPTER FOUR: RESULTS AND DISCUSSION

4.1 Preparation of silver and zinc oxide nanoparticles

Bidens pilosa contains bio-molecules (**Section 2.2**) such as polyphenols which aid in the synthesis of silver and zinc oxide nanoparticles. These biomolecules present in the *Bidens pilosa* acted as the reducing, capping and stabilizing agents during the synthesis of the nanoparticles (Cortés-Rojas *et al*., 2013; Iravani, 2011). During the preparation of ZnONPs, the colour changed from that of the extract to a bright yellow after 5 minutes indicating the formation of ZnONPs. In the case of the AgNPs, the colour changed from the colour of the extracts, according to A, B and C in **Figure 7**, to a dark grey after 5 minutes indicating the formation of AgNPs. For ZnO-AgNPs, the colour changed from the colour of the extracts to a brown colour. The colours of the extracts are shown in **Figure 7 A, B** and **C**. The colour of the ZnO-AgNPs was an intermediate of the colour of ZnONP solution and AgNP solution that is a brown colour as shown in **Figure 7 (G)**. There was no observable colour change with change in the composition of ZnO-AgNP solution as shown in **Figure 7 (G)**.

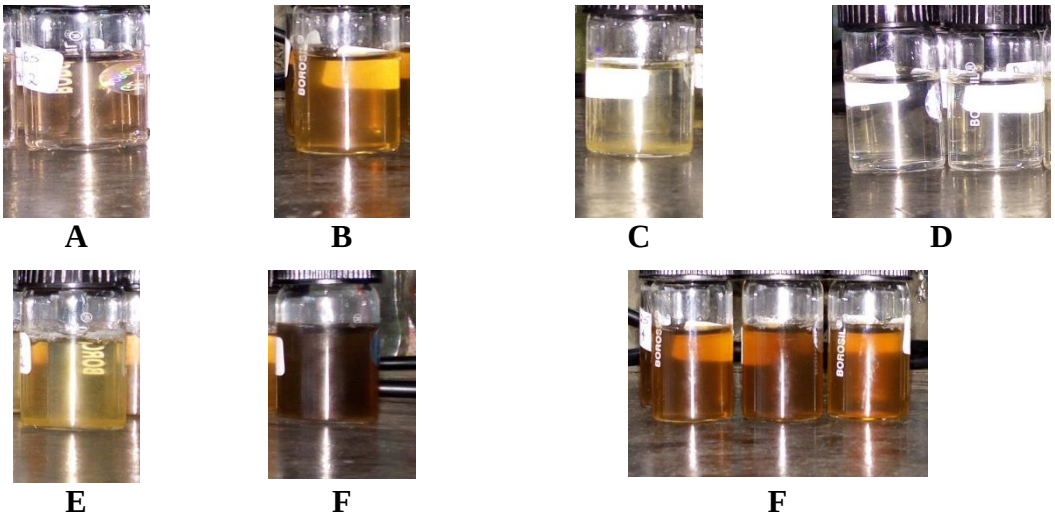

Figure 7: (A) Seed extract (B) Leaf extract (C) Root extract (D) Silver nitrate and Zinc nitrate (E) Solution containing ZnONPs (F) Soluton containing AgNPs (G) Solutions containing ZnO-AgNPs.

4.2. Effect of Temperature on Percentage yield of AgNPs, ZnONPs and ZnO-AgNPs

The percentage yields of the synthesized AgNPs, ZnONPs and ZnO-AgNPs were determined and summarized in **Figure 8A - C (Appendix A, Table 6)**. The result as expected show that the percentage yields increased with increase in extraction temperature. This implies that as the extraction temperature increases the solubility of water soluble biomolecules increases and thus increasing the reducing and stabilizing ability of the extract. Also increase in temperature increases the kinetic energy of the reacting species hence increasing the rate of collision of the reacting species with a higher part of collisions exceeding the threshold of activation energy. This in turn increases the amount of nanoparticles produced as the tempearture of the extract increases.

Figure 8A indicates that the seed extract gave generally higher percentage yield of ZnONPs compared to the leaf and root extracts. This could imply that the seed extract contains more reducing and stabilizing agents for the ZnONPs compared to the leaf and root extracts there by giving a generally higher yield. However, for AgNPs the leaf extract gave higher yield compared to the seed and root extracts, **Figure 8B**. This could mean that the leaf extract contains more bio-molecule compounds for the reduction and stabilization of Ag^{+} to AgNPs hence giving a higher yield of AgNPs. In the case of ZnO-AgNPs, the root extract gave the highest yield, **Figure 8C**. This could be due to the root extract having compounds with a higher reducing and stabilising ability for the ZnO-AgNPs than the seed and leaf extracts.

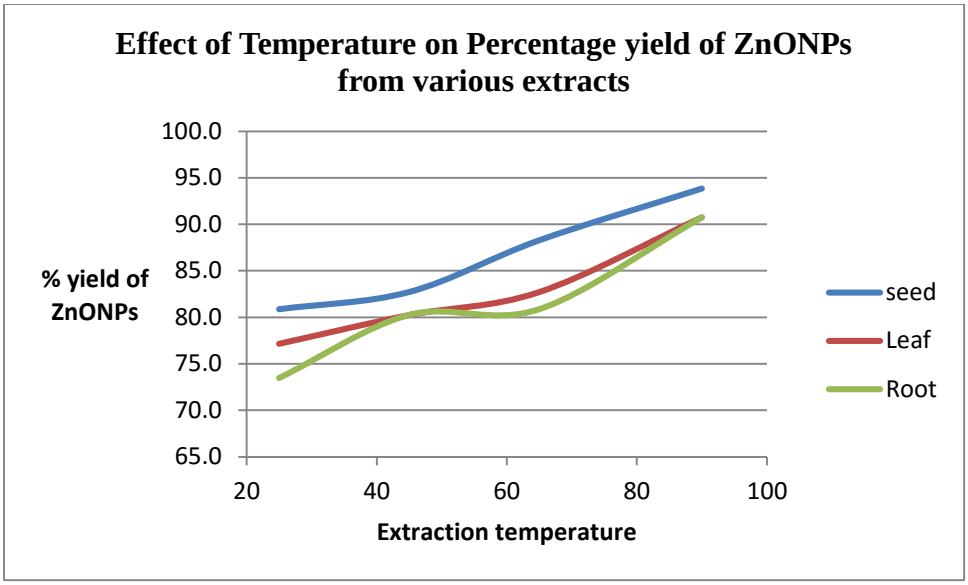

Figure 8A: Percentage yield of ZnONPs versus temperature for seed, leaf and root extracts.

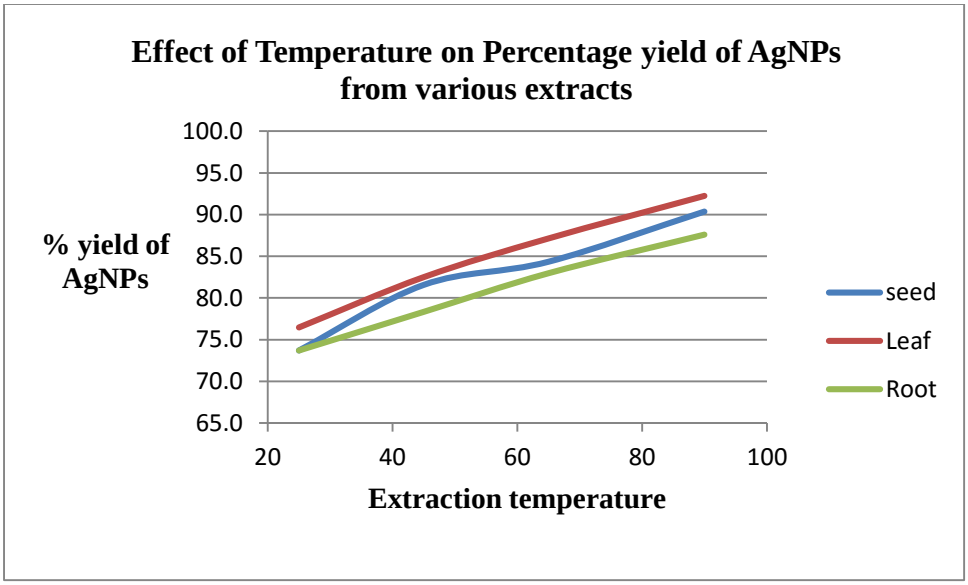

Figure 8B: Percentage yield of AgNPs versus temperature for seed, leaf and root extracts.

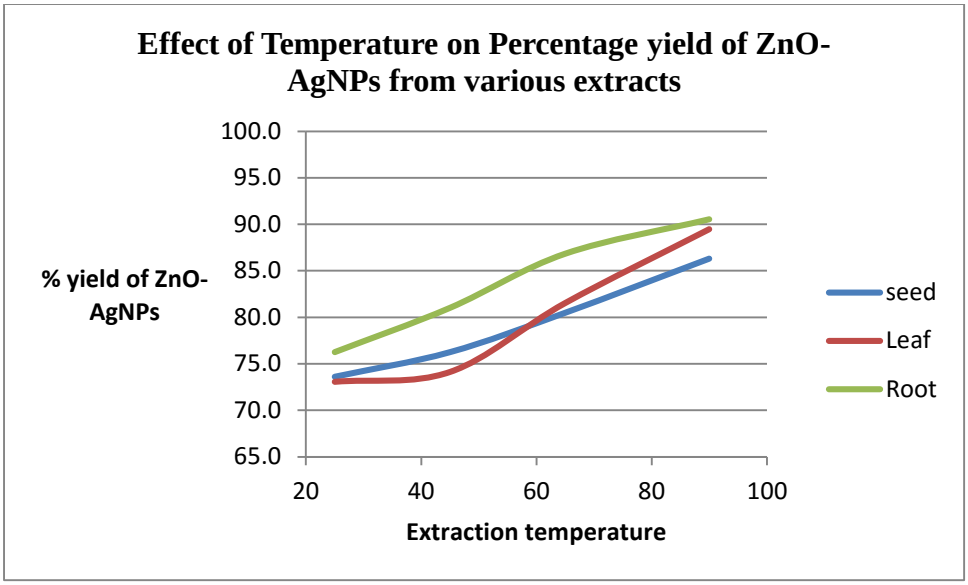

Figure 8C: Percentage yield of ZnO-AgNPs versus temperature for seed, leaf and root extracts. The ratio of Ag: ZnO in this ZnO-AgNPs is 1:1.

4.3 Characteristion of extracts, precursors and nanoparticles using UV-Visible Spectroscopy

4.3.1 UV-Vis spectra of extracts, silver nitrate and zinc nitrate

The UV-Vis spectroscopy of the extracts (seed, leaf and root) and the metal salts (silver and zinc nitrate) was determined as a baseline for comparison with the behavior of nanoparticles in UV-Vis region.

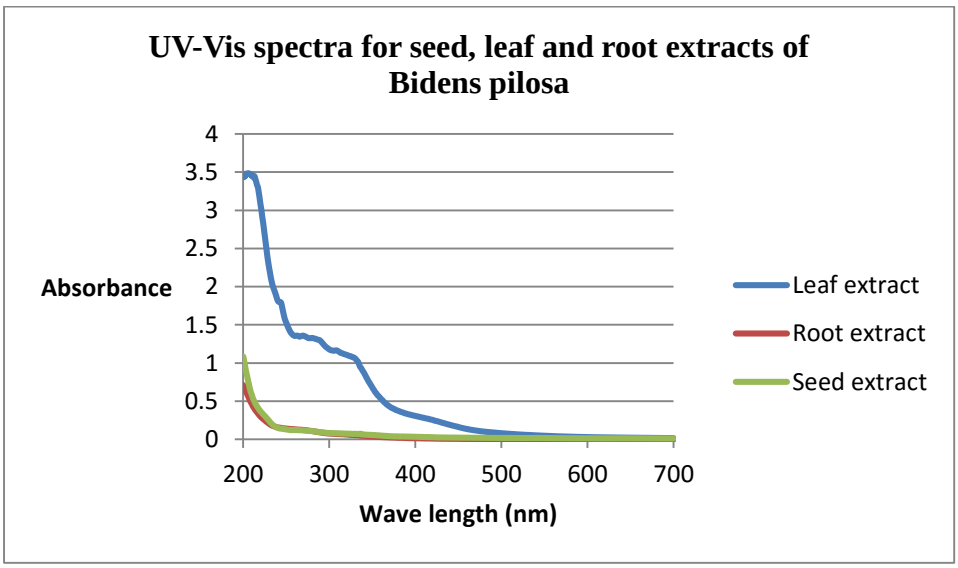

Figure 9A: UV-Vis spectra for seed extract, leaf extract and root extract

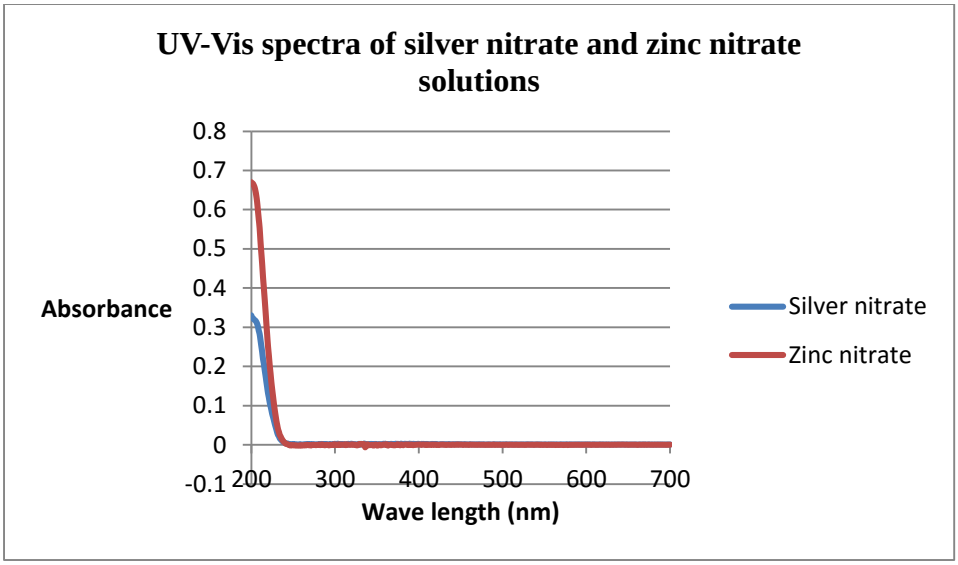

Figure 9B: UV-Vis spectra for silver nitrate and zinc nitrate solutions

4.3.2 Characterization of the nanoparticles using UV-Vis of the nanoparticles

The UV-Vis spectra of the nanoparticles of the three extracts were measured at four different temperatures, 25, 45, 65 and 90°C, to determine the effect of temperature on yield of nanoparticles.

4.3.2.1 Characterization of AgNPs using UV-Vis spectroscopy

The UV-Vis spectra of the silver nanoparticles of the three different extracts were measured and discussed in the following sections.

4.3.2.1.1 UV-Vis spectra of silver nanoparticles from leaf, seed and root extracts from *Bidens pilosa* at a particular temperature.

Surface plasmon resonance consists of a collective oscillation of conduction electrons excited by the electromagnetic field of light. The particles absorb light and the electrons move to the excited state and resonate with a certain frequency known as the resonant frequency (Garcia, 2011). The surface plasmon bands for AgNPs synthesized using seed extract at the four temperatures were at 410, 410, 410 and 411nm, respectively, **Figure 10A - D**. For the leaf extract AgNPs at the four temperatures, the surface plasmon resonances were at 408, 405, 404 and 410nm, respectively, **Figure 10A - D**. For the AgNPs obtained using root extract at theses temperatures the

resonances were at 411, 411, 411 and 410nm, respectively, **Figure 10A - D**. The agreement in band occurrence shows, all the extracts of the AgNPs absorbed within a narrow range of 404 – 411nm, that AgNPs were successfully produced using the selected parts of the *Bidens pilosa* plant. The above bands all show a slight blue shift of the absorption bands of the nanoparticles presented with respect to the Surface Plasmon band of silver nanoparticles of other extracts that is around 420 - 500nm (Desai *et al*., 2012). This could be due to the silver nanoparticles produced had a very small diameter since decrease in size of silver nanoparticles causes a blue shift in the absorbance spectrum (Desai *et al*., 2012; Saion *et al*., 2013; Raza *et al*., 2013).The size of nanoparticles obtained in this study was 2-20nm as compared to Kumar *et al*., 2012 whose nanoparticles had a size range of 50-100nm with a surface plasmon band at 452nm. This is a clear indication that decreased size of nanoparticles causes a blue shift in the surface plasmon peak of the nanoparticles. The other factors such as surrounding medium and interparticle interactions could also contribute to the low band values (Mankad *et al*., 2013; Desai *et al*., 2012).

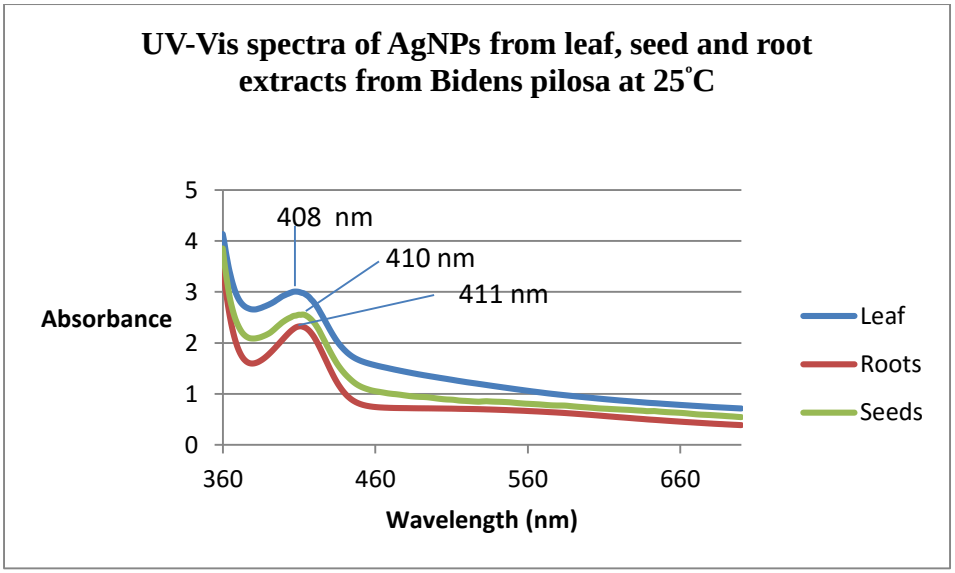

Figure 10A: UV-Vis spectra for AgNPs from extracts at 25˚C

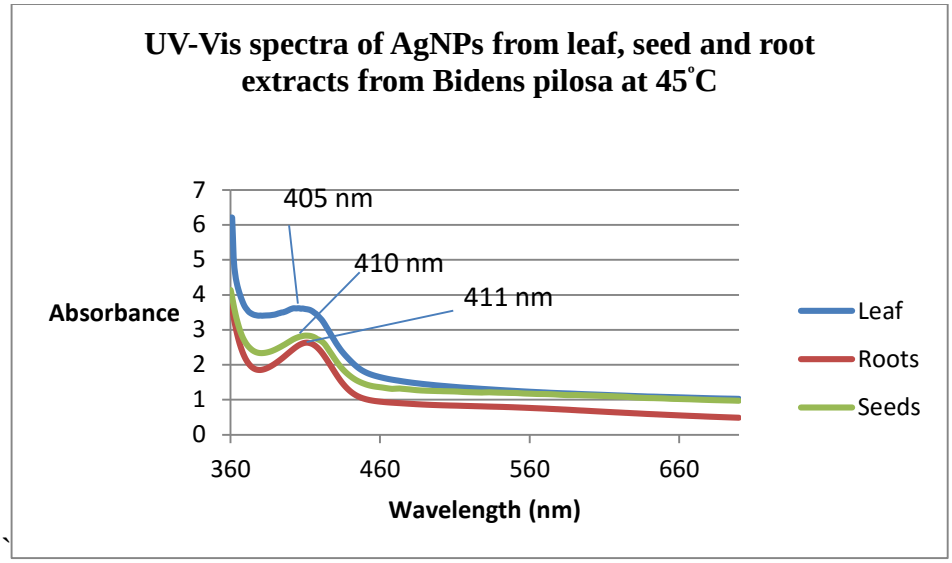

Figure 10B: UV-Vis spectra for AgNPs from extracts at 45°C

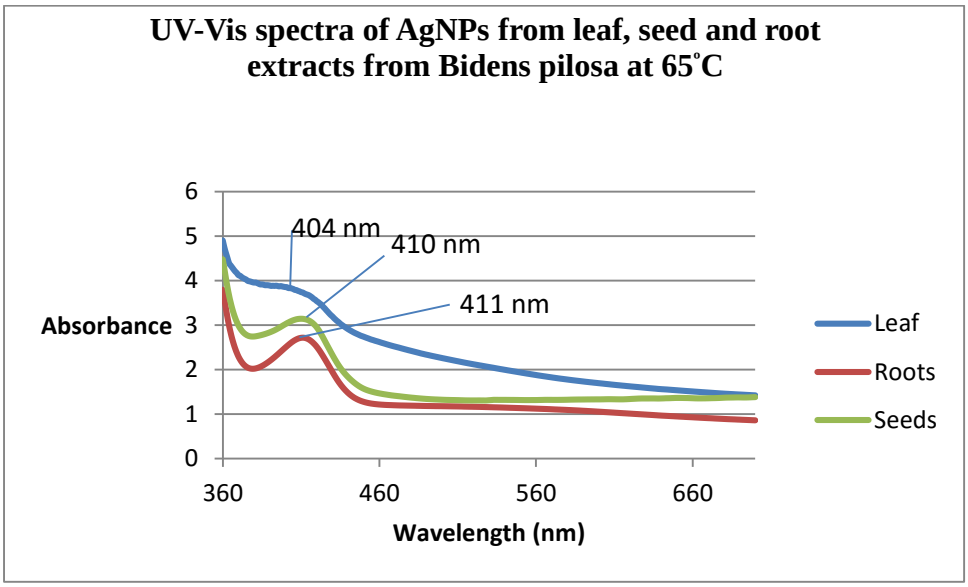

Figure 10C: UV-Vis spectra for AgNPs from extracts at 65°C

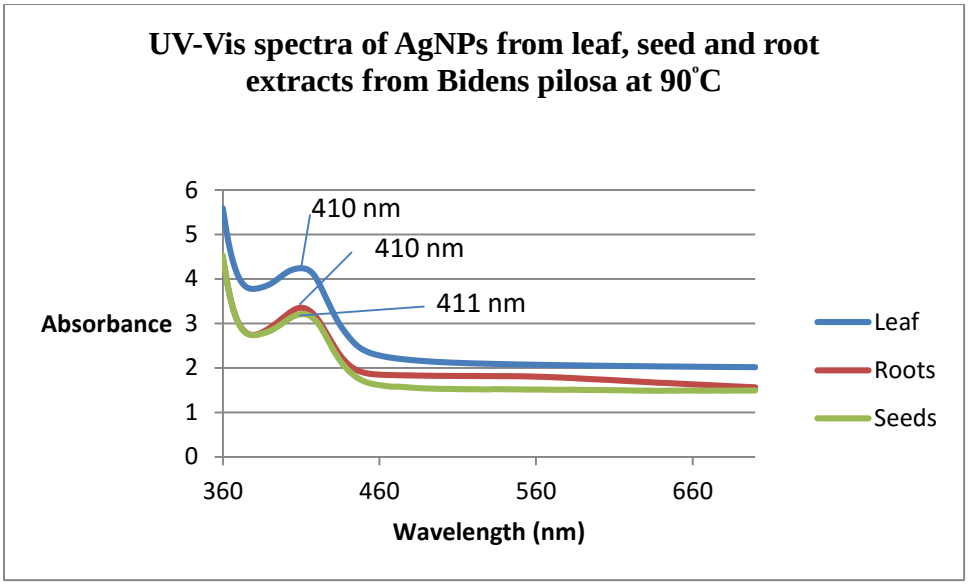

Figure 10D: UV-Vis spectra for AgNPs from extracts at 90°C

4.3.2.1.2 Effect of extraction temperature of seed, leaf and root extracts on synthesis of silver nanoparticles

As shown in **Figure 11A - C**, absorbance increased with increase in extraction temperature. The extraction temperature of 90°C gave the highest band intensity of the UV spectrum. This implies that the concentration of nanoparticles formed increases with increase in extraction temperature since the solubility of the reducing and capping agents in the extracts is also high. According to (Dai and Mumper, 2010), the solubility of water soluble biomolecules, such as polyphenols and heterocyclic compounds, increases with increase in temperature. This in the end increases the reducing and capping power of the plant extract during nanoparticle synthesis.

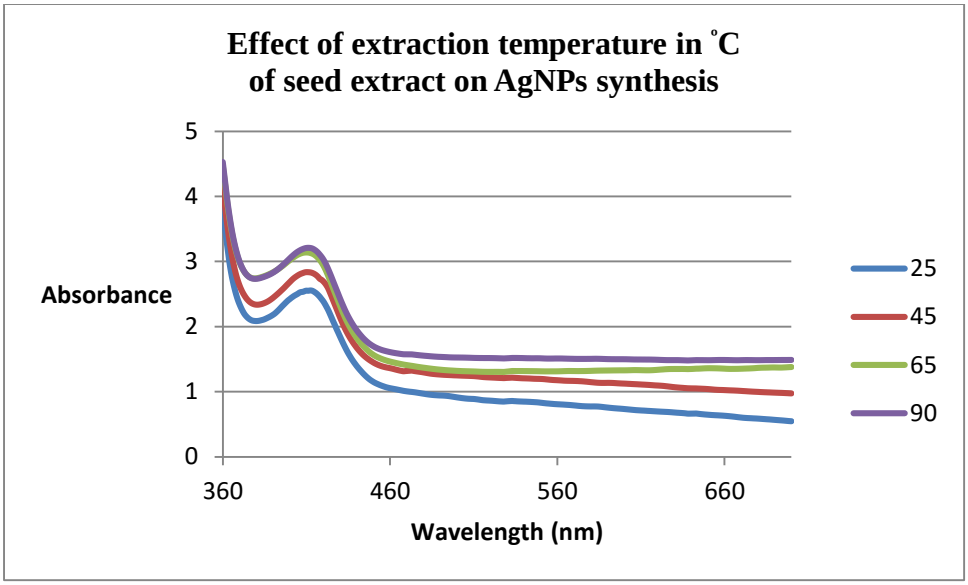

Figure 11A: UV-Vis spectra for AgNPs synthesized from seed extract at various temperatures

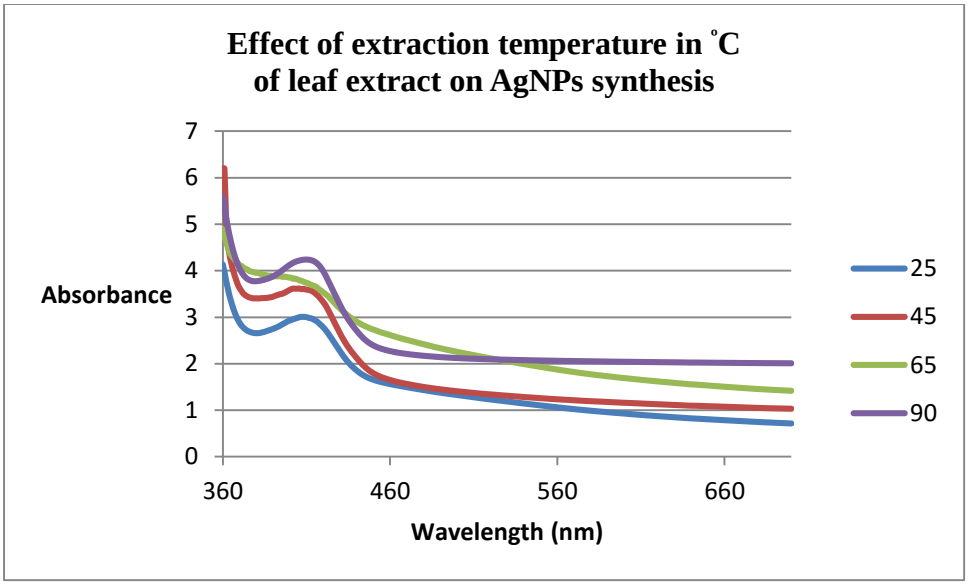

Figure 11B: UV-Vis spectra for AgNPs from leaf extract at various temperatures

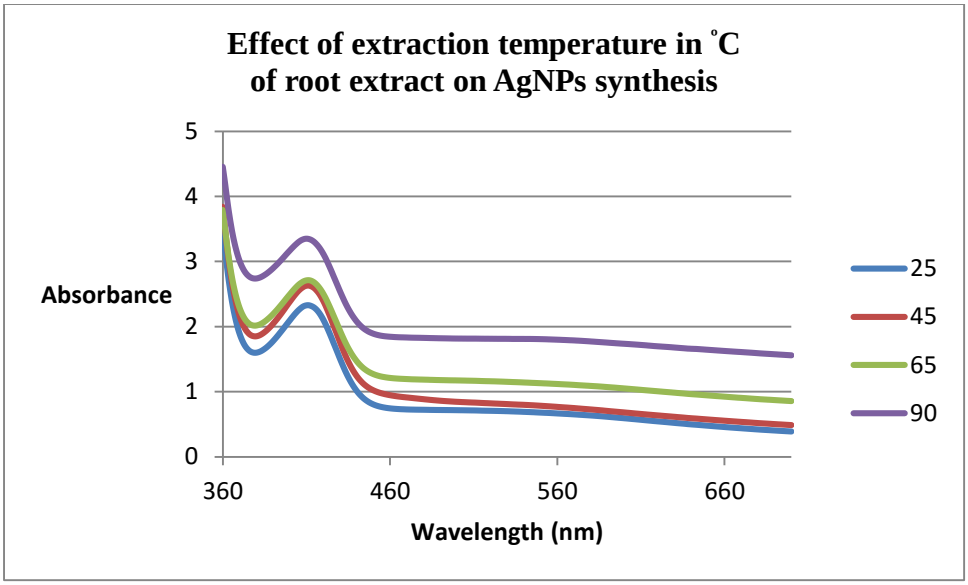

Figure 11C: UV-Vis spectra for AgNPs from root extract at various temperatures

4.3.2.2 Characterization of ZnONPs using UV-Vis spectroscopy

The UV-Vis spectra of the ZnONPs were measured at the four different temperatures and the spectra are given in **Figures 12A–D**. The results are discussed in the following section.

4.3.2.2.1 UV-Vis spectra of zinc oxide nanoparticles from leaf, seed and root extracts from *Bidens pilosa* at a particular temperature.

The surface plasmon bands for ZnONPs synthesized using seed extract at the four temperatures were 372, 368, 370 and 368nm, respectively. For the ZnONPs obtained using leaf extract at 25, 45, 65 and 90^{o}C, the bands were observed at 365, 368, 361 and 363nm respectively. For the ZnONPs obtained using root extract at 25, 45, 65 and 90^{o}Cthese temperatures were 371,370, 370 and 370nm, respectively. From the absorption bands obtained, all the values do not correspond to the band gap wavelength of 388nm of bulk zinc oxide (Bagabas *et al*., 2013) that is, they all indicated a blue shift in their absorption spectra. The decrease in λ_{max} could be due to increase in particle size which in turn increases its Rayleigh scattering (Bagabas *et al*., 2013). This could also be attributed to aggregation and agglomeration leading to particle size increment as the material settle down at the bottom of the container thus causing a decrease in absorbance (Rani *et al*., 2014). According to (Ghosh and

Raychaudhuri, 2008), shape transition of zinc oxide nanoparticles from spherical to hexagonal morphology occurs with increase in size of the nanoparticles leading to a blue shift of the absorption spectrum.

Different plant extracts have been used in the synthesis of zinc oxide nanoparticles and the UV-Vis absorption bands obtained vary according to the conditions at which the extracts are obtained and the type of plants used. Since absorption spectrum depends on many factors such as the refractive index of the surrounding medium, particle size, particle shape and absorption substance on the surface of the nanoparticles, the chemical compounds in the extracts of *Bidens pilosa* could also have contributed to the shift of the surface Plasmon peak of zinc oxide nanoparticles (Mankad *et al*., 2013).

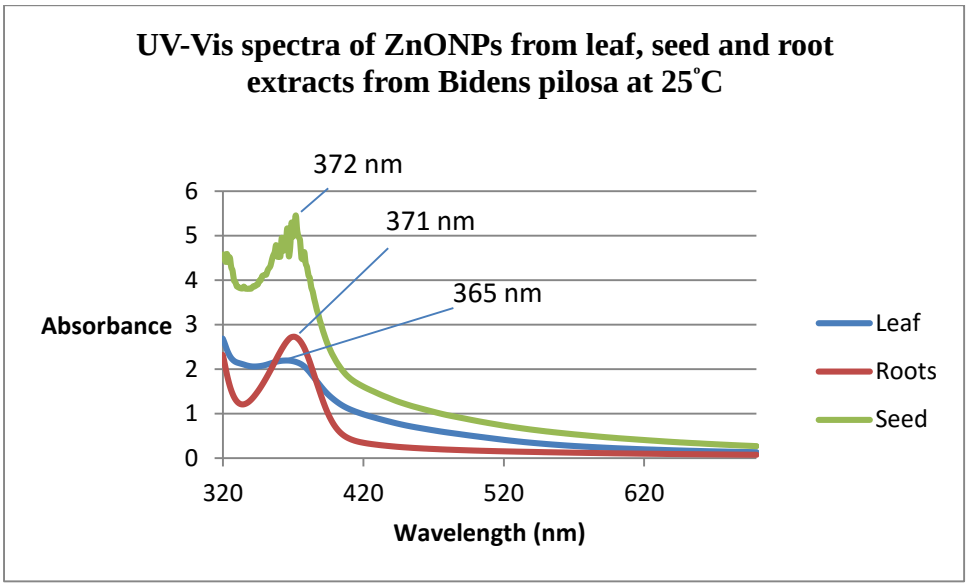

Figure 12A: UV-Vis spectra for ZnONPs from extracts at 25°C

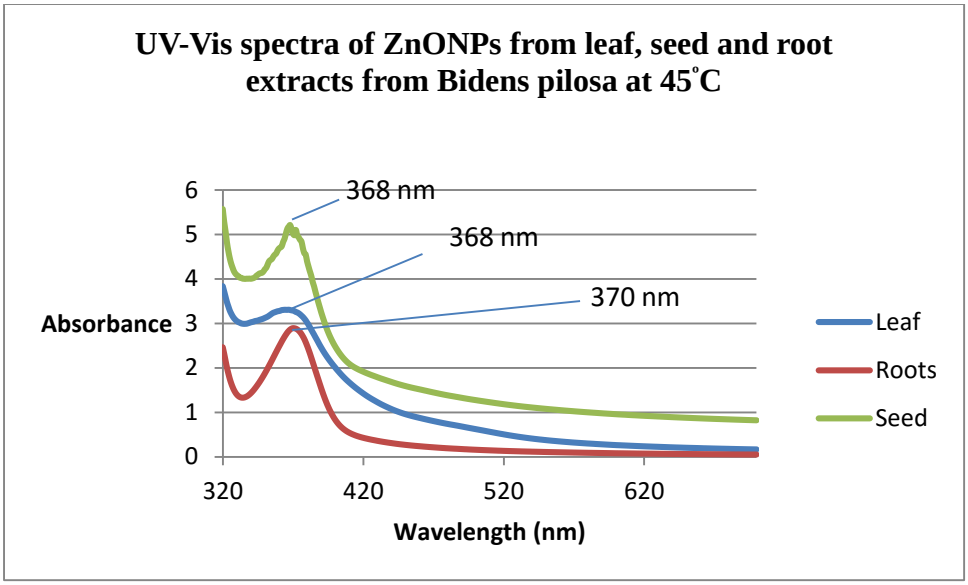

Figure 12B: UV-Vis spectra for ZnONPs from extracts at 45°C

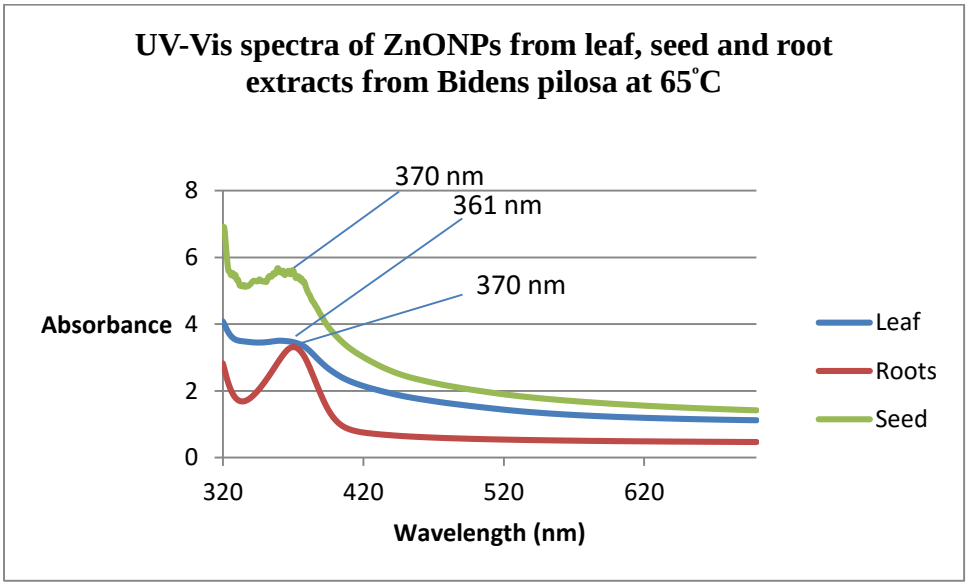

Figure 12C: UV-Vis spectra for ZnONPs from extracts at 65°C

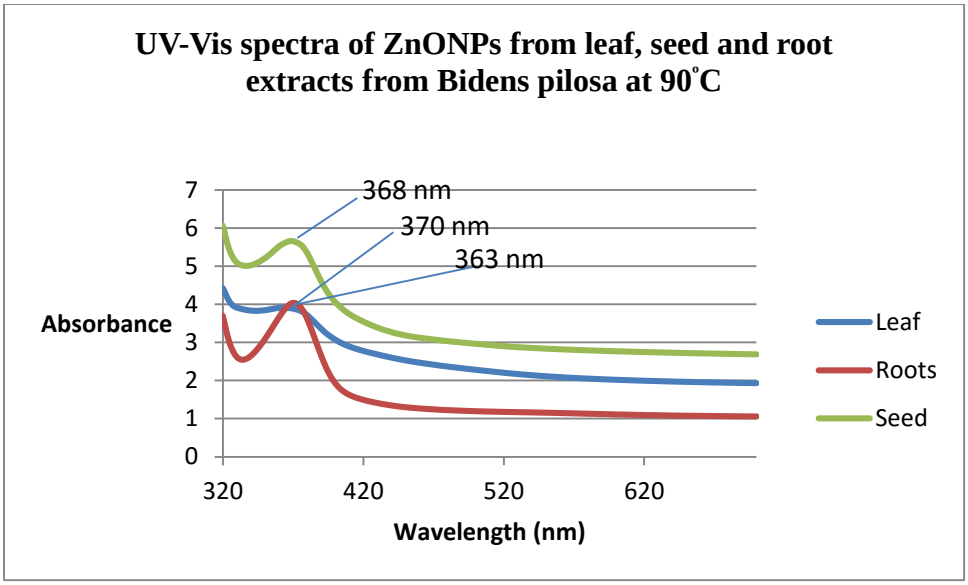

Figure 12D: UV-Vis spectra for ZnONPs from extracts at 90°C

Figures 12A–D indicate that the seed extract gave the highest absorption bands for ZnONPs implying that higher concentration of nanoparticles were formed using the seed extract. This could be due to the differences in the reducing and stabilizing agents present in the extracts. Plant extracts contain high levels of polyphenols containing hydroxyl and carboxylic functional groups. These functional groups bind to the metal ions and provide stability during the reduction process of the metal salts. The extracts also contain proteins and enzymes which combine with the metal ion to form enzyme-substrate complex. The enzymes work on the metal ions by reducing them to their respective metals hence forming metal capped nanoparticles (Matinise *et al*., 2017). In the formation of AgNPs and ZnONPs the mechanism could slightly differ. That is during formation of AgNPs; only reduction of Ag+ to Ag metal is needed, while during the formation of ZnONPs, oxidation of Zn^{2+} to ZnO is required. This means that the capping and stabilizing compounds must be in position to donate the O^{2-} to Zn^{2+} hence the seed extract could be containing more compounds that can stabilize ZnONPs compared to the root and leaf extract.

4.3.2.2.2 Effect of extraction temperature of seed, leaf and root extracts on synthesis of zinc oxide nanoparticles

The UV-Vis spectra of the ZnONPs were measured at the four different temperatures, **Figures 13A – C**. Just in the case of the AgNPs absorbance increased with increase in

extraction temperature. The extraction temperature of 90°C gave the highest band intensity of the spectrum. This implies that the concentration of nanoparticles formed increases with increase in extraction temperature since the solubility of the reducing and capping agents in the extracts is also high. According to (Dai and Mumper, 2010), the solubility of water soluble biomolecules, such as polyphenols and heterocyclic compounds, increases with increase in temperature. This in the end increases the reducing and capping power of the plant extract during nanoparticle synthesis.

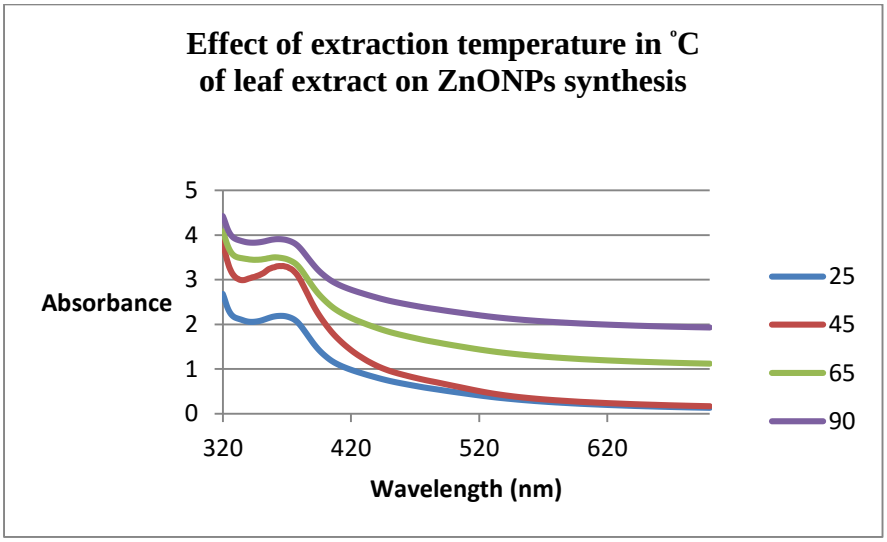

Figure 13A: UV-Vis spectra for ZnONPs from leaf extract at various temperatures

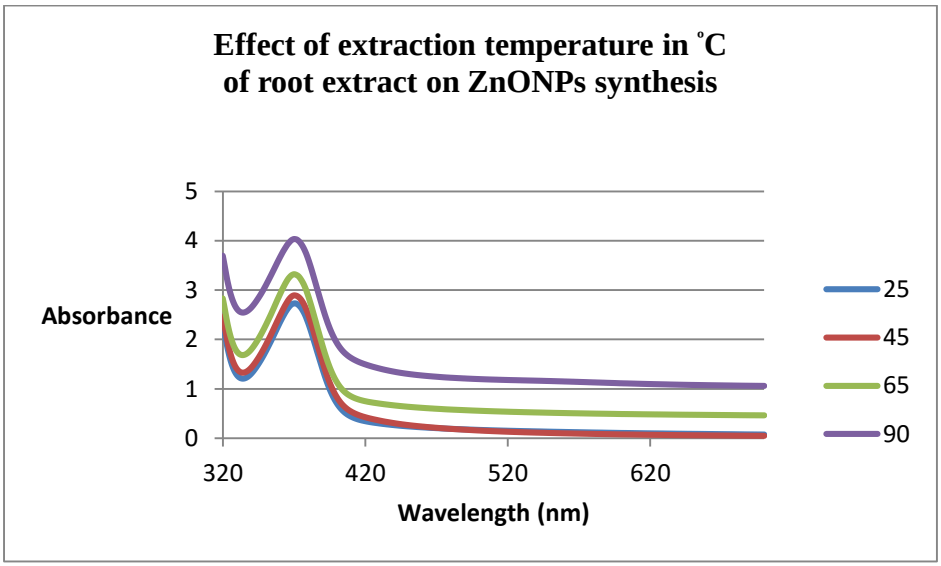

Figure 13B: UV-Vis spectra for ZnONPs from root extract at various temperatures

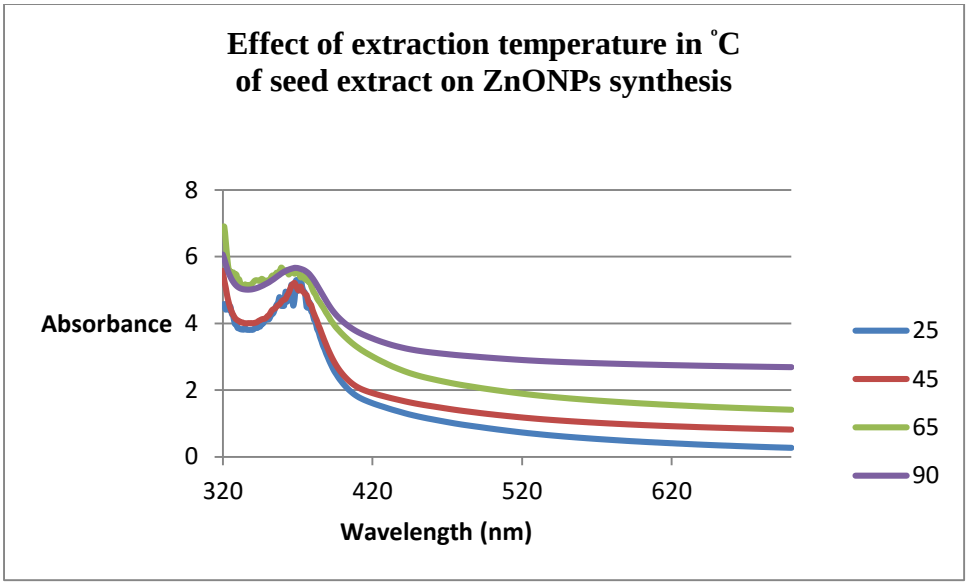

Figure 13C: UV-Vis spectra for ZnONPs from seed extract at various temperatures

4.3.2 3 Characterization of ZnO-AgNPs using UV-Vis spectroscopy

The UV-Vis spectra for ZnO-AgNPs, **Figure 14A - C**, were also measured for the three extracts at different ratios of AgNPs:ZnONPs. The ZnO-AgNPs gave two surface plasmon bands, one at 302nm corresponding to ZnONPs and another at 438nm corresponding to AgNPs. The band corresponding to AgNPs increases in intensity with increase in composition of AgNPs, **Figure 14A - C**. This implies that the yield of AgNPs increases with increase the amount of silver nitrate added to the extract and zinc nitrate mixture. However, the same trend is not observed for the ZnONPs. The change in their composition does not affect their absorbance intensity. As shown in **Section 4.3.2** the λ_{max} for ZnONPs and AgNPs were at 370 and 410nm respectively. However, in the composites, the surface plasmon bands shifted to 302 and 428nm, respectively for ZnONPs and AgNPs. The surface plasmon resonance depends on particle size, composition and dielectric constant of surrounding materials (Baba *et al*., 2014). The shifts in the surface plasmon bands for AgNPs and ZnONPs as compared to the bands in individual nanoparticles could be due to electromagnetic coupling between the nanoparticles. Electromagnetic coupling leads to an enhancement of the intense electric field which depends the distance between the nanoparticles (Tao *et al*., 2007; Chen *et al*., 2008; Liz-Marzán, 2006)

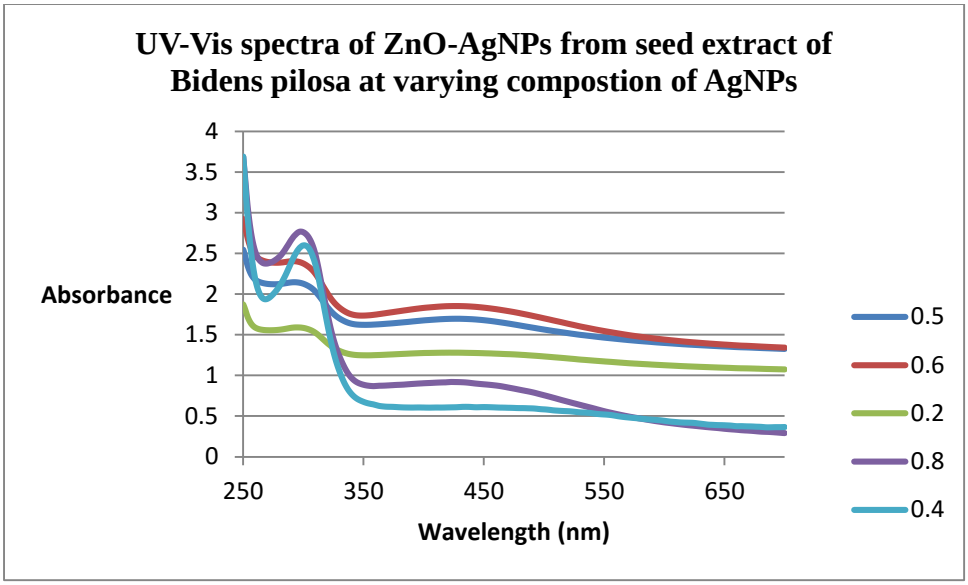

Figure 114A: UV-Vis spectra for ZnO-AgNPs from seed extract at various compositions of AgNPs 0.0, 0.2, 0.4, 0.5, 0.6, 0.8 and 1.0

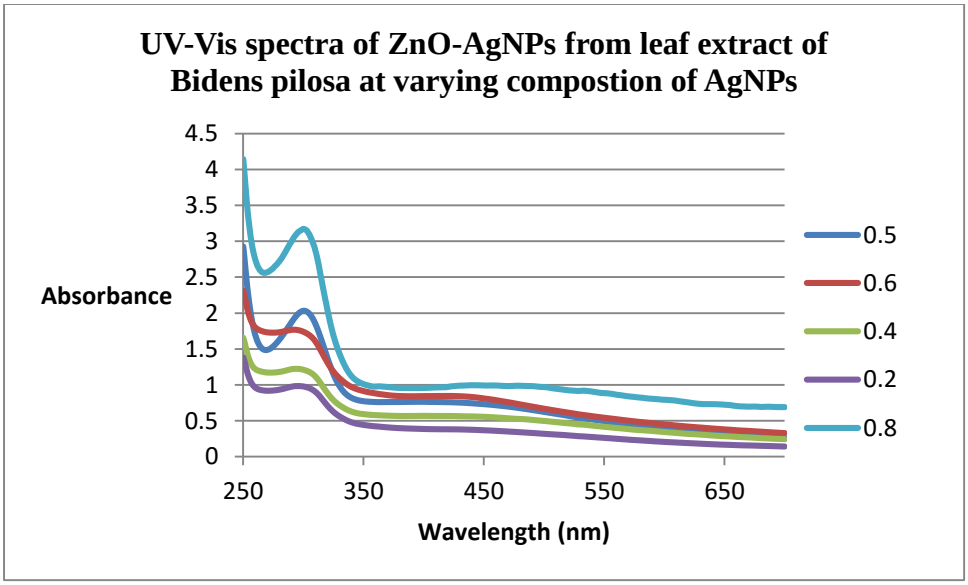

Figure 114B: UV-Vis spectra for ZnO-AgNPs from leaf extract at various compositions of AgNPs 0.0, 0.2, 0.4, 0.5, 0.6, 0.8 and 1.0

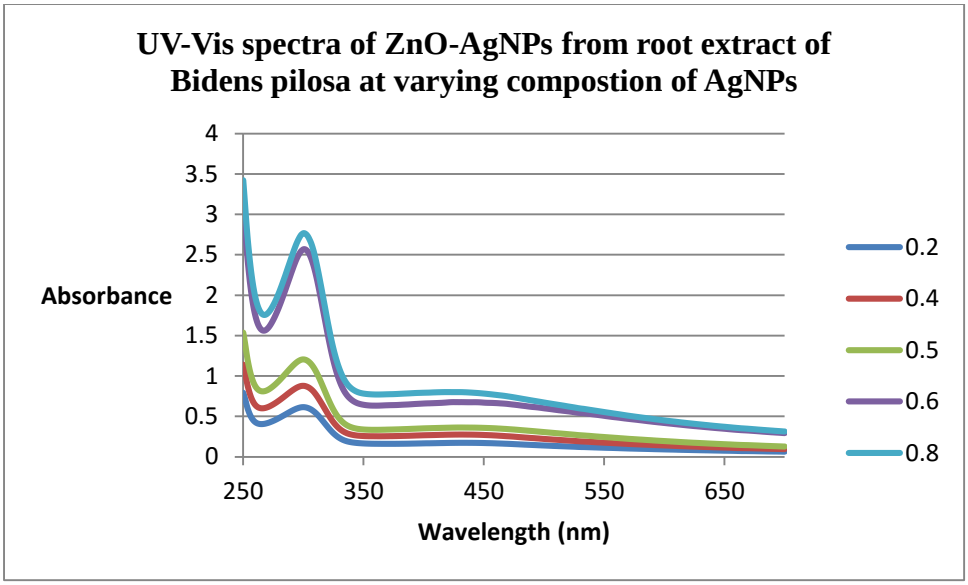

Figure 14C: UV-Vis spectra for ZnO-AgNPs from root extract at various compositions of AgNPs 0.0, 0.2, 0.4, 0.5, 0.6, 0.8 and 1.0

4.4 Characterization of AgNPs, ZnONPs and ZnO-AgNPs using Fourier Transform Infrared spectroscopy

4.4.1 FTIR spectrum for AgNPs

The IR bands obtained for the leaf extract, **Figure 15A**, include; 2772 cm^{-1} for carboxylic acid O-H stretch, 1151 cm^{-1} for C-O stretch, 912 cm^{-1} for =C-H bending and 728 cm^{-1} for aromatic C-H bending. The IR bands obtained from the AgNPs include, **Figure 15B**; 3448 cm^{-1} which corresponds to free O-H, 1560 cm^{-1} which corresponds to aromatic C=C stretch and 112 cm^{-1} which corresponds to C-O stretch.

The functional groups mainly OH and –C=C– derived from heterocyclic compounds (flavonoids) and aliphatics among others (**Section 2.2**) present in *Bidens pilosa* leaf extract and are the capping ligands of the nanoparticles. This shows that the compounds from the leaf extract cap and stabilize the AgNPs during the synthesis process.

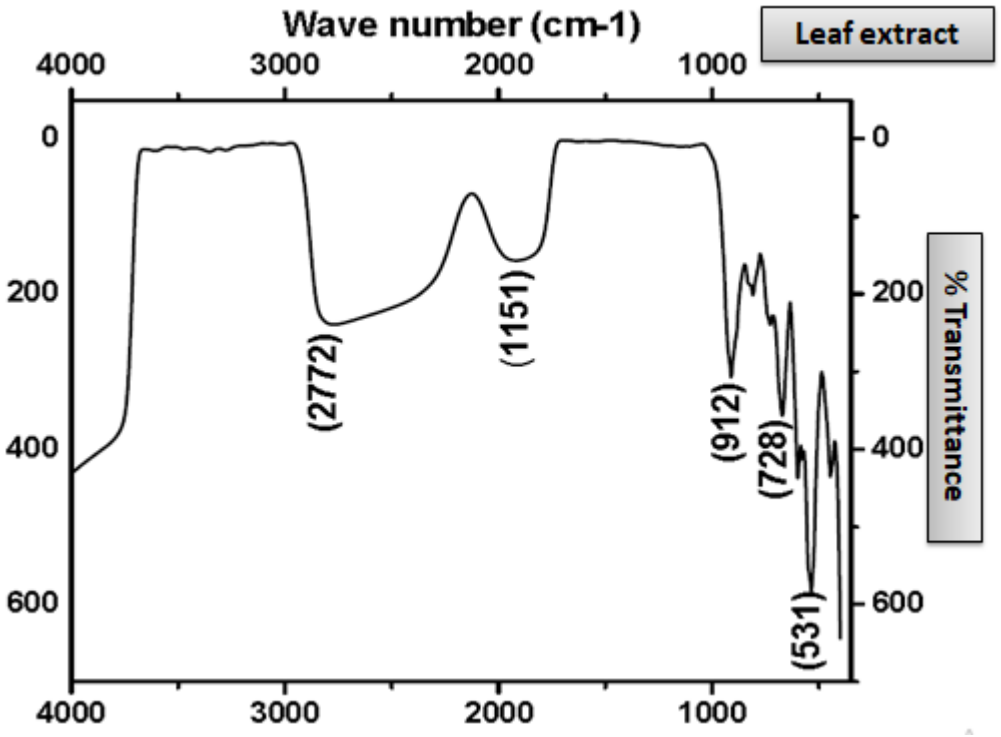

Figure 15A: IR spectra of the leaf extract

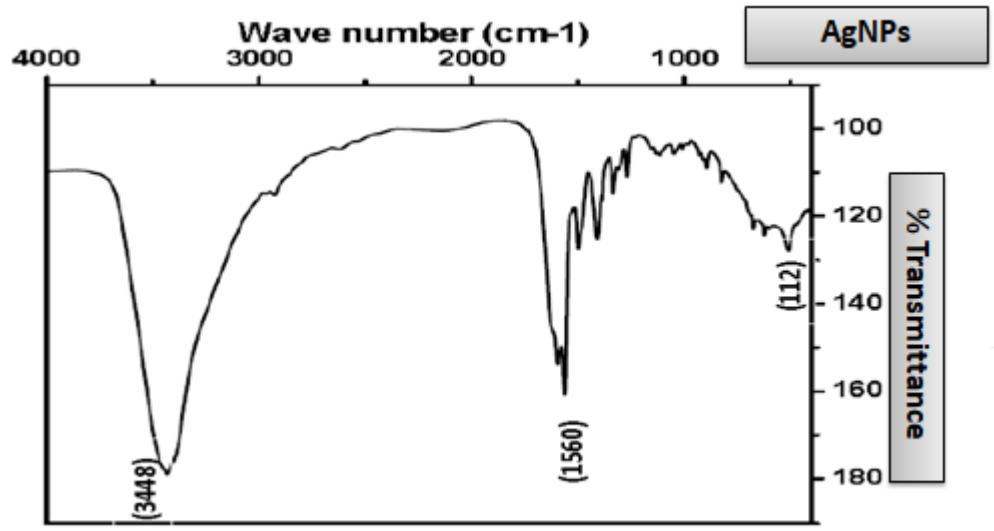

Figure 15B: Infrared spectra for leaf extract AgNPs

4.4.2 FTIR spectrum for ZnONPs

The IR bands obtained from the seed extract, **Figure 16A**, include; 2772 cm^{-1} for carboxylic acid O-H stretch, 1151 cm^{-1} for C-O stretch, 912 cm^{-1} for =C-H bending and 728 cm^{-1} for aromatic C-H bending. The bands obtained for ZnONPs, **Figure 16B**, include; 3432 cm^{-1} which corresponds to free O-H, 1559 cm^{-1} which corresponds to aromatic C=C stretch.

The functional groups mainly OH and –C=C– derived from heterocyclic compounds (flavonoids) and aliphatics among others (**Section 2.2**) present in *Bidens pilosa* seed extract and are the capping ligands of the nanoparticles. This shows that the compounds from the seed extract cap and stabilize the ZnONPs during the synthesis process.

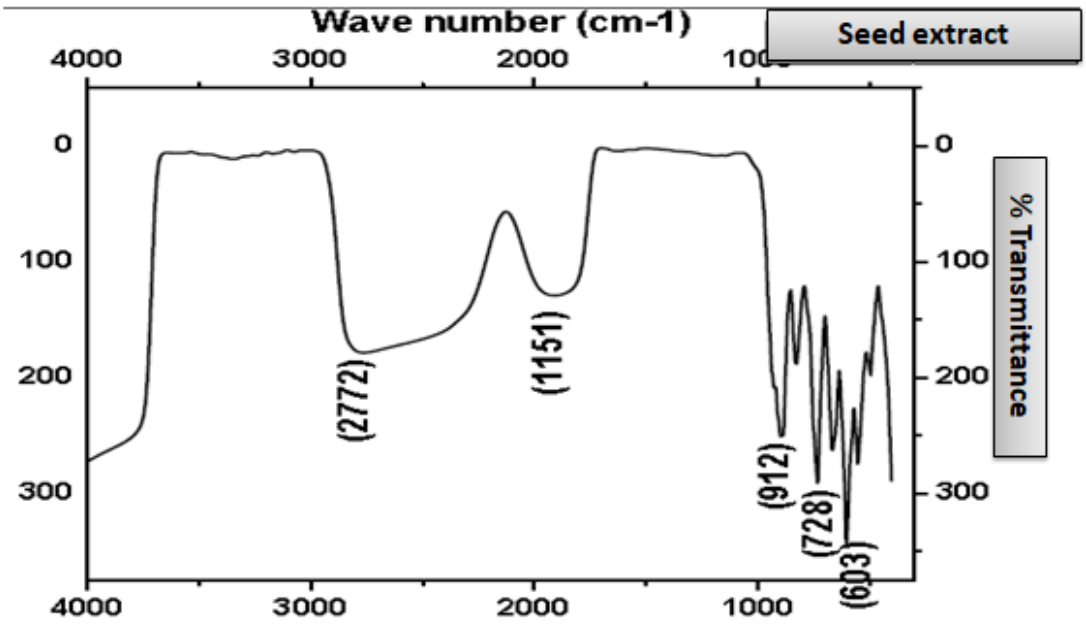

Figure 16A: IR spectra for *Bidens pilosa* seed extracts

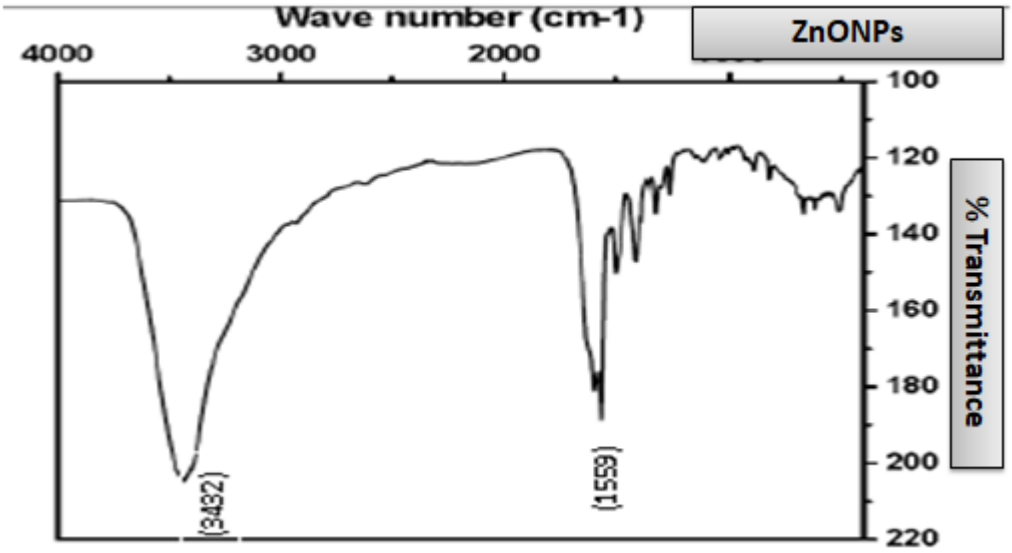

Figure 16A: Infrared spectra for seed extract ZnONPs

4.4.3FTIR spectrum for ZnO-AgNPs

The IR bands obtained from the root extract, **Figure 17A**, include; 1151 cm^{-1} for C-O stretch, 728 cm^{-1} for aromatic C-H bending and 912 cm^{-1} for =C-H bending. The bands obtained for ZnO-AgNPs, **Figure 17B**, include; 3432 cm^{-1} which corresponds to free O-H and 1564 cm^{-1} which corresponds to aromatic C=C stretch.

The functional groups mainly OH and –C=C– derived from heterocyclic compounds (flavonoids) and aliphatics among others (**Section 2.2**) present in *Bidens pilosa* root extract and are the capping ligands of the nanoparticles. This shows that the compounds from the root extract cap and stabilize the ZnO-AgNPs during the synthesis process.

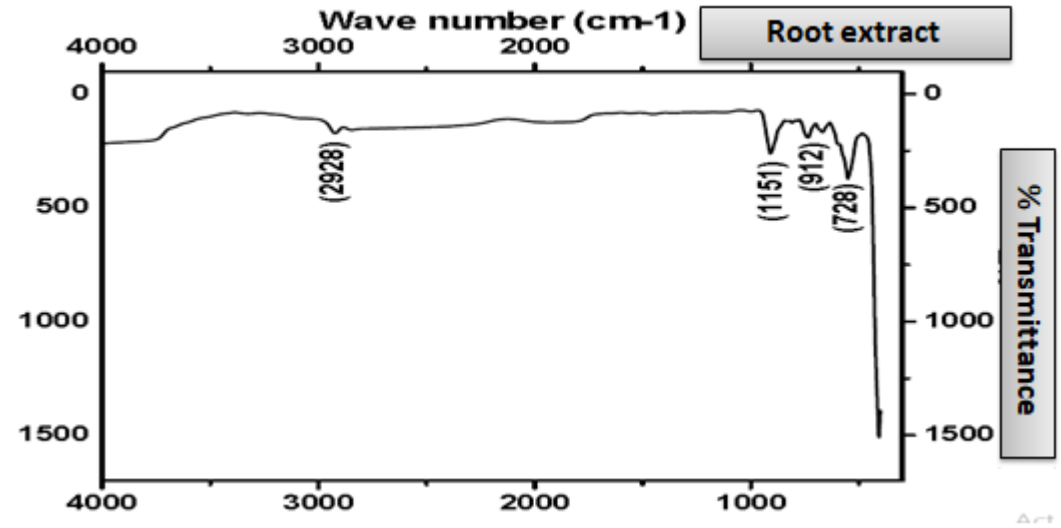

Figure 17A: IR spectrum of the root extract of *Bidens pilosa*

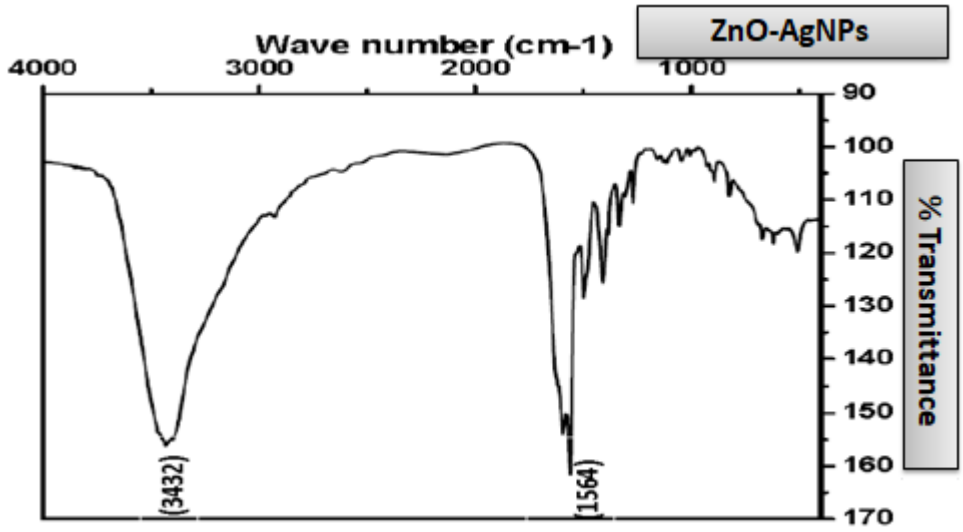

Figure 17B: Infrared spectra for root extract ZnO-AgNPs

4.5 Characterization of AgNPs, ZnONPs and ZnO-AgNPs using Raman spectroscopy

4.5.1 Raman spectrum for leaf extract AgNPs

The bands for AgNPs obtained include; 356 cm^{-1} corresponding to C-C aliphatic chains, 484 cm^{-1} corresponding to S-S bonds, 1350 cm^{-1} corresponding to carboxylate salt, 1578 cm^{-1} corresponding to aromatic ring and 2435 cm^{-1} corresponding to thiol

group, **Section 2.2**. However, no metabolite with a S-S bond and thiol functional group has been reported from the plant. The functional groups attached to the AgNPs confirm that the leaf extract contains compounds that reduce the Ag^{+} to Ag^{0} and also stabilize the AgNPs formed.

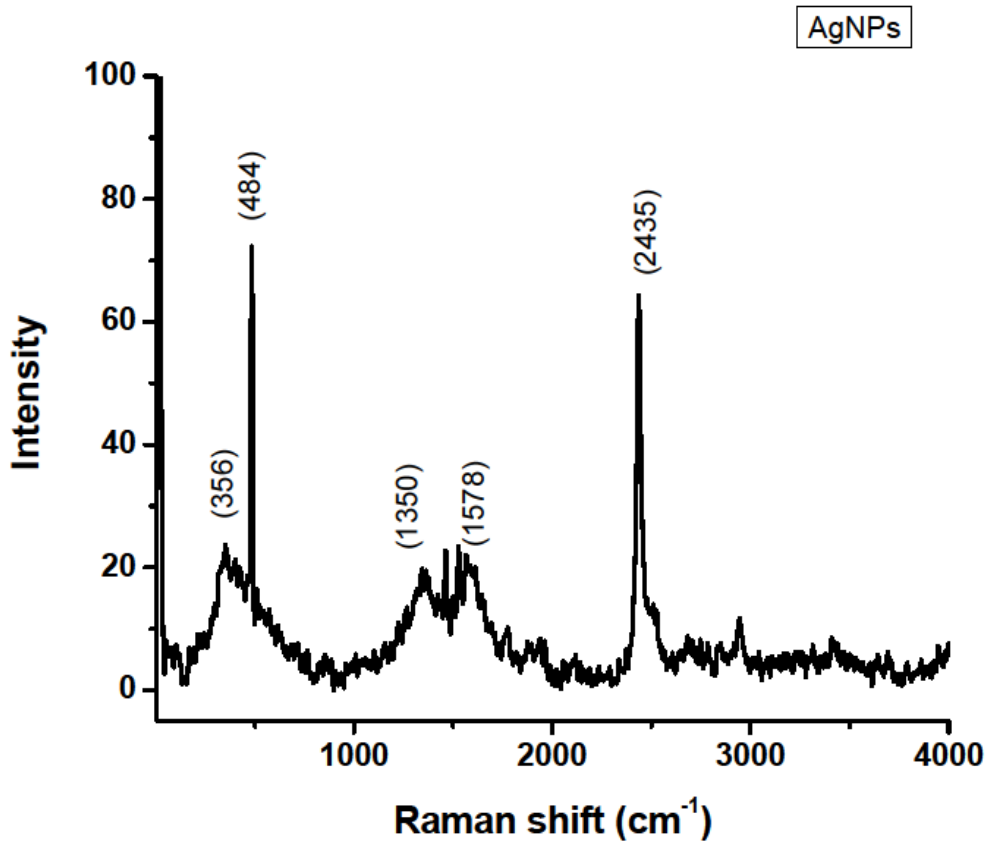

Figure 18: Raman spectrum for AgNPs

4.5.2 Raman spectrum for ZnONPs

The Raman spectrum bands for ZnONPs obtained include; 1909 cm^{-1} corresponding to C=C bond, 1253 cm^{-1} corresponding to C-C aliphatic chains vibrations, 2439 cm^{-1} corresponding to thiol group and 3419 cm^{-1} corresponding to O-H group, **Section 2.2**. The functional groups attached to the ZnONPs confirm that the seed extract contains compounds that reduce the zinc nitrate to zinc oxide nanoparticles and also stabilize the ZnONPs formed.

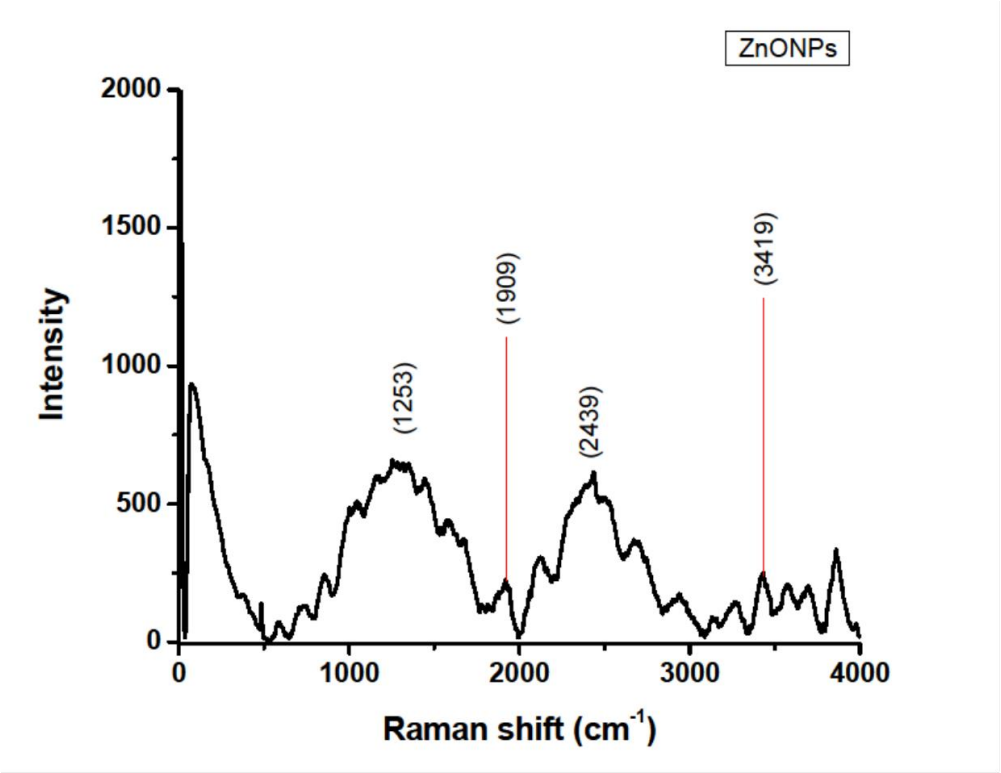

Figure 19: Raman spectrum for ZnONPs

4.5.3 Raman spectrum for ZnO-AgNPs

The bands obtained for ZnO-AgNPs include; 482 cm^{-1} corresponding to S-S bond, 1350 cm^{-1} corresponding to carboxylate salt, 1575 cm^{-1} corresponding to aromatic ring, 2432 cm^{-1} corresponding to thiol group and 2944 cm^{-1} corresponding to O-H group, **Section 2.2**. The functional groups attached to the ZnO-AgNPs confirm that the root extract contains compounds that reduce the silver nitrate and zinc nitrate to ZnO-AgNPs and also stabilize the ZnO-AgNPs formed.

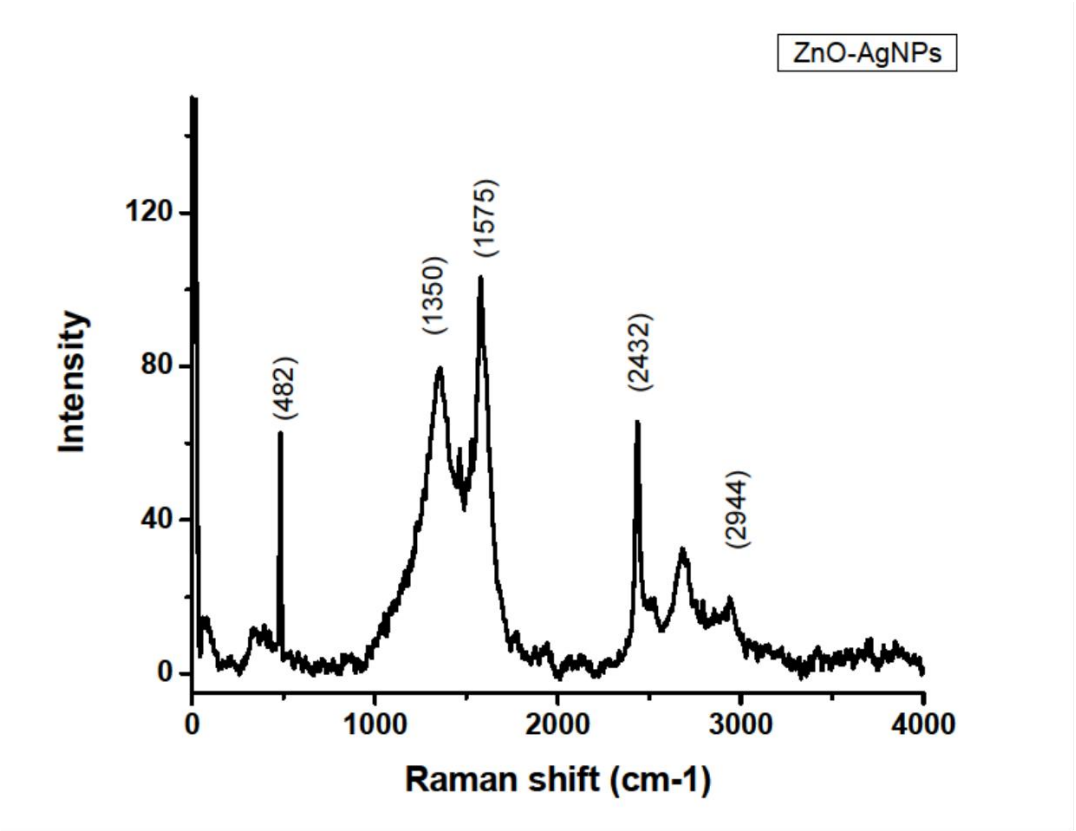

Figure 20: Raman spectrum for ZnO-AgNPs

4.6 Characterization of AgNPs, ZnONPs and ZnO-AgNPs using Transmission Electron Microscopy

4.6.1 Transmission Electron Microscopy for leaf extract AgNPs

Scanning under TEM revealed different sizes for the leaf extract AgNPs ranging from 2 – 20nm. In all the cases, the particles were spherical in nature without significant agglomeration as shown in **Figure 21A**. Energy Dispersive X-ray Spectroscopy was used to verify the presence of Ag in the sample. The curve showed two peaks of elemental silver in the silver region, **Figure 21B,** hence confirming formation of AgNPs.

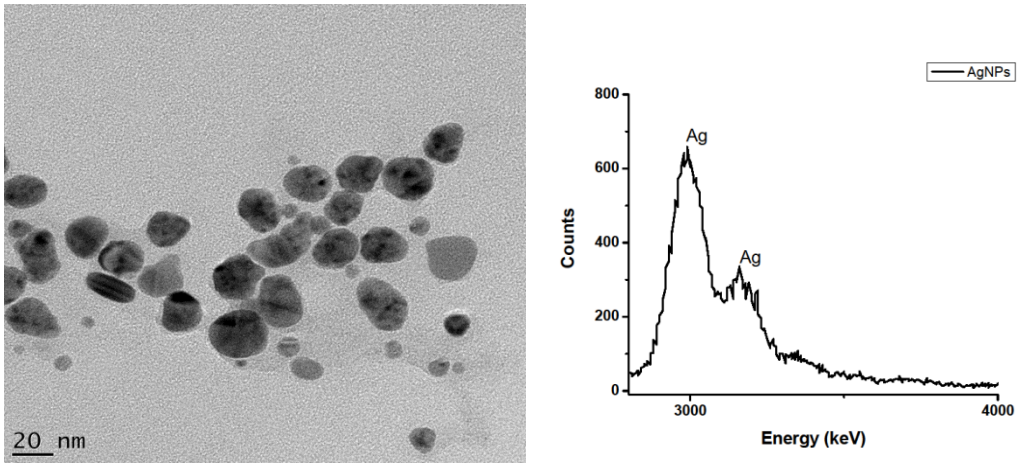

A B

Figure 21: (A) TEM image for AgNPs (B) An EDS spectrum for AgNPs

4.6.2 Transmission Electron Microscopy for seed extract ZnONPs

Scanning under TEM revealed different sizes of ZnONPs ranging from 2 – 20nm as shown in **Figure 22A**. Energy Dispersive X-ray Spectroscopy was used to verify the presence of ZnO in the sample, **Figure 22B**. The curve showed a peak of zinc nanoparticles and a peak of oxygen hence confirming formation of ZnONPs.

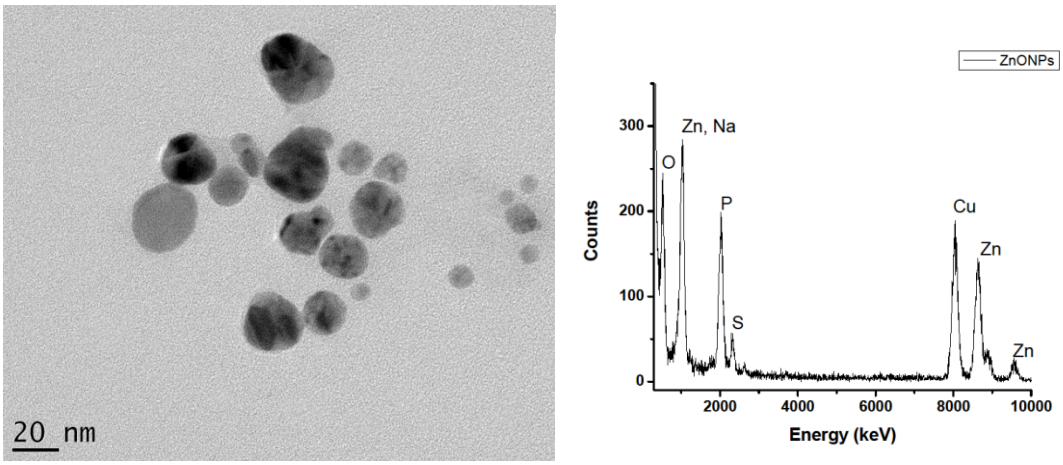

A B

Figure 22: (A) TEM image for ZnONPs (B) EDS spectrum for ZnONPs

The copper appearing in the EDX spectrum is due to the copper grid used holding the sample for analysis and the phosphorous and sulphur could be due to capping agents from the plant extract that were utilized during the synthesis of the ZnONPs

4.6.3 Transmission Electron Microscopy ZnO-AgNPs

Scanning under TEM revealed different sizes of ZnO-AgNPs produced ranging from 2 – 20nm. In all the cases, the particles were spherical in nature without significant agglomeration as shown in **Figure 23A**. Energy Dispersive X-ray Spectroscopy was used to verify the presence of ZnO and Ag in the sample **Figure 23(B)**. The curve showed three major peaks of interest that is, zinc silver and oxygen. The peak corresponding to copper is due to the copper grid used as the sample holder during the analysis.

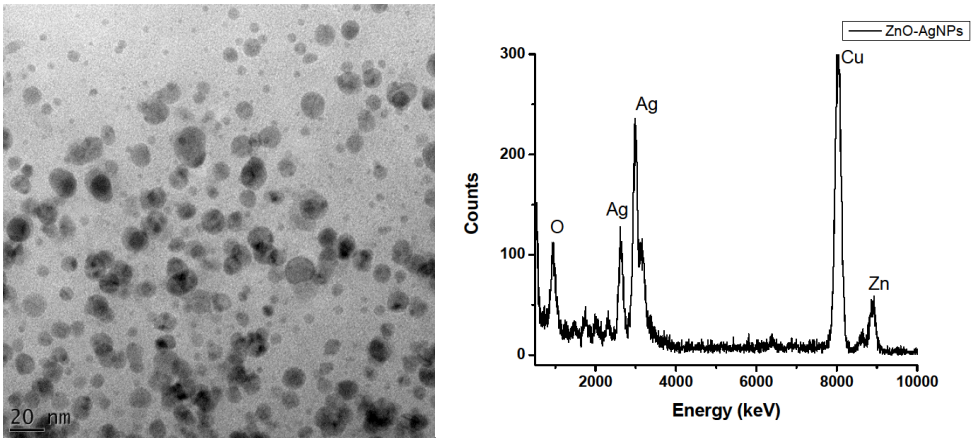

A B

Figure 23: (A) TEM image for ZnO-AgNPs (B) EDS spectrum for ZnO-AgNPs

4.7 Characterization of AgNPs, ZnONPs and ZnO-AgNPs using Scanning Electron Microscopy

4.7.1 SEM of leaf extract AgNPs

The SEM micrograph shows the leaf extract AgNPs aggregates, **Figure 24**. In this micrograph spherical nanoparticles with average mean size in the range 2-20nm were observed. The nanoparticles were not in direct contact even within the aggregates, indicating stabilization of the nanoparticles by the capping agent (Vijayakumar *et al*., 2013).

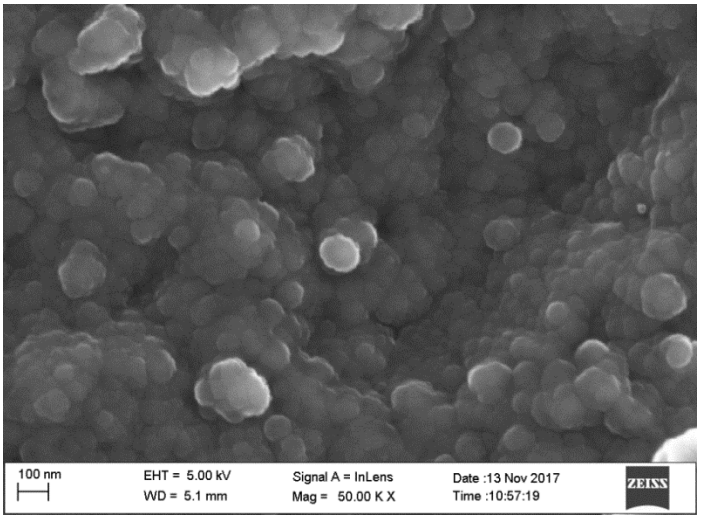

Figure 24: SEM image showing spherical AgNPs (X50,000)

4.7.2 Scanning Electron Microscopy for seed extract ZnONPs

The SEM micrograph shows seed extract ZnONPs aggregates, **Figure 25**. In this micrograph spherical nanoparticles with average mean size in the range 2-20nm were observed. The nanoparticles were not in direct contact even within the aggregates, indicating stabilization of the nanoparticles by the capping agent (Elumalai & Velmurugan, 2015)

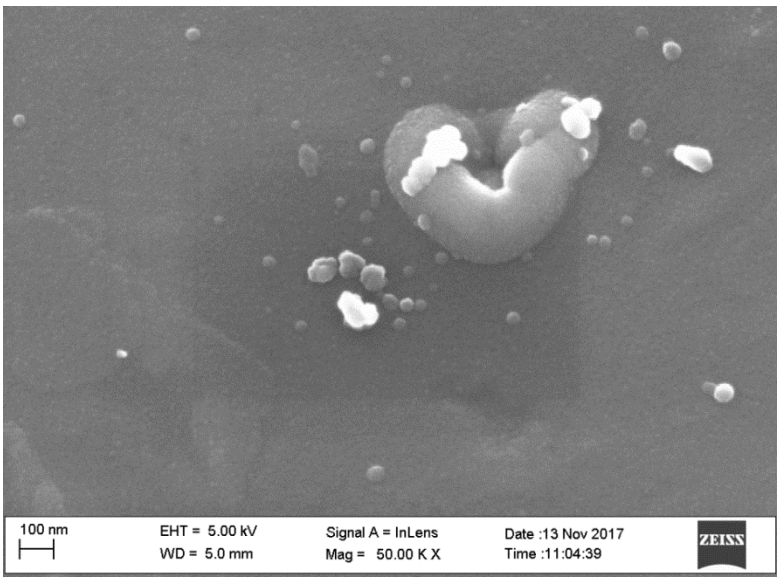

Figure 25: SEM image showing spherical ZnONPs (X50,000)

4.7.3 Scanning Electron Microscopy for root extract ZnO-AgNPs

The SEM micrograph shows root extract ZnO-AgNPs aggregates **Figure 26**. In this micrograph spherical nanoparticles with average mean size in the range 2-20nm were observed. The nanoparticles were not in direct contact even within the aggregates, indicating stabilization of the nanoparticles by the capping agent (Vijayakumar *et al*., 2013; Elumalai & Velmurugan, 2015).

.

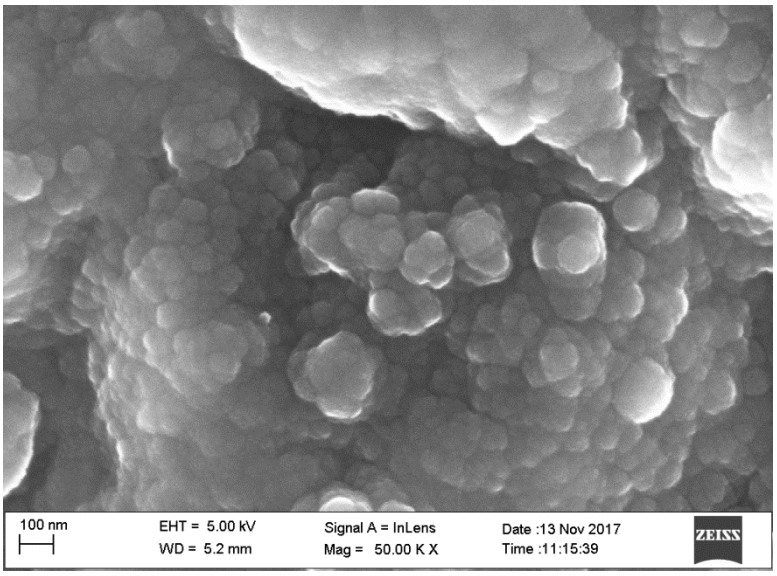

Figure 26: SEM image showing spherical ZnO-AgNPs (X50,000)

4.8 Characterization of AgNPs, ZnONPs and ZnO-AgNPs using X-ray Diffraction Spectroscopy

4.8.1 X-ray Diffraction Spectroscopy for leaf extract AgNPs

XRD analysis of the leaf extract AgNPs showed three distinct diffraction peaks at 38.05, 45.35 and 64.42°, **Figure 27,** and can be indexed 2θ of (111), (200) and (220) for the face-centered cubic silver as per the JCPDS card no. 89–3722 (Vivek *et al*., 2012). The well resolved and intense XRD pattern clearly showed that the AgNPs formed by the reduction of Ag^+ ions using *Bidens pilosa* leaf extract were crystalline in nature (Das *et al*., 2017).

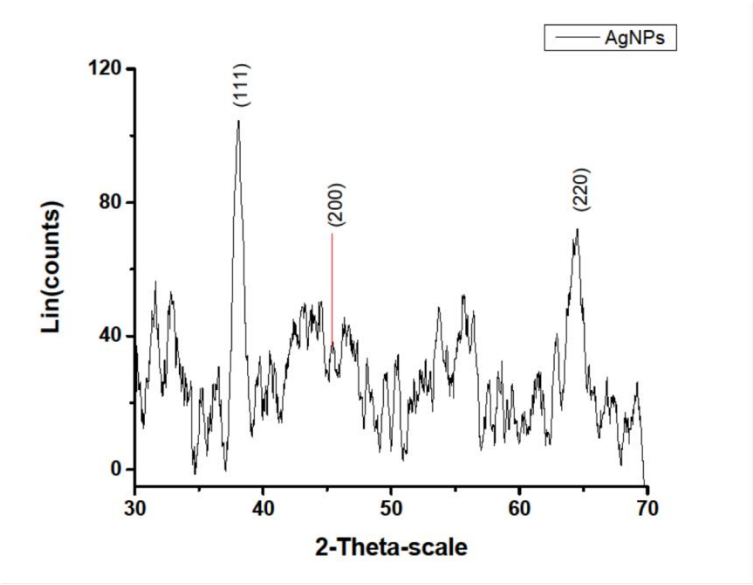

Figure 27: XRD pattern for biosynthesized AgNPs

4.8.2 X-ray Diffraction Spectroscopy for seed extract ZnONPs

The XRD pattern of bio-synthesized seed extract ZnONPs from seed extracts of *Bidens pilosa* is shown in **Figure 28**. The XRD analysis gave diffraction peaks at 30.15, 35.74, 47.16 and 56.67° corresponding to 100, 101, 102 and 110, respectively. The peaks confirm ZnO hexagonal phase as compared to JCPDS card No. 89-7102 (Rajiv *et al*., 2013; Selvarajan and Mohanasrinivasan, 2013). The well resolved and sharp peaks show that the nanoparticles are crystalline in nature (Bagabas *et al*., 2013).

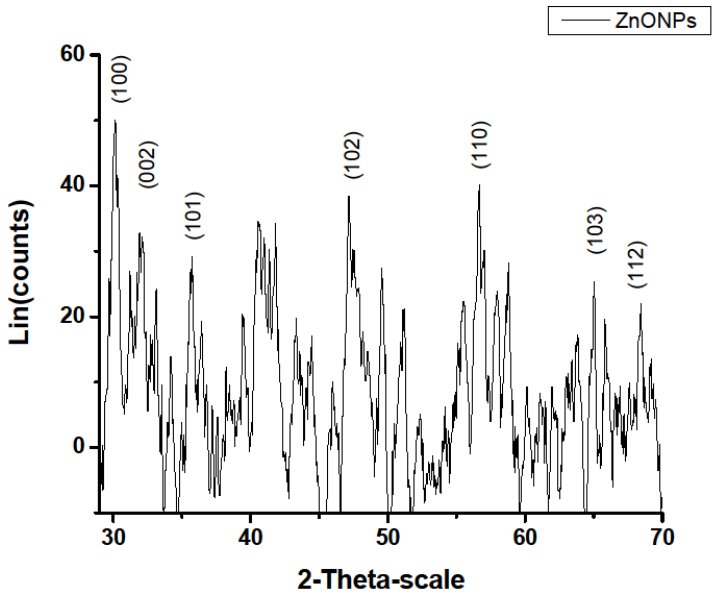

Figure 28: XRD pattern for biosynthesized ZnONPs

4.8.3 X-ray Diffraction Spectroscopy for root extract ZnO-AgNPs

XRD analysis for the root extract ZnO-AgNPs showed distinct diffraction peaks, **Figure 29**, at 38.05, 45.35 and 64.42° of (111), (200) and (220) for the face-centered cubic silver as per the JCPDS card no. 89–3722 and 30.15, 35.74, 47.16 and 56.67° corresponding to 100, 101, 102 and 110 for hexagonal ZnONPs as per JCPDS card No. 89-7102 (Rajiv *et al*., 2013; Selvarajan and Mohanasrinivasan, 2013; Vivek *et al*., 2012), respectively. The peaks confirm biosynthesis of ZnO-AgNPs from the root extracts of *Bidens pilosa*.

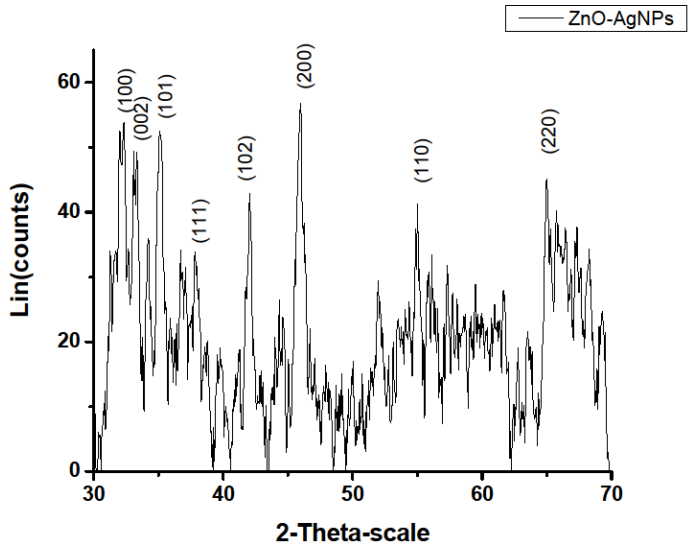

Figure 29: XRD pattern for biosynthesized ZnO-AgNPs

4.9 Characterization of AgNPs, ZnONPs and ZnO-AgNPs using Atomic Force Microscopy

4.9.1 Atomic Force Microscopy for leaf extract AgNPs

Figures 30A and 30B show two and three dimensional view of sample surface over a 24.8 x 24.8 µm scan for the leaf extract AgNPs, respectively. The atomic force microscopy is performed to identify the topological appearance of the nanoparticles.

The AFM images are also used for the analysis of the fractal behavior of the deposited and annealed films. The results depict polycrystalline with porous nature of AgNPs (Ethiraj *et al*, 2016).

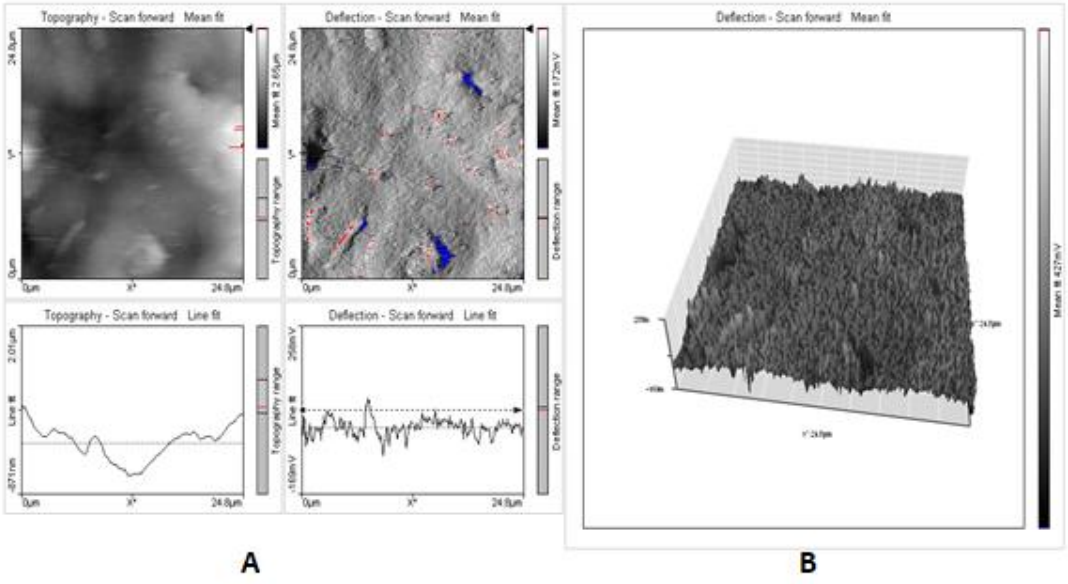

Figure 30: AFM images showing the topography of the AgNPs, (A) 2D image, (B) 3D image

4.9.2 Atomic Force Microscopy for ZnONPs

Figures 31(A) and **31(B)** show two and three dimensional view of sample surface over a 24.8 x 24.8 µm scan respectively. AFM analysis is used to show topography and roughness of nanoparticles. AFM image shows polycrystalline with porous nature of ZnONPs with capping of phytochemicals over the surface of ZnONPs (Elumalai & Velmurugan, 2015).

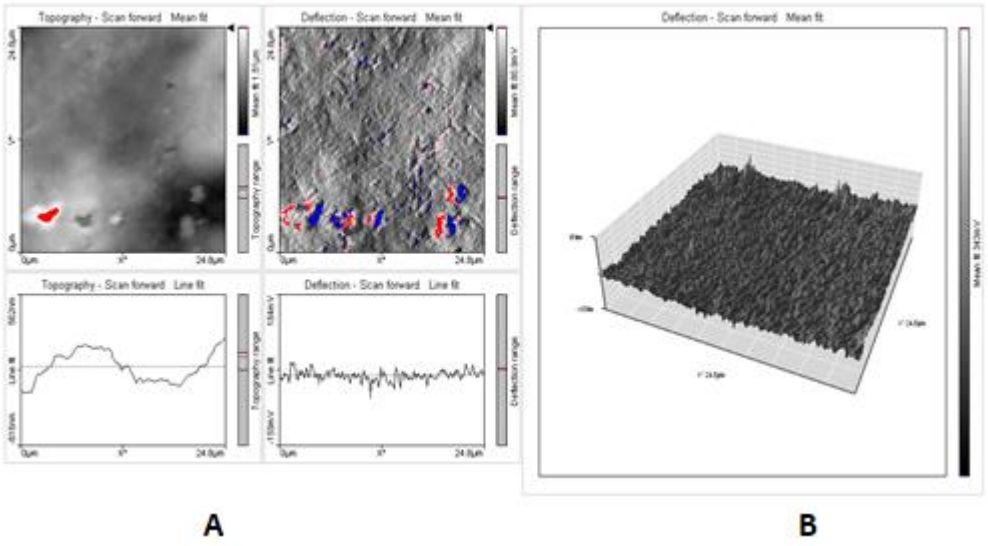

Figure 31: AFM images showing the topography of the ZnONPs, (A) 2D image, (B) 3D image

4.9.3 Atomic Force Microscopy for root extract ZnO-AgNPs

Figure 32 shows two and three dimensional view of sample surface over a 24.8 µm x 24.8 µm scan for the root extract ZnO-AgNPs. AFM analysis is used to show topography and roughness of nanoparticles. AFM image shows smooth nanoparticles with capping of phytochemicals over the surface of nanoparticles (Ethiraj *et al*, 2016).

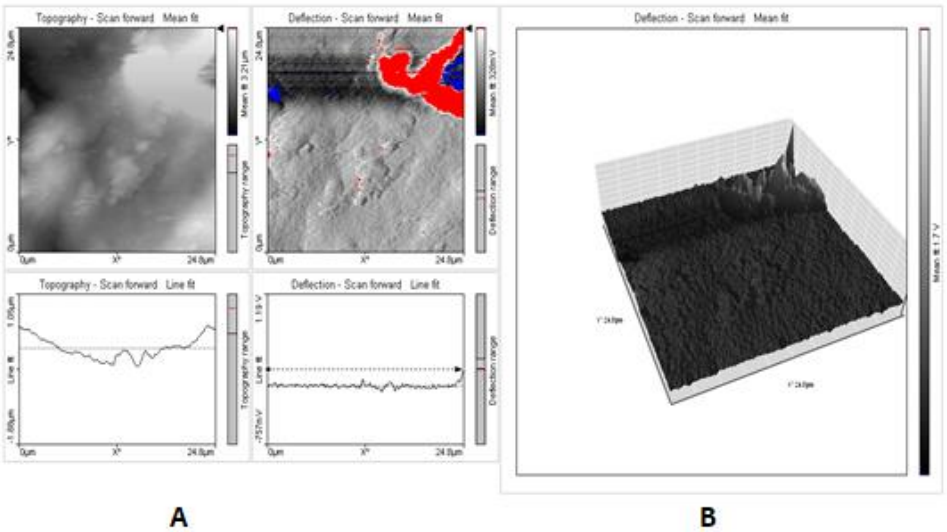

Figure 32: AFM images showing the topography of the ZnO-AgNPs, (A) 2D image, (B) 3D image

4.10 Antimicrobial activity of AgNPs, ZnONPs and ZnO-AgNPs

Metal and metal oxide nanoparticles have very small size and a high surface area to volume ratio and can closely interact with the microbial cell membranes (Ruparelia *et al*., 2008). The nanoparticles attach themselves to the cell wall and damage the cell membrane. This causes leakage of intracellular components and thus leading to cell death (Sondi and Salopek-Sondi, 2004; Ruparelia *et al*., 2008; Ibrahim, 2015). More so the nanoparticles permeate the cell wall and denature the DNA, proteins and lipids there by the cell losing it replication ability (Ibrahim, 2015; Okafor *et al*., 2013).

AgNPs release Ag+ into the cell. The Ag+ denatures the DNA of the cell by reacting with sulphur and phosphorous and also react with the thiol groups of the enzymes in the cell there by deactivating them (Matsumura *et al*., 2003). This eventually leads to cell death (Ruparelia *et al*., 2008; Hatchett and Henry, 1996). AgNPs when attached to the cell membrane release free radicals which cause membrane disruption (Prabhu and Poulose, 2012).

ZnONPs produce reactive oxygen species such as hydroxyl radicals, superoxide anion and hydrogen peroxide (Okafor *et al*., 2013). These species damage cellular components such as DNA, proteins and lipids and eventually lead to cell death (Raghupathi *et al*., 2011)

In the testing of antimicrobial activity of the nanoparticles, two bacteria and one fungus were used. The gram positive bacterium used was *S. aureus* and the gram negative bacterium used was *E. coli*. The fungus used was *C. albicans*. In all the tests carried out, clear inhibition zones were observed in all the nanoparticle compositions used, as shown in **Figures 33 - 35 (A – C)**, thus indicating inhibition of microbial growth by the nanoparticles.

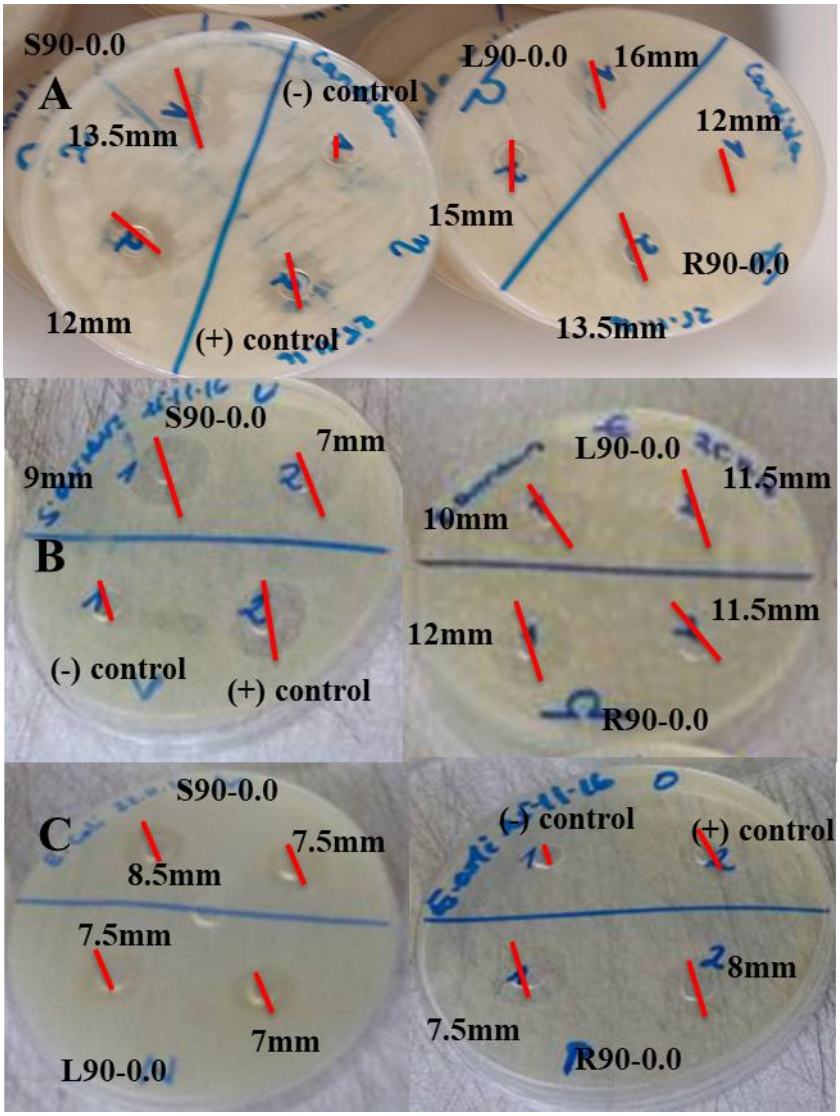

Figure 33: Zones of inhibition for *C. albicans* (A) *S. aureus* (B) and *E. coli*(C), for the ZnONPs

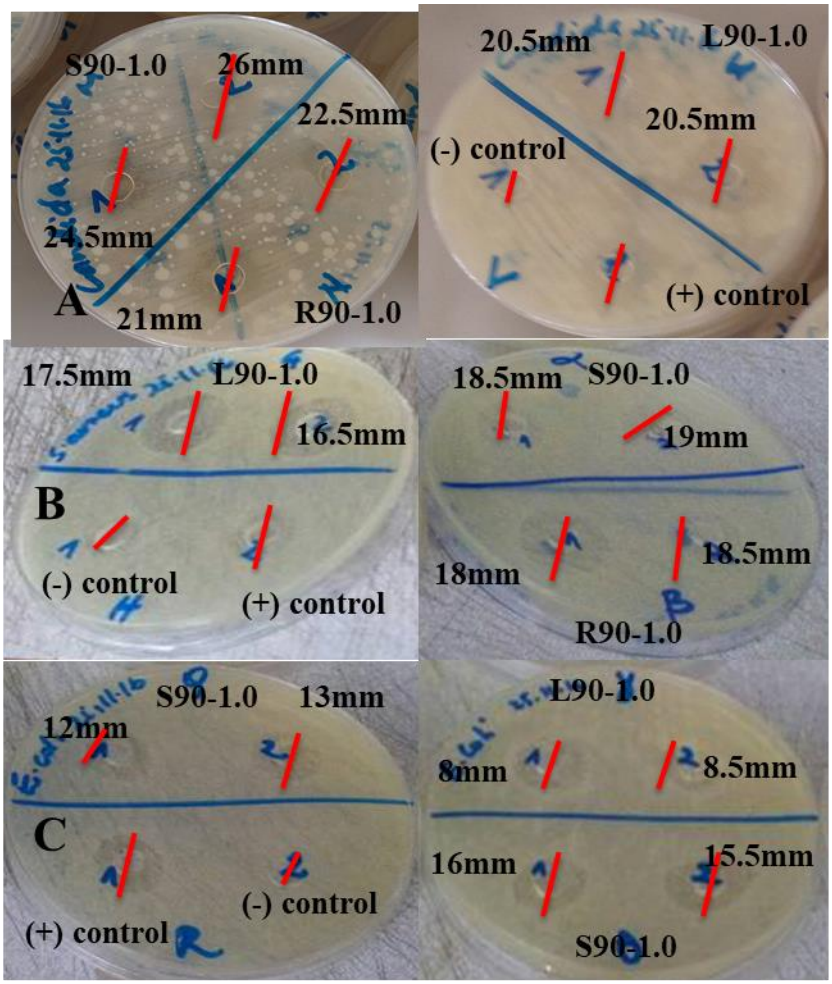

Figure 34: Zones of inhibition for *C. albicans* (A) *S. aureus* (B) and *E. coli*(C), for the AgNPs nanoparticles

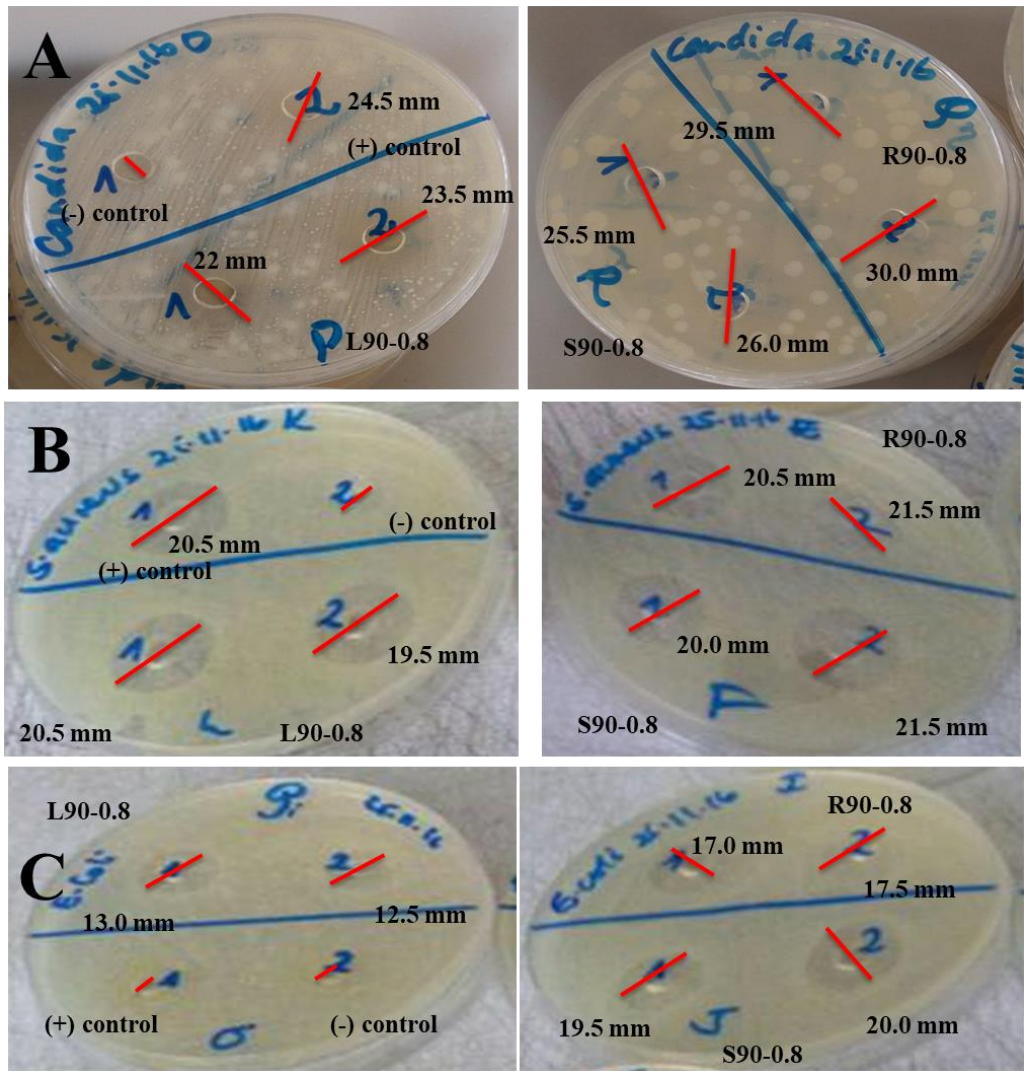

Figure 35: Zones of inhibition for *C. albicans* (A) *S. aureus* (B) and *E. coli*(C), for the ZnO-AgNPs.

The zones of inhibition were recorded and tabulated in **Appendix B Table 7** and it was observed the composition of 0.8 AgNPs gave the highest values of zones of inhibition as shown in **Figure 36A - C**. This implies that the composition of 0.8 Ag/0.2 ZnO ZnO-AgNPs had the highest antimicrobial activity.

The positive control used for *E. coli* and *S. aureus* was the antibiotic chloramphenicol (1000 ppm). In the case of *E, coli* there were no zones of inhibition identified. This implies that the culture of *E. coli* that was used was resistant to the positive control. For the case of *S. aureus*, the positive control gave a zone of inhibition of 26.25 $\pm$ 0.17mm. The positive control used for *C. albicans* was Fluconazole (1000 ppm) and gave an average diameter of zone of inhibition of 24.75 $\pm$ 0.17mm. The negative

control used for all the microorganisms was distilled water since it was used to dissolve the nanoparticles. The negative control did not show any zones of inhibition for all the microorganisms.

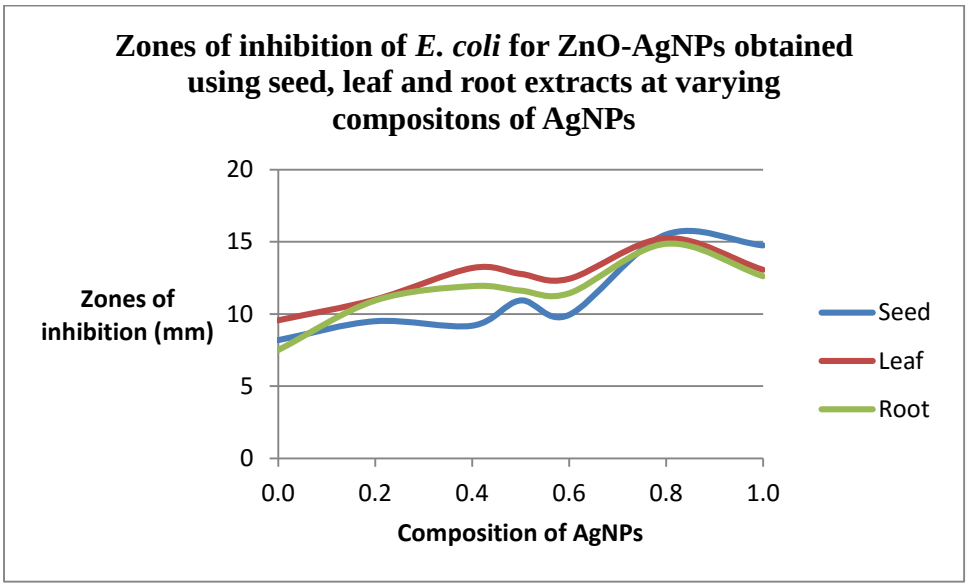

Figure: 36A: Mean diameters of zones of inhibition of *E. coli* by nanoparticles from extracts against composition of AgNPs of 0.0, 0.2, 0.4, 0.5, 0.6, 0.8 and 1.0

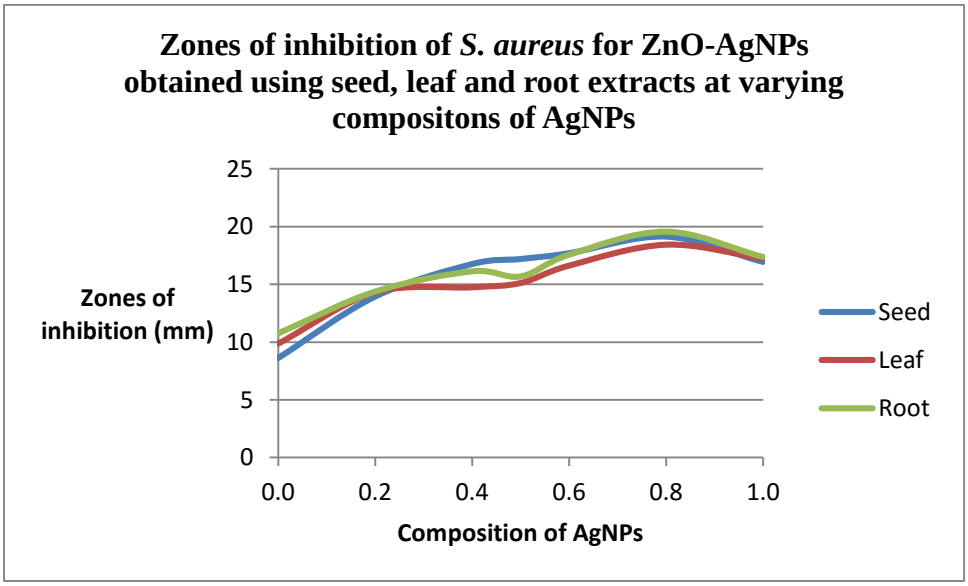

Figure: 36B: Mean diameters of zones of inhibition of *S. aureus* by nanoparticles from extracts against composition of AgNPs of 0.0, 0.2, 0.4, 0.5, 0.6, 0.8 and 1.0

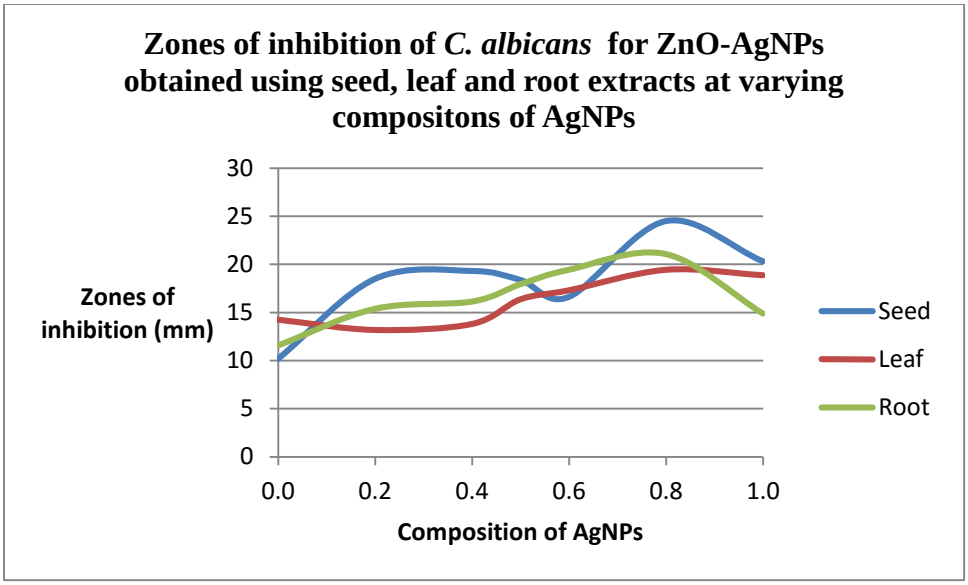

Figure: 36C: Mean diameters of zones of inhibition of *C. albicans* by nanoparticles from extracts against composition of AgNPs of 0.0, 0.2, 0.4, 0.5, 0.6, 0.8 and 1.0

The nanoparticles that gave the highest antimicrobial activity were 0.2 ZnO/0.8 Ag ZnO-AgNPs obtained using leaf extract at 90^{o}C (L90-0.8), 0.2 ZnO/0.8 Ag ZnO-AgNPs obtained using seed extract at 90^{o}C (S90-0.8) and 0.2 ZnO/0.8 Ag ZnO-AgNPs obtained using root extract at 90^{o}C (R90-0.8). The percentage enhancement in microbial inhibition of the extracts by the nanoparticles with the optimal antimicrobial activity is shown in **Table 3** below.

From the **Table 3** the ZnO-AgNPs improved the antimicrobial activity of the extracts by over 50%. This shows that nanotization of bioactive compounds improves on their efficacy.

Table 3: Percentage enhancement of zone of inhibition of extracts by the ZnO-AgNPs

Type of inhibiting material	Concentration of inhibiting material (ppm)	Microbe	Diameter of zone of inhibition	Percentage enhancement of inhibition (%)
Seed extract	8000	*E. coli*	7.25	
		S. aureus	8.5	
		C. albicans	10.75	
Leaf extract	8000	*E. coli*	7.6	
		S. aureus	8.5	
		C. albicans	11.0	
Root extract	8000	*E. coli*	7.3	
		S. aureus	8.25	
		C. albicans	10.25	
S90-0.8 (seed originating ZnO-AgNPs of 0.8AgNPs and 0.2 ZnONPs)	100	*E. coli*	15.5	113.79
		S. aureus	19.13	125.06
		C. albicans	24.5	127.91
L90-0.8 (leaf originating ZnO-AgNPs of 0.8AgNPs and 0.2 ZnONPs)	100	*E. coli*	15.25	100.66
		S. aureus	18.44	116.94
		C. albicans	19.44	76.73
R90-0.8 (root originating ZnO-AgNPs of 0.8AgNPs and 0.2 ZnONPs)	100	*E. coli*	14.88	103.84
		S. aureus	19.56	137.09
		C. albicans	21.06	105.46

From the above results, the nanoparticles that exhibited highest antimicrobial activity were used to determine their Minimum Inhibition Concentration (MIC). MIC is the

lowest concentration of antimicrobial agent that completely inhibits growth of the microorganism in the tubes or microdilution wells as detected by the naked eye (Balouiri *et al*., 2016). The MIC was determined to identify the lowest effective concentration of the three types of nanoparticles against *E. coli*, *S. aureus* and *C. albicans*. The results for MIC are as shown in **Table 4** below.

According to **Table 4**, S90-0.8 and L90-0.8 show a MIC of 10 ppm for *E. coli* and 1ppmfor *S. aureus* and *C. albicans.* R90-0.8 shows a MIC of 1ppmfor *E. coli, S. aureus* and *C. albicans*. This implies that R90-0.8 has the lowest concentration for MIC for all the three tested microorganisms compared to S90-0.8 and L90-0.8.

Table 4: Minimum Inhibition Concentrations for S90-0.8, L90-0.8 and R90-0.8 nanoparticles

Microorganism	MIC (ppm)		
	S90-0.8	L90-0.8	R90-0.8
E. coli	10	10	1
S. aureus	1	1	1
C. albicans	1	1	1

From the above analysis only the silver nanoparticles obtained using leaf extract, zinc oxide nanoparticles obtained using seed extract and the zinc oxide-silver nanocomposite obtained using the root extract were characterized using TEM, EDS, SEM, FTIR and XRD methods.

4.11 Formation of an antiseptic

The antiseptic formed was of yellowish-brown colour as shown in **Figure 37**.

Figure 37: Hand sanitizing antiseptic containing ZnO-AgNPs as active ingredient

4.11.1 Percentage composition of the antiseptic (%w/w)

The percentage composition of the components of the antiseptic was obtained from **Equation (5)** below.

$$\%composition\ of\ component = \frac{Mass\ of\ component}{\text{Mass of the antiseptic}} \text{ X } 100 \quad (5)$$

The composition of the various components in the antiseptic is shown in **Table 5** below.

Table 5: Percentage composition (%w/w) of the different components in the antiseptic

Component	Mass (g)	Composition (%w/w)
Deionized water	77.10	88.52
Guar gum (gelling agent)	0.70	0.80
α-tocopherol (emollient)	2.00	2.30
ZnO-AgNPs (active ingredient)	0.10	0.11
Glycerin (humectant)	7.00	8.04
Fragrance	0.20	0.23
Total	87.10	100.00

4.11.2 Antimicrobial activity of the antiseptic

In the testing of antimicrobial activity of the antiseptic, two bacteria and one fungus were used. The Gram positive bacteria used was *S. aureus* and the Gram negative bacteria used was *E. coli*. The fungus used was *C. albicans*. In all the tests carried out, clear halos were observed as shown in **Figure 38**, thus indicating inhibition of microbial growth by the antiseptic. The values of zones of inhibition were 14mm for *E. coli*, 20.5mm for *S. aureus* and 24.5mm for *C. albicans*. These values for the zones of inhibition indicate that the hand sanitizer that has been made has antimicrobial activity.

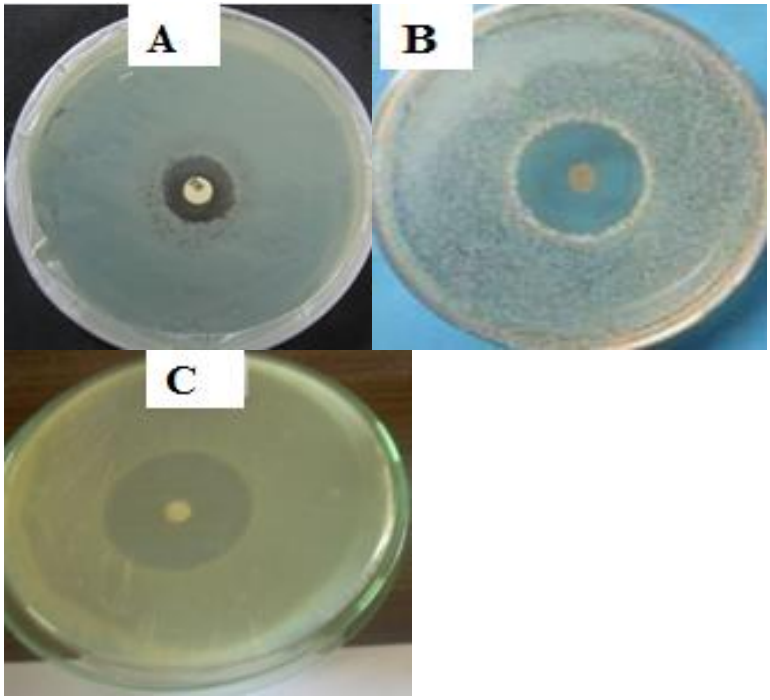

Figure 38: Zones of inhibition for (A) *E. coli*, (B) *S. aureus* and (C) *C. albicans* by the hand sanitizing antiseptic formed.

CHAPTER FIVE: CONCLUSION AND RECOMMENDATIONS

5.1 Conclusion

In this study AgNPs, ZnONPs and ZnO-AgNPs of the seed, leaf and root extracts of *Bidens pilosa* were synthesized. The nanoparticles were characterized using a number of techniques. In addition the antimicrobial activities of the nanoparticles were determined and antiseptic from the most active nanoparticles was formulated. The conclusions drawn from this study are:

1. AgNPs, ZnONPs and ZnO-AgNPs were synthesized using the seed, leaf and root extracts of *Bidens pilosa*. The seed extract gave the highest yield for ZnONPs; the leaf extract gave the highest yield for AgNPs while the root extract gave the highest yield for the ZnO-AgNPs.
2. The characterization of the synthesized AgNPs, ZnONPs and ZnO-AgNPs was successful. UV-Visible spectra gave the surface plasmon band for AgNPs at around 410nm and ZnONPs at around 370nm. For the ZnO-AgNPs two bands were obtained at 302 and 438nm for ZnONPs and AgNPs respectively. FT-IR and Raman spectra of the nanoparticles revealed the presence of functional groups O-H, C=C, C-H aromatic, and =C–H which were responsible for reduction and stabilization of the nanoparticles. The particles were found to have average mean size of 2-20nm and were spherical in shape without significant agglomeration as revealed from the SEM and TEM analysis. EDX spectrum revealed the strong signal in the silver region confirming the presence of Ag and in the zinc region confirming the presence of ZnO. The synthesized nanoparticles exhibited face–centered cubic crystals as demonstrated from XRD studies.
3. The results confirmed that in the medium treated with AgNPs, ZnONPs and ZnO-AgNPs, *E.coli*, *S. aureus* and *C. albicans* growth was inhibited. The ZnO-AgNPs with composition of 0.8 Ag/ 0.2 ZnO gave the highest antimicrobial activity regardless of the extract used. From the ZnO-AgNPs of the three extracts, those originating from the root extract showed the lowest Minimum Inhibition Concentration.

4. The root extract ZnO-AgNPs (0.2:0.8) were used as active ingredients to formulate a hand sanitizing antiseptic. The antiseptic formed exhibited strong antimicrobial activity.

5.2 Recommendations

The recommendations of this study are:

1. Nanoparticles of pure compounds of this plant (*Bidens pilosa*) to be synthesized and their antimicrobial activity assayed
2. In this study, antimicrobial activity was only determined for three species and it is good if they are tested against a battery of microbes
3. This research recommends the standardization of the antiseptic and its toxicity determined

APPENDICES

Appendix A

Table 6: Mass and percentage yield of silver and zinc oxide nanoparticles synthesized using different parts of *Bidens pilosa*.

Sample code	Volume of Zinc nitrate (ml)	Volume of silver nitrate (ml)	Expected mass (g)	Actual mass (g)	Percentage yield	Temperature (°C)
S25-0.0	80.0	0.0	0.00648	0.00524	80.9	25
S45-0.0	80.0	0.0	0.00648	0.00536	82.7	45
S65-0.0	80.0	0.0	0.00648	0.00572	88.3	65
S90-0.0	80.0	0.0	0.00648	0.00608	93.8	90
S25-0.2	64.0	16.0	0.00691	0.00508	73.5	25
S45-0.2	64.0	16.0	0.00691	0.00532	77.0	45
S65-0.2	64.0	16.0	0.00691	0.00516	74.7	65
S90-0.2	64.0	16.0	0.00691	0.00592	85.7	90
S25-0.4	48.0	32.0	0.00734	0.00552	75.2	25
S45-0.4	48.0	32.0	0.00734	0.00568	77.4	45
S65-0.4	48.0	32.0	0.00734	0.00588	80.1	65
S90-0.4	48.0	32.0	0.00734	0.00636	86.6	90
S25-0.5	40.0	40.0	0.00756	0.00556	73.6	25
S45-0.5	40.0	40.0	0.00756	0.00576	76.2	45
S65-0.5	40.0	40.0	0.00756	0.00608	80.5	65
S90-0.5	40.0	40.0	0.00756	0.00652	86.3	90
S25-0.6	32.0	48.0	0.00777	0.00544	70.0	25
S45-0.6	32.0	48.0	0.00777	0.00560	72.1	45
S65-0.6	32.0	48.0	0.00777	0.00592	76.2	65
S90-0.6	32.0	48.0	0.00777	0.00668	86.0	90
S25-0.8	16.0	64.0	0.00820	0.00596	72.7	25
S45-0.8	16.0	64.0	0.00820	0.00624	76.1	45
S65-0.8	16.0	64.0	0.00820	0.00644	78.5	65
S90-0.8	16.0	64.0	0.00820	0.00748	91.2	90
S25-1.0	0.0	80.0	0.00863	0.00636	73.7	25
S45-1.0	0.0	80.0	0.00863	0.00704	81.6	45
S65-1.0	0.0	80.0	0.00863	0.00728	84.4	65
S90-1.0	0.0	80.0	0.00863	0.00780	90.4	90
L25-0.0	80.0	0.0	0.00648	0.00500	77.2	25
L45-0.0	80.0	0.0	0.00648	0.00520	80.2	45
L65-0.0	80.0	0.0	0.00648	0.00536	82.7	65

Sample code	Volume of Zinc nitrate (ml)	Volume of silver nitrate (ml)	Expected mass (g)	Actual mass (g)	Percentage yield	Temperature (^{o}C)
L90-0.0	80.0	0.0	0.00648	0.00588	90.7	90
L25-0.2	64.0	16.0	0.00691	0.00528	76.4	25
L45-0.2	64.0	16.0	0.00691	0.00576	83.4	45
L65-0.2	64.0	16.0	0.00691	0.00568	82.2	65
L90-0.2	64.0	16.0	0.00691	0.00612	88.6	90
L25-0.4	48.0	32.0	0.00734	0.00552	75.2	25
L45-0.4	48.0	32.0	0.00734	0.00568	77.4	45
L65-0.4	48.0	32.0	0.00734	0.00588	80.1	65
L90-0.4	48.0	32.0	0.00734	0.00652	88.8	90
L25-0.5	40.0	40.0	0.00756	0.00552	73.1	25
L45-0.5	40.0	40.0	0.00756	0.00560	74.1	45
L65-0.5	40.0	40.0	0.00756	0.00616	81.5	65
L90-0.5	40.0	40.0	0.00756	0.00676	89.5	90
L25-0.6	32.0	48.0	0.00777	0.00596	76.7	25
L45-0.6	32.0	48.0	0.00777	0.00648	83.4	45
L65-0.6	32.0	48.0	0.00777	0.00660	84.9	65
L90-0.6	32.0	48.0	0.00777	0.00672	86.5	90
L25-0.8	16.0	64.0	0.00820	0.00680	82.9	25
L45-0.8	16.0	64.0	0.00820	0.00692	84.4	45
L65-0.8	16.0	64.0	0.00820	0.00728	88.8	65
L90-0.8	16.0	64.0	0.00820	0.00748	91.2	90
L25-1.0	0.0	80.0	0.00863	0.00660	76.5	25
L45-1.0	0.0	80.0	0.00863	0.00712	82.5	45
L65-1.0	0.0	80.0	0.00863	0.00752	87.1	65
L90-1.0	0.0	80.0	0.00863	0.00796	92.2	90
R25-0.0	80.0	0.0	0.00648	0.00476	73.5	25
R45-0.0	80.0	0.0	0.00648	0.00520	80.2	45
R65-0.0	80.0	0.0	0.00648	0.00524	80.9	65
R90-0.0	80.0	0.0	0.00648	0.00588	90.7	90
R25-0.2	64.0	16.0	0.00691	0.00504	72.9	25
R45-0.2	64.0	16.0	0.00691	0.00512	74.1	45
R65-0.2	64.0	16.0	0.00691	0.00540	78.1	65
R90-0.2	64.0	16.0	0.00691	0.00604	87.4	90
R25-0.4	48.0	32.0	0.00734	0.00528	71.9	25
R45-0.4	48.0	32.0	0.00734	0.00564	76.8	45
R65-0.4	48.0	32.0	0.00734	0.00592	80.7	65
R90-0.4	48.0	32.0	0.00734	0.00648	88.3	90
R25-0.5	40.0	40.0	0.00756	0.00576	76.2	25

Sample code	Volume of Zinc nitrate (ml)	Volume of silver nitrate (ml)	Expected mass (g)	Actual mass (g)	Percentage yield	Temperature (^{o}C)
R45-0.5	40.0	40.0	0.00756	0.00612	81.0	45
R65-0.5	40.0	40.0	0.00756	0.00656	86.8	65
R90-0.5	40.0	40.0	0.00756	0.00684	90.5	90
R25-0.6	32.0	48.0	0.00777	0.00656	84.4	25
R45-0.6	32.0	48.0	0.00777	0.00668	86.0	45
R65-0.6	32.0	48.0	0.00777	0.00636	81.9	65
R90-0.6	32.0	48.0	0.00777	0.00716	92.1	90
R25-0.8	16.0	64.0	0.00820	0.00584	71.2	25
R45-0.8	16.0	64.0	0.00820	0.00604	73.7	45
R90-0.8	16.0	64.0	0.00820	0.00652	79.5	65
R65-0.8	16.0	64.0	0.00820	0.00724	88.3	90
R25-1.0	0.0	80.0	0.00863	0.00636	73.7	25
R45-1.0	0.0	80.0	0.00863	0.00676	78.3	45
R65-1.0	0.0	80.0	0.00863	0.00716	83.0	65
R90-1.0	0.0	80.0	0.00863	0.00756	87.6	90

Appendix B

Table 7: Zones of inhibition for the synthesized nanoparticles on *E. coli, S. aureus* and *C. albicans*

Sample	Sample code	Composition of ZnO-AgNPs	*E. coli*		*S. aureus*		*C. albicans*	
Positive control	+		0	0	26	26	25	24.5
Negative control	-		0	0	0	0	0	0
Seed extract			7	7.5	8.5	8.5	10.5	11
Leaf extract			7.5	7.7	8	9	11	11
Root extract			6.9	7.7	8.5	8	11	11.5
A	S25-0.0	0.0	8	7.5	7	8.5	8.5	10
H	S45-0.0	0.0	7	8.5	8	7.5	8.5	7.5
A1	S65-0.0	0.0	9	9.5	11.5	10.5	10	11.5
D2	S90-0.0	0.0	7.5	8.5	7	9	12	13.5
B	S25-0.2	0.2	11	11.5	13.5	14.5	17.5	19.5
I	S45-0.2	0.2	11.5	11	14	12.5	22	21.5
A2	S65-0.2	0.2	7.5	8.5	12	13.5	20.5	21.5
E1	S90-0.2	0.2	8	7	16.5	15	13.5	12
C	S25-0.4	0.4	8	10.5	19	18.5	20	21.5
J	S45-0.4	0.4	11	10.5	15.5	15	25.5	25
B1	S65-0.4	0.4	7	8	18.5	16.5	19.5	19
E2	S90-0.4	0.4	8.5	10	18	16	12.5	11.5
D	S25-0.5	0.5	8	9.5	17.5	18.5	28.5	27
K	S45-0.5	0.5	11.5	10.5	17.5	17	11	8
B2	S65-0.5	0.5	15.5	16	18	15.5	18	21.5
F1	S90-0.5	0.5	8.5	8	16.5	17	14.5	18.5
E	S25-0.6	0.6	11	12	18.5	19.5	22.5	25
L	S45-0.6	0.6	12	12	17.5	18.5	8	8.5
C1	S65-0.6	0.6	8	8.5	15	16	16.5	18
F2	S90-0.6	0.6	8	8	19	17.5	16.5	18
F	S25-0.8	0.8	12	11.5	18.5	18	28	26.5
M	S45-0.8	0.8	14	14.5	18	19.5	28	28.5
C2	S65-0.8	0.8	16	16.5	19	18.5	17	16.5
G1	S90-0.8	0.8	19.5	20	20	21.5	25.5	26
G	S25-1.0	1.0	10.5	11	18	18	16	13
N	S45-1.0	1.0	12.5	13	15.5	16	26	27.5
D1	S65-1.0	1.0	15.5	15	15	15.5	15	14.5

Sample	Sample code	Composition of ZnO-AgNPs	*E. coli*		*S. aureus*		*C. albicans*	
G2	S90-1.0	1.0	20	20.5	18.5	19	24.5	26
H1	L25-0.0	0.0	12.5	11.5	12	13	16.5	15.5
K2	L45-0.0	0.0	10	11.5	8	9	11.5	12
O1	L65-0.0	0.0	8.5	8	7.5	8	13.5	14
R2	L90-0.0	0.0	7.5	7	10	11.5	15	16
H2	L25-0.2	0.2	12.5	12	13.5	13.5	14.5	15
L1	L45-0.2	0.2	8	8.5	15.5	16.5	14	14.5
O2	L65-0.2	0.2	16.5	15	16.5	17.5	12.5	13
S1	L90-0.2	0.2	8	7.5	11.5	10	11.5	10.5
I1	L25-0.4	0.4	21	20.5	11.5	12	11	10.5
L2	L45-0.4	0.4	8.5	9	18.5	19	15.5	15
P1	L65-0.4	0.4	15	16	17.5	17	17.5	18
S2	L90-0.4	0.4	7.5	8	11.5	11	11	12
I2	L25-0.5	0.5	16.5	15.5	13	12.5	17	18.5
M1	L45-0.5	0.5	15.5	16	16.5	15.5	15.5	16
P2	L65-0.5	0.5	16.5	16	18	19	21.5	20.5
T1	L90-0.5	0.5	7	8	14	12.5	11.5	10.5
J1	L25-0.6	0.6	14.5	13.5	14.5	13.5	13	12.5
M2	L45-0.6	0.6	15	15	18	17.5	18.5	19
Q1	L65-0.6	0.6	13.5	13	18.5	19.5	23.5	24.5
T2	L90-0.6	0.6	7.5	7.5	15	16.5	14	13.5
J2	L25-0.8	0.8	16.5	16	16.5	17.5	14.5	14
N1	L45-0.8	0.8	15.5	16	17	18.5	16.5	15.5
Q2	L65-0.8	0.8	16.5	16	18.5	19.5	24.5	25
U1	L90-0.8	0.8	12.5	13	20.5	19.5	22	23.5
K1	L25-1.0	1.0	14.5	14.5	18	17.5	14.5	13.5
N2	L45-1.0	1.0	14.5	13.5	16.5	15.5	20	21.5
R1	L65-1.0	1.0	15.5	15.5	18	18.5	20.5	20
U2	L90-1.0	1.0	8.5	8	17.5	16.5	20.5	20.5
V1	R25-0.0	0.0	7.5	7	10	10.5	10.5	11.5
Y2	R45-0.0	0.0	7.5	7	9.5	8.5	10	11
η1	R65-0.0	0.0	7.5	8	11.5	12	11.5	12.5
Ω2	R90-0.0	0.0	8	7.5	12.5	11.5	12	13.5
V2	R25-0.2	0.2	8.5	8.5	15.5	16	18	18
Z1	R45-0.2	0.2	11.5	11	14	14.5	13.5	13.5
η2	R65-0.2	0.2	8	7.5	13.5	14.5	13	14.5
γ1	R90-0.2	0.2	16.5	16	14	13	16	16.5
W1	R25-0.4	0.4	13.5	14	13	13.5	19	19.5
Z2	R45-0.4	0.4	11.5	10.5	20	19	13	14.5

Sample	Sample code	Composition of ZnO-AgNPs	*E. coli*		*S. aureus*		*C. albicans*	
ɽ1	R65-0.4	0.4	10	10.5	16.5	16.5	17	16.5
γ2	R90-0.4	0.4	12	13.5	15.5	15	14.5	15
W2	R25-0.5	0.5	16.5	15.5	15.5	16	20.5	21.5
α1	R45-0.5	0.5	7	7	15.5	15.5	13.5	14
ɽ2	R65-0.5	0.5	8.5	10	15	14.5	14.5	14
Θ1	R90-0.5	0.5	14.5	14	16.5	17	22.5	23
X1	R25-0.6	0.6	12.5	11.5	16	15.5	24.5	24
α2	R45-0.6	0.6	7	7	17.5	18	14	14.5
€ 1	R65-0.6	0.6	13.5	12.5	20.5	19.5	16	18
Θ2	R90-0.6	0.6	13.5	14	16.5	17	22.5	22
X2	R25-0.8	0.8	14	14.5	17.5	18.5	20.5	21.5
β1	R45-0.8	0.8	12.5	12	19.5	20.5	15	16.5
€ 2	R65-0.8	0.8	15.5	16	19.5	19	17.5	18
ρ1	R90-0.8	0.8	17.5	17	21.5	20.5	30	29.5
Y1	R25-1.0	1.0	13.5	13	15.5	16	12.5	13.5
β2	R45-1.0	1.0	8	7.5	16	17.5	11.5	12
Ω1	R65-1.0	1.0	13.5	14	18.5	19	13.5	12.5
ρ2	R90-1.0	1.0	16	15.5	18	18.5	21	22.5

Appendix C

Table 8: Mean diameter and standard deviation of zones of inhibition for *E. coli*, *S. aureus* and *C. albicans* at varying compositions of ZnO-AgNPs

Sample	Sample code	Composition of ZnO-AgNPs	*E. coli*		*S. aureus*		*C. albicans*	
			Mean	Standard deviation	Mean	Standard deviation	Mean	Standard deviation
Positive control	+		0.00	0.00	26.00	0.00	24.75	0.354
Negative control	-		0.00	0.00	0.00	0.00	0.00	0.00
Seed extract			7.25	0.354	8.5	0.00	10.75	0.354
Leaf extract			7.6	0.141	8.5	0.707	11.0	0.00
Root extract			7.3	0.565	8.25	0.354	11.25	0.354
A	S25-0.0	0	7.75	0.354	7.75	1.061	9.25	1.061
H	S45-0.0	0	7.75	1.061	7.75	0.354	8.00	0.707
A1	S65-0.0	0	9.25	0.354	11.00	0.707	10.75	1.061
D2	S90-0.0	0	8.00	0.707	8.00	1.414	12.75	1.061
B	S25-0.2	0.2	11.25	0.354	14.00	0.707	18.50	1.414
I	S45-0.2	0.2	11.25	0.354	13.25	1.061	21.75	0.354
A2	S65-0.2	0.2	8.00	0.707	12.75	1.061	21.00	0.707
E1	S90-0.2	0.2	7.50	0.707	15.75	1.061	12.75	1.061
C	S25-0.4	0.4	9.25	1.768	18.75	0.354	20.75	1.061
J	S45-0.4	0.4	10.75	0.354	15.25	0.354	25.25	0.354
B1	S65-0.4	0.4	7.50	0.707	17.50	1.414	19.25	0.354
E2	S90-0.4	0.4	9.25	1.061	17.00	1.414	12.00	0.707
D	S25-0.5	0.5	8.75	1.061	18.00	0.707	27.75	1.061
K	S45-0.5	0.5	11.00	0.707	17.25	0.354	9.50	2.121
B2	S65-0.5	0.5	15.75	0.354	16.75	1.768	19.75	2.475
F1	S90-0.5	0.5	8.25	0.354	16.75	0.354	16.50	2.828
E	S25-0.6	0.6	11.50	0.707	19.00	0.707	23.75	1.768
L	S45-0.6	0.6	12.00	0.000	18.00	0.707	8.25	0.354

Sample	Sample code	Composition of ZnO-AgNPs	*E. coli*		*S. aureus*		*C. albicans*	
			Mean	Standard deviation	Mean	Standard deviation	Mean	Standard deviation
C1	S65-0.6	0.6	8.25	0.354	15.50	0.707	17.25	1.061
F2	S90-0.6	0.6	8.00	0.000	18.25	1.061	17.25	1.061
F	S25-0.8	0.8	11.75	0.354	18.25	0.354	27.25	1.061
M	S45-0.8	0.8	14.25	0.354	18.75	1.061	28.25	0.354
C2	S65-0.8	0.8	16.25	0.354	18.75	0.354	16.75	0.354
G1	S90-0.8	0.8	19.75	0.354	20.75	1.061	25.75	0.354
G	S25-1.0	1	10.75	0.354	18.00	0.000	14.50	2.121
N	S45-1.0	1	12.75	0.354	15.75	0.354	26.75	1.061
D1	S65-1.0	1	15.25	0.354	15.25	0.354	14.75	0.354
G2	S90-1.0	1	20.25	0.354	18.75	0.354	25.25	1.061
H1	L25-0.0	0	12.00	0.707	12.50	0.707	16.00	0.707
K2	L45-0.0	0	10.75	1.061	8.50	0.707	11.75	0.354
O1	L65-0.0	0	8.25	0.354	7.75	0.354	13.75	0.354
R2	L90-0.0	0	7.25	0.354	10.75	1.061	15.50	0.707
H2	L25-0.2	0.2	12.25	0.354	13.50	0.000	14.75	0.354
L1	L45-0.2	0.2	8.25	0.354	16.00	0.707	14.25	0.354
O2	L65-0.2	0.2	15.75	1.061	17.00	0.707	12.75	0.354
S1	L90-0.2	0.2	7.75	0.354	10.75	1.061	11.00	0.707
I1	L25-0.4	0.4	20.75	0.354	11.75	0.354	10.75	0.354
L2	L45-0.4	0.4	8.75	0.354	18.75	0.354	15.25	0.354
P1	L65-0.4	0.4	15.50	0.707	17.25	0.354	17.75	0.354
S2	L90-0.4	0.4	7.75	0.354	11.25	0.354	11.50	0.707
I2	L25-0.5	0.5	16.00	0.707	12.75	0.354	17.75	1.061
M1	L45-0.5	0.5	15.75	0.354	16.00	0.707	15.75	0.354
P2	L65-0.5	0.5	16.25	0.354	18.50	0.707	21.00	0.707
T1	L90-0.5	0.5	7.50	0.707	13.25	1.061	11.00	0.707
J1	L25-0.6	0.6	14.00	0.707	14.00	0.707	12.75	0.354
M2	L45-0.6	0.6	15.00	0.000	17.75	0.354	18.75	0.354
Q1	L65-0.6	0.6	13.25	0.354	19.00	0.707	24.00	0.707
T2	L90-0.6	0.6	7.50	0.000	15.75	1.061	13.75	0.354
J2	L25-0.8	0.8	16.25	0.354	17.00	0.707	14.25	0.354
N1	L45-0.8	0.8	15.75	0.354	17.75	1.061	16.00	0.707
Q2	L65-0.8	0.8	16.25	0.354	19.00	0.707	24.75	0.354
U1	L90-0.8	0.8	12.75	0.354	20.00	0.707	22.75	1.061
K1	L25-1.0	1	14.50	0.000	17.75	0.354	14.00	0.707

Sample	Sample code	Composition of ZnO-AgNPs	*E. coli*		*S. aureus*		*C. albicans*	
			Mean	Standard deviation	Mean	Standard deviation	Mean	Standard deviation
N2	L45-1.0	1	14.00	0.707	16.00	0.707	20.75	1.061
R1	L65-1.0	1	15.50	0.000	18.25	0.354	20.25	0.354
U2	L90-1.0	1	8.25	0.354	17.00	0.707	20.50	0.000
V1	R25-0.0	0	7.25	0.354	10.25	0.354	11.00	0.707
Y2	R45-0.0	0	7.25	0.354	9.00	0.707	10.50	0.707
η1	R65-0.0	0	7.75	0.354	11.75	0.354	12.00	0.707
Ω2	R90-0.0	0	7.75	0.354	12.00	0.707	12.75	1.061
V2	R25-0.2	0.2	8.50	0.000	15.75	0.354	18.00	0.000
Z1	R45-0.2	0.2	11.25	0.354	14.25	0.354	13.50	0.000
η2	R65-0.2	0.2	7.75	0.354	14.00	0.707	13.75	1.061
γ1	R90-0.2	0.2	16.25	0.354	13.50	0.707	16.25	0.354
W1	R25-0.4	0.4	13.75	0.354	13.25	0.354	19.25	0.354
Z2	R45-0.4	0.4	11.00	0.707	19.50	0.707	13.75	1.061
ζ1	R65-0.4	0.4	10.25	0.354	16.50	0.000	16.75	0.354
γ2	R90-0.4	0.4	12.75	1.061	15.25	0.354	14.75	0.354
W2	R25-0.5	0.5	16.00	0.707	15.75	0.354	21.00	0.707
α1	R45-0.5	0.5	7.00	0.000	15.50	0.000	13.75	0.354
ζ2	R65-0.5	0.5	9.25	1.061	14.75	0.354	14.25	0.354
Θ1	R90-0.5	0.5	14.25	0.354	16.75	0.354	22.75	0.354
X1	R25-0.6	0.6	12.00	0.707	15.75	0.354	24.25	0.354
α2	R45-0.6	0.6	7.00	0.000	17.75	0.354	14.25	0.354
€ 1	R65-0.6	0.6	13.00	0.707	20.00	0.707	17.00	1.414
Θ2	R90-0.6	0.6	13.75	0.354	16.75	0.354	22.25	0.354
X2	R25-0.8	0.8	14.25	0.354	18.00	0.707	21.00	0.707
β1	R45-0.8	0.8	12.25	0.354	20.00	0.707	15.75	1.061
€ 2	R65-0.8	0.8	15.75	0.354	19.25	0.354	17.75	0.354
ρ1	R90-0.8	0.8	17.25	0.354	21.00	0.707	29.75	0.354
Y1	R25-1.0	1	13.25	0.354	15.75	0.354	13.00	0.707
β2	R45-1.0	1	7.75	0.354	16.75	1.061	11.75	0.354
Ω1	R65-1.0	1	13.75	0.354	18.75	0.354	13.00	0.707
ρ2	R90-1.0	1	15.75	0.354	18.25	0.354	21.75	1.061

REFERENCE

Abat, C., Chaudet, H., Rolain, J.-M., Colson, P., & Raoult, D. (2016). Traditional and syndromic surveillance of infectious diseases and pathogens. *International Journal of Infectious Diseases*, **48**, 22–28.

Abd El-Gawad, A. M., Mashaly, I. A., Abu Ziada, M. E., & Deweeb, M. R. (2015). Phytotoxicity of three Plantago species on germination and seedling growth of hairy beggarticks (*Bidens pilosa* L.). *Egyptian Journal of Basic and Applied Sciences*, **2**(4), 303–309.

Abdel-Fatah, W. I., Gobara, M. M., Mustafa, S. F. M., Ali, G. W., & Guirguis, O. W. (2016). Role of silver nanoparticles in imparting antimicrobial activity of titanium dioxide. *Materials Letters*, **179**, 190–193.

Abdulaziz Bagabas, Ahmad Alshammari, Mohamed F. A. Aboud, & Hendrik Kosslick. (2013). Room-temperature Synthesis of Zinc oxide Nanoparticles in different media and their Application in Cyanide Photodegradation. *Nano Research Letters* **8**(1), 516–525.

Adedapo, A., Jimoh, F., & Afolayan, A. (2011). Comparison of the nutritive value and biological activities of the acetone, methanol and water extracts of the leaves of *Bidens pilosa* and *Chenopodium album*. *Acta Pol Pharm,* **68**(1), 83–92.

Adhikari, S. R., Sapkota, V. P., Khan, M., & Maskay, N. M. (2016). A study of the relationship between infectious diseases and health economics: some evidences from Nepal. *Asian Pacific Journal of Tropical Disease*, **6**(6), 437–442.

Agarwal, H., Venkat Kumar, S., & Rajeshkumar, S. (2017). A review on green synthesis of zinc oxide nanoparticles – An eco-friendly approach. *Resource-Efficient Technologies*, **3**(4) 406-413.

Ahamed, M., Alsalhi, M. S., & Siddiqui, M. K. (2010). Silver nanoparticle applications and human health. *Clin Chim Acta* **411**(23–24), 1841–1848.

Ahmad, S., AbdEl-Salam, N. M., & Ullah, R. (2016). In Vitro Antimicrobial Bioassays, DPPH Radical Scavenging Activity, and FTIR Spectroscopy Analysis of *Heliotropium bacciferum*. *BioMed Research International*, **2016**, 1–12.

Ahmed, S., Ahmad, M., Swami, B. L., & Ikram, S. (2016). A review on plants extract mediated synthesis of silver nanoparticles for antimicrobial applications: A green expertise. *Journal of Advanced Research*, **7**(1), 17–28.

Alagummuthu, G., & Kirubha, R. (2012). Green synthesis of silver nanoparticles using *Cissus quandrangularis* plant extract and their antibacterial activity. *Nanomaterials and Biostructures*, **2**(3), 30–33.

Alvarez-Ordóñez, A., & Prieto, M.(2012). Fourier Transform Infrared Spectroscopy in Food Microbiology. *In SpringerBriefs in Food, Health, and Nutrition*. Retrieved from http://link.springer.com/10.1007/978-1-4614-3813-7 on 5/16/2017 at 1: 06: 18 PM

Amábile-Cuevas, C. F., Cabrera, R., Valenzuela, F., & Fuchs, L. Y. (1998). 11.3 Antibiotic Resistance and Prescription Practices in Developing Countries. In J. K. and G. S. Peter Williams (Ed.), *Methods in Microbiology* (pp. 587–594). Retrieved from http://www.sciencedirect.com/science/article/pii/S0580951708703143 on 7/4/2017 at 7: 06: 37 PM

Atomic World - Transmission electron microscope(TEM) - Principle of TEM. (n.d.). Retrieved, from http://www.hk-phy.org/atomic_world/tem/tem02_e.html on 14/4/2019 at 1:44:06 PM

Awwad, A. M., Albiss, B., & Ahmad, A. L. (2014). Green synthesis, characterization and optical properties of zinc oxide Nano sheets using *Olea europea* leaf extract. *Advanced Materials Letters*, **5**(9), 520–524.

Aysaa, N. H., & Salman, H. D. (2016). Antibacterial activity of modified zinc oxide nanoparticles against *Pseudomonas aeruginosa* isolates of burn infections. *World Scientific News*, **33**, 1-14.

Baba, A., Imazu, K., Yoshida, A., Tanaka, D., & Tamada, K. (2014). Surface plasmon resonance properties of silver nanoparticle 2D sheets on metal gratings. *SpringerPlus*, **3**, 284-294.

Bagherzade, G., Tavakoli, M. M., & Namaei, M. H. (2017). Green synthesis of silver nanoparticles using aqueous extract of saffron (*Crocus sativus* L.) wastages and its

antibacterial activity against six bacteria. *Asian Pacific Journal of Tropical Biomedicine*, **7**(3), 227–233.

Balouiri, M., Sadiki, M., & Ibnsouda, S. K. (2016). Methods for in vitro evaluating antimicrobial activity: A review. *Journal of Pharmaceutical Analysis*, **6**(2), 71–79.

Bar, H., Bhui, D. K., Sahoo, G. P., Sarkar, P., De, S. P., & Misra, A. (2009). Green synthesis of silver nanoparticles using latex of *Jatropha curcas*. Colloids and Surfaces A: *Physicochemical and Engineering Aspects*, **339**(1–3), 134–139.

Bartolome, A. P., Villaseñor, I. M., & Yang, W.-C. (2013). *Bidens pilosa* L. (Asteraceae): Botanical Properties, Traditional Uses, Phytochemistry, and Pharmacology. *Evidence-Based Complementary and Alternative Medicine*, **2013**, 1–51.

Basha, S. K., Lakshmi, K. V., & Kumari, V. S. (2016). Ammonia sensor and antibacterial activities of green zinc oxide nanoparticles. *Sensing and Bio-Sensing Research*, **10**, 34–40.

Bhainsa, K. C., & Souza, S. (2006). Extracellular biosynthesis of silver nanoparticles using fungus *Aspergillus fumigates*. *Colloids Surf B Biointerfaces* **47**(2), 160–164.

Binnig, G., Quate, C. F., & Gerber, C. (1986). Atomic force microscope. *Physical Review Letters*, **56**(9), 930.

Bloomfield, S. F., Martin, Exner, Gaetano, Fara, M., Kumar, Jyoti, Nath, Elizabeth, Scott, A., & Carolien, Van der, Voorden,. (2009). The global burden of hygiene-related diseases in relation to the home and community (Simmons College, Boston, MA USA). Retrieved from http://www.ifh-homehygiene.org/sites/default/files/publications/The%20global%20burden%20of%20hygiene-related%20diseases%20in%20relation%20to%20the%20home%20and%20community_16022012.pdf on 8/9/2017 at 4: 25: 38 PM

Bouchard, M., & Bouchard, J.M. (2011). Disinfectant cleaner. Retrieved from http://www.google.com/patents/US20110195131 on 15/9/2017 at 11: 22: 13 AM

Bowen, D. K., & Tanner, B. K. (1998). High resolution X-ray diffractometry and topography. London: Taylor & Francis, 1-5.

Brandao, M. G. L., Nery, C. G. C., Mamao, M. A. S & Krettli, A. U (1998). Two Methoxylated Flavone Glycosides from *Bidens pilosa*. *Phytochemistry* **48**(2), 397–399.

Brent, Fultz, & James, M. Howe. (2008). Transmission Electron Microscopy and Diffractometry of Materials (3rd ed.). Springer Berlin Heidelberg, 1-8.

Brian C. Smith. (1999). Infrared Spectra Interpretation; A Systematic Approach. CRC press, Boca Raton, 1-5.

Brian C. Smith. (2002). Quantitative Spectroscopy; Theory and Practice. Academic Press, San Diego, 1-4.

Brian. C. Smith. (2011). Fundamentals of Fourier Transform Infrared Spectroscopy (2nd ed.). USA: CRC press, Taylor and Francis group, 1-7.

Bumbrah, G. S., & Sharma, R. M. (2016). Raman spectroscopy – Basic principle, instrumentation and selected applications for the characterization of drugs of abuse. *Egyptian Journal of Forensic Sciences*, **6**(3), 209–215.

Chaloupka, K., Malam, Y., & Seifalian, A. M. (2010). Nanosilver as a new generation of nanoproduct in biomedical applications. *Trends in Biotechnology*, **28**(11), 580–588.

Chang, C. L. T., Kuo, H. K & Chang, S. L (2005). The distinct effects of a butanol fraction of *Bidens pilosa* plant extract on the development of Th1-mediated diabetes and Th2-mediated airway inflammation in mice. *J Biomed Sci*, **12**(1), 79–89.

Chen, C. F., Tzeng, S. D., Chen, H. Y., Lin, K. J., & Gwo, S (2008). Tunable Plasmonic Response from Alkanethiolate-Stabilized Gold Nanoparticle Superlattices: Evidence of Near-Field Coupling. *Journal of the American Chemical Society*, **130**(3), 824–826.

Chen, M., Feng, Y. M., Wang, X., Li, T. C., Zhang, J. Y., & Qian, D. J. (2007). Silver nanoparticles capped by oleylamine: formation, growth, and self-organization. *Langmuir* **23**(10), 5296–5304.

Chen, S. F & Zhang, H. (2012). Aggregation kinetics of nanosilver in different water condition. *Adv. Nat. Sci.: Nanosci. Nanotechnol* **3**, 035006-1–7.

Chiang, M. (2003). Patent No. US20030008791 A1. Retrieved from http://www.google.com/patents/US20030008791 on 5/8/2017 at 3: 05: 40 PM

Chiang, M. Y.C. (2003). Non alcoholic hand sanitizer (Vol. 1), 131-138.

Chien, S. C., Young, P. H., Hsu, Y. J., Chen, C. H., Tien, Y. J., Shiu, S. Y., … Yang, W. C. (2009). Anti-diabetic properties of three common *Bidens pilosa* variants in Taiwan. *Phytochemistry*, **70**(10), 1246–1254.

Chung, C. Y., Yang, W. C., Liang, C. L., Liu, H. Y., Lai, S. K., & Chang, C. L. T. (2016). Cytopiloyne, a polyacetylenic glucoside from *Bidens pilosa*, acts as a novel anticandidal agent via regulation of macrophages. *Journal of Ethnopharmacology*, **184**, 72–80.

Cortés-Rojas, D. F., Chagas-Paula, D. A., Da Costa, F. B., Souza, C. R. F., & Oliveira, W. P. (2013). Bioactive compounds in *Bidens pilosa* L. populations: a key step in the standardization of phytopharmaceutical preparations. *Revista Brasileira de Farmacognosia*, **23**(1), 28–35.

Dai, J & Mumper, R. J (2010). Plant Phenolics: Extraction, Analysis and their Antioxidant and Anticamcer Properties. *Molecules*, **15**(10) 7320–7330.

Dang, T. M. D., Le, T. T. T., Blance, E. F. M., & Dang, C. (2012). Influence of surfactant on the preparation of silver nanoparticles by polyol method. *Journal of Nanotechnology* **3**, 035004-1–4.

Das, B., Dash, S. K., Mandal, D., Ghosh, T., Chattopadhyay, S., Tripathy, S., … Roy, S. (2017). Green synthesized silver nanoparticles destroy multidrug resistant bacteria via reactive oxygen species mediated membrane damage. *Arabian Journal of Chemistry*, **10**(6), 862–876.

De, M., Ghosh, P. S., & Rotello, V. M. (2008). Applications of Nanoparticles in Biology. *Advanced Materials*, **20**(22), 4225–4241.

Deba, F., Xuan, T. D., Yasuda, M & Tawata, S (2007). Herbicidal and fungicidal activities and identification of potential phytotoxins from *Bidens pilosa* L. var. radiata scherf. *Weed Biology and Management* **7**(2), 77–83.

Deba, F., Xuan, T. D., Yasuda, M., & Tawata, S. (2008). Chemical composition and antioxidant, antibacterial and antifungal activities of the essential oils from *Bidens pilosa* Linn. var. Radiata. *Food Control*, **19**(4), 346–352.

Desai, R., Mankad, V., Gupta, S., & Jha, P. (2012). Size Distribution of Silver Nanoparticles: UV-Visible Spectroscopic Assessment. *Nanoscience and Nanotechnology Letters*, **4**(1), 30–34.

Devi, R. S., & Gayathri, R. (2014). Green Synthesis of zinc oxide nanoparticles by using *Hibiscus rosa-sinensis*. *Int J Curr Eng Technol*, **4**, 2444–2446.

Dhand, C., Dwivedi, N., Loh, X. J., Ying, A. N. J., Verma, N. K., Beuerman, R. W., … Ramakrishna, S. (2015). Methods and strategies for the synthesis of diverse nanoparticles and their applications: a comprehensive overview. *RSC Advances*, **5**(127), 105003–105037.

Dharmanada, S. (2013). A popular Remedy Escapes Notice of Westen Practitioners. Retrieved from http://www.itmonline.org/arts/bidens.html on 31/5/2018 at 3: 38: 05 PM

Dimo, T., Azay, J & Tan, P. V (2001). Effects of the aqueous and methylene chloride extracts of *Bidens pilosa* leaf on fructose-hypertensive rats. *J Ethnopharmacol* **76**(3), 215–221.

Dizaj, S. M., Lotfipour, F., Barzegar-Jalali, M., Zarrintan, M. H., & Adibkia, K. (2014). Antimicrobial activity of the metals and metal oxide nanoparticles. *Materials Science and Engineering:* C, **44**, 278–284.

Durán, N., Durán, M., de Jesus, M. B., Seabra, A. B., Fávaro, W. J., & Nakazato, G. (2016). Silver nanoparticles: A new view on mechanistic aspects on antimicrobial activity. *Nanomedicine: Nanotechnology, Biology and Medicine*, **12**(3), 789–799.

Dutta, R. K., Bhavani, P. N., Mahesh, K. G., & Reddy, A. V. R. (2012). Studies on antibacterial activity of ZnO nanoparticles by ROS induced lipid peroxidation. *Colloids Surf B Biointerfaces* **94**, 143–150.

Dyer D. L, Gerenraich K. B, & Wadhams P. S. (1998). Testing a new Alcohol-free Sanitizer to Combat Infection. *AORN J*, **68**(2), 239–251.

Dyer, D. L., Shinder, A., & Shinder, F. (2000). Alcohol-free instant hand sanitizer reduces elementary school illness absenteeism. *Family Medicine-Kansas City*, **32**(9), 633–638.

Edison, T. J. I., & Sethuraman, M. G. (2012). Instant green synthesis of silver nanoparticles using *Terminalia chebula* fruit extract and evaluation of their catalytic activity on reduction of methylene blue. *Process Biochemistry*, **47**(9), 1351–1357.

Elizabeth, Varghese, & Mary, George. (2015). Green synthesis of zinc oxide nanoparticles. *IJARSE* **4**(1), 307-314.

Elumalai, K., & Velmurugan, S. (2015). Green synthesis, characterization and antimicrobial activities of zinc oxide nanoparticles from the leaf extract of *Azadirachta indica* (L.). *Applied Surface Science*, **345**, 329–336.

Emmanuel, R., Palanisamy, S., Chen, S.-M., Chelladurai, K., Padmavathy, S., Saravanan, M., … Al-Hemaid, F. M. A. (2015). Antimicrobial efficacy of green synthesized drug blended silver nanoparticles against dental caries and periodontal disease causing microorganisms. *Materials Science and Engineering*: C, **56**, 374–379.

Espitia, P., de Fátima Ferreira Soares, N., Coimbra, J., José de Andrade, N., Cruz, R., & Medeiros, E. (2012). Zinc Oxide Nanoparticles: Synthesis, Antimicrobial Activity and Food Packaging Applications. *Food and bioprocess technology*. **5**, 1447-1464

Ethiraj, A. S., Jayanthi, S., Ramalingam, C., & Banerjee, C. (2016). Control of size and antimicrobial activity of green synthesized silver nanoparticles. *Materials Letters*, **185**, 526–529.

Ezzati, M., Lopez, A. D., Rodgers, A. A & Murray, C. J. L (2004). Comparative quantification of health risks: global and regional burden of disease attributable to selected major risk factors Volume 1. Geneva: *World Health Organization*, 1-20.

Farnsworth, N. R., Akerele, O., Bingel, A. S., Soejarto, D. D., & Guo, Z. (1985). Medicinal plants in therapy. *Bulletin of the World Health Organization*, 63(6), 965.

Fayaz, A. M., Balaji, K., Girilal, M., Yadav, R., Kalaichelvan, P. T., & Venketesan, R. (2010). Biogenic synthesis of silver nanoparticles and their synergistic effect with antibiotics: a study against gram-positive and gram-negative bacteria. Nanomedicine: *Nanotechnology, Biology and Medicine*, **6**(1), 103–109.

Feris, K., Otto, C., & Tinker, J. (2010). Electrostatic Interactions affect nanoparticle-mediated toxicity to Gram (-) bacterium, *Pseudomonas aeruginosa*. *Langmuir*, **26**(6), 4429–4436.

Ferni, V., Prabha, P. H., Sudha, P., Devibala, B & Jerald, A (2011). Antibacterial effect of ZnO-Au nanocomposites. *Colloids Surf B Biointerfaces*, **1**, 1–8.

Ferraro, J. R., Nakamoto, K., & Brown, C. W. (2003). Introductory Raman spectroscopy (2nd ed). Amsterdam ; Boston: Academic Press, 1-5.

Fitchmun, M. (2007). Surface sanitizer. Retrieved from http://www.google.com/patents/US20080045491 on 16/05/2017 at 1: 22: 02 PM

Fultz, B., & Howe, J. (2008). Transmission Electron Microscopy and Diffractometry of Materials (3rd ed.). Springer Berlin Heidelberg, 1-8.

Gale, S. D., Erickson, L. D., Berrett, A., Brown, B. L., & Hedges, D. W. (2016). Infectious disease burden and cognitive function in young to middle-aged adults. *Brain, Behavior, and Immunity*, **52**, 161–168.

Garcia, M. A. (2011). Surface plasmons in metallic nanoparticles: fundamentals and applications. *Journal of Physics D: Applied Physics*, **44**(28), 283001.

Gaynes, R. (2017). The discovery of penicillin—new insights after more than 75 years of clinical use. *Emerging Infectious Diseases*, **23**(5), 849.

Geissberger, peter, & Séquin, U. (1991). Constituents of *Bidens pilosa* L.: Do the components found so far explain the use of this plant in traditional medicine? *Acta Trop* **48**, 251–261.

Gelbrand, H., Miller-Petrie, M., Pant, S., Gandra, S., Levinson, J., Barter, D., … others. (2015). The State of the World's Antibiotics 2015. *Wound Healing Southern Africa*, **8**(2), 30–34.

Ghosh Chaudhuri, Rajib, & Paria, Santanu. (2012). Core/Shell Nanoparticles: Classes, Properties, Synthesis Mechanisms, Characterization, and Applications. *Chem Rev*, **112**(4), 2373-2433.

Ghosh, M., & Raychaudhuri, A. K. (2008). Shape transition in ZnO nanostructures and its effect on blue-green photoluminescence. *Nanotechnology*, **19**(44), 445704.

Gibson, K., & Toscano, J. (2012). Urinary Tract Infection Update. Retrieved from http://www.aapsus.org/wp-content/uploads/uti82.pdf on 15/10/2017 at 10: 17: 25 AM

Griffiths, P. R., & DeHaseth, J. A. (2007). Fourier transform infrared spectrometry (2. ed). In Chemical Analysis: Vol. 171 (2. ed). Hoboken, NJ: Wiley-Interscience, 1-5.

Grombone-Guaratini, M. T., Silva-Brandão, K. L., Solferini, V. N., Semir, J., & Trigo, J. R. (2005). Sesquiterpene and polyacetylene profile of the *Bidens pilosa* complex (Asteraceae: Heliantheae) from Southeast of Brazil. *Biochemical Systematics and Ecology*, **33**(5), 479–486.

Gunalan, S., Rajeswari, S., & venckatesh, R. (2012). Green synthesized zinc oxide nanoparticles against bacterial and fungal pathogens. *Progress in Natural Science: material International*, **22**(6), 693–700.

Gurunathan, S. (2015). Biologically synthesized silver nanoparticles enhances antibiotic activity against Gram-negative bacteria. *Journal of Industrial and Engineering Chemistry*, **29**, 217–226.

Guzman, M., Dille, J., & Godet, S. (2012). Synthesis and antibacterial activity of silver nanoparticles against gram-positive and gram-negative bacteria. *Nanomedicine: Nanotechnology, Biology and Medicine*, **8**(1), 37–45.

Hajipour, M. J., Fromm, K. M., Akbar Ashkarran, A., Jimenez de Aberasturi, D., Larramendi, I. R. de, Rojo, T., … Mahmoudi, M. (2012). Antibacterial properties of nanoparticles. *Trends in Biotechnology*, **30**(10), 499–511.

Hansen, C., & Paintsil, E. (2016). Infectious Diseases of Poverty in Children. *Pediatric Clinics of North America*, **63**(1), 37–66.

Harvey, S. (1980). Antiseptics and Disinfectants, Fungicides, Ectoparasiticides. In Goodman, L. S, Gilman, A. G, & Gilman, A., The Pharmacological Basis of Therapeutics (6th Edition, p. Chapter 41). New York: Macmillan Publishing Company, Inc, p974.

Hatchett, D. W & Henry, S (1996). Electrochemistry of sulfur adlayers on low-index faces of silver. *J Phys Chem*, **100**, 9854–9859.

Hebeish, A., El-Rafie, M. H., EL-Sheikh, M. A., Seleem, A. A., & El-Naggar, M. E. (2014). Antimicrobial wound dressing and anti-inflammatory efficacy of silver nanoparticles. *International Journal of Biological Macromolecules*, **65**, 509–515.

Henry, D., Eby, N., Goodge, J., & Mogk, D. (2004). BraggsLaw. Retrieved, from Geochemical Instrumentation and Analysis website: https://serc.carleton.edu/research_education/geochemsheets/BraggsLaw.html on 14/4/2019 at 2:04:12 PM

Hoffmann, B., & Hölzl, J. (1989). Chalcone glucosides from *Bidens pilosa*. *Phytochemistry*, **28**(1), 247–249.

Hopp, S., Quest, T. L., & Wanat, K. A. (2016). Infectious Disease Practice Gaps in Dermatology. *Dermatologic Clinics*, **34**(3), 281–289.

Huh, A. J., & Kwon, Y. J. (2011). "Nanoantibiotics": A new paradigm for treating infectious diseases using nanomaterials in the antibiotics resistant era. *Journal of Controlled Release*, **156**(2), 128–145.

Ibrahim, H. M. M. (2015). Green synthesis and characterization of silver nanoparticles using banana peel extract and their antimicrobial activity against representative microorganisms. *Journal of Radiation Research and Applied Sciences*, **8**(3), 265–275.

Iravani, S (2011). Green Synthesis of Metal nanoparticles using plants. *Advances in Nanoparticles* **13**(10), 2638–2650.

Jaggi, N., & Vij, D. R. (2006). Fourier transform infrared spectroscopy. In Handbook of Applied Solid State Spectroscopy (pp. 411–450). Retrieved from http://link.springer.com/chapter/10.1007/0-387-37590-2_9 on 5/12/2017 at 9: 10: 16 AM

Janaki, A. C., Sailatha, E., & Gunasekaran, S. (2015). Synthesis, characteristics and antimicrobial activity of ZnO nanoparticles. *Spectrochimica Acta Part A: Molecular and Biomolecular Spectroscopy*, **144**, 17–22.

Jeffrey, D. J. (1995). Chemicals used as disinfectants: Active ingredients and enhancing additives. *Rev. Sci. tech. Off. int. Epiz*, **14**(1), 57–70.

Jia, J., Wang, B., Wu, A., Cheng, G., Li, Z., & Dong, S. (2002). A Method to Construct a Third-Generation Horseradish Peroxidase Biosensor: Self-Assembling Gold Nanoparticles to Three-Dimensional Sol−Gel Network. *Analytical Chemistry*, **74**(9), 2217–2223.

Jim, O'Neill. (2014). Antimicrobial Resistance: Tackling a crisis for the health and wealth of nations.

Joshi, M., Bhattacharyya, A., & Wazed, Ali, S. (2008). Characterisation techniques for nanotechnology applications in textiles. *Indian Journal of Fibre and Textile Research* **33**, 304–317.

Ju-Nam, Y., & Lead, J. R. (2008). Manufactured nanoparticles: an overview of their chemistry, interctions and potential environmental implications. *Sci Total Environ*, **400**(1–3), 396–414.

Jyoti, K., Baunthiyal, M., & Singh, A. (2016). Characterization of silver nanoparticles synthesized using Urtica dioica Linn. leaves and their synergistic effects with antibiotics. *Journal of Radiation Research and Applied Sciences*, **9**(3), 217–227.

Kaviya, S., Santhanalakshmi, J., Viswanathan, B., Muthumary, J., & Srinivasan, K. (2011). Biosynthesis of silver nanoparticles using citrus sinensis peel extract and its antibacterial activity. *Spectrochimica Acta Part A: Molecular and Biomolecular Spectroscopy*, **79**(3), 594–598.

Khan, M. R., Kihara, M & Omoloso, A. D (2001). Antimicrobial Activity of *Bidens pilosa*, Bischofia javanica, Elmerillia papuana and Sigesbekia orientalis. *Fitoterapia* **72**, 662–665.

Khoza, B. S., Gbashi, S., Steenkamp, P. A., Njobeh, P. B., & Madala, N. E. (2016). Identification of hydroxylcinnamoyl tartaric acid esters in *Bidens pilosa* by UPLC-tandem mass spectrometry. *South African Journal of Botany*, **103**, 95–100.

Kim, J. S., Lee, H. J., Lee, M. H., Kim, J., Jin, C & Ryu, J. H. (2006). Luteolin inhibits LPS-stimulated inducible nitric oxide synthase expression in BV-2 micrglial cells. *Planta Med* **72**(1), 65–68.

Krishnaraj, C., Jagan, E. G., Rajasekar, S., Selvakumar, P., Kalaichelvan, P. T., & Mohan, N. (2010). Synthesis of silver nanoparticles using *Acalypha indica* leaf

extracts and its antibacterial activity against water borne pathogens. *Colloids and Surfaces B: Biointerfaces*, **76**(1), 50–56.

Krutyakov, Y. A., Kudrinskiy, A. A., Olenin, A. Y., & Lisichkin, G. V. (2008). Synthesis and properties of silver nanoparticles: advances and prospects. *Russian Chemical Reviews*, **77**(3), 233–257.

Kumar, C. S. S. R. (Ed.). (2014). Transmission electron microscopy characterization of nanomaterials. Berlin: Springer, 1-5.

Larkin, P. (2011). Infrared and Raman spectroscopy: principles and spectral interpretation. Amsterdam ; Boston: Elsevier, 1-8.

Le Ouay, B., & Stellacci, F. (2015). Antibacterial activity of silver nanoparticles: A surface science insight. *Nano Today*, **10**(3), 339–354.

Leece, S. (2004). Topical antimicrobial composition having improved moisturization properties. Retrieved from http://www.google.com/patents/US20060074029 on 4/8/2017 at 2: 08: 16 PM

Leid, J. G., Ditto A. J., Knapp, A., Shah, P. N., Wright, B. D., Blust, R.,… Cope, E. K (2012). In vitro antimicrobial studies of silver carbene complexes: activity of free and nanoparticle carbene formulation against clinical isolates of pathogenic bacteria. *J Antimicrob Chemother* **67**, 138–148.

Levy, S. B., & Marshall, B. (2004). Antibacterial resistance worldwide: causes, challenges and responses. *Nature Medicine*, **10**(12s), S122–S129.

Li, Q., Mahendra, S., Lyon, D. Y., Brunet, L., Liga, M. V., Li, D., & Alvarez, P. J. J. (2008). Antimicrobial nanomaterials for water disinfection and microbial control: Potential applications and implications. *Water Research*, **42**(18), 4591–4602.

Liz-Marzán, L. M. (2006). Tailoring Surface Plasmons through the Morphology and Assembly of Metal Nanoparticles. *Langmuir*, **22**(1), 32–41.

Lu, H., Salabas, E. L., & Schuth, F. (2007). Magnetic nanoparticles: synthesis, protection, functionalization and application. *Angew Chem Int Ed Engl* **46**(8), 1222–1244.

Lu, P. J., Huang, S. C., Chen, Y. P., Chiueh, L. C., & Shih, D. Y. C (2015). Analysis of titanium dioxide and zinc oxide nanoparticles in cosmetics. *Journal of Food and Drug Analysis*, **23**(3), 587–594.

Macinga, D. R., Sattar, S. A., Jaykus, L. A., & Arbogast, J. W. (2008). Improved Inactivation of Nonenveloped Enteric Viruses and Their Surrogates by a Novel Alcohol-Based Hand Sanitizer. *Applied and Environmental Microbiology*, **74**(16), 5047–5052.

Madsen, J. B. (2016). Barriers to Prosperity: Parasitic and Infectious Diseases, IQ, and Economic Development. *World Development*, **78**, 172–187.

Mah, T. F & Otoole, G. A (2001). Mechanisms of biofilm resistance to antimicrobial agents. *Trends Microbiol*, **9**, 34–39.

Mankad, V., Kumar, R. K., & Jha, P. (2013). Investigation of Blue-Shifted Plasmon Resonance: An Optical Properties Study of Silver Nanoparticles. *Nanoscience and Nanotechnology Letters*, **5**(8), 889–894.

Martin, Y., Williams, C. C & Wickramasinghe, H. K (1987). Atomic Force Microscope-force Mapping and Profiling on a Sub 100-A Scale. **61**(10), 4723.

Mason, C., Vivekanandha, S., Misra, M., & Mohanty, A. K. (2012). Switch grass (*Panicum virgatum*) extract medicated green synthesis of silver nanoparticles. *World Journal of Nano Science and Engineering* **12**, 47–52.

Matinise, N., Fuku, X. G., Kaviyarasu, K., Mayedwa, N & Maaza, M (2017). ZnO nanoparticles via *Moringa oleifera* green synthesis: Physical properties and mechanism of formation. *Applied Surface Science* **406**, 339–347.

Matsumura, Y., Yoshikata, K., Kunisaki, S & Tsuchido, T (2003). Mode of bacterial action of silver zeolite and its comparison with that of silver nitrate. *Applied Environmental Microbiology*, **69**, 4278–4281.

McMurray L. M, Oethinger M, & Levy S. B. (1998). Triclosan Targets Lipid Synthesis. *Nature* **39**(2), 531–532.

Michaels, B., Gangar, V., Lin, C.-M., & Doyle, M. (2003). Use limitations of alcoholic instant hand sanitizer as part of a food service hand hygiene program. *Food Service Technology*, **3**(2), 71–80.

Mirzajani, F., Ghassempour, A., Aliahmadi, A., & Esmaeili, M. A. (2011). Antibacterial effect of silver nanoparticles on Staphylococcus aureus. *Research in Microbiology*, **162**(5), 542–549.

Mishra, V., & Sharma, R. (2015). Green Synthesis of Zinc Oxide Nanoparticles Using Fresh Peels Extract of *Punica granatum* and its Antimicrobial Activities. *International Journal of Pharma Research and Health Sciences* **3**(3), 694–699.

Mohan Kumar, K., Sinha, M., Mandal, B. K., Ghosh, A. R., Siva Kumar, K., & Sreedhara Reddy, P. (2012). Green synthesis of silver nanoparticles using *Terminalia chebula* extract at room temperature and their antimicrobial studies. *Spectrochimica Acta Part A: Molecular and Biomolecular Spectroscopy*, **91**, 228–233.

Motshekga, S. C., Ray, S. S., Onyango, M. S., & Momba, M. N. (2015). Preparation and antibacterial activity of chitosan-based nanocomposites containing bentonite-supported silver and zinc oxide nanoparticles for water disinfection. *Applied Clay Science*, **114**, 330–339.

Mott, P. J., Sisk, B. W., Arbogast, J. W., Ferrazzano-Yaussy, C., Bondi, C. A., & Sheehan, J. J. (2007). Alcohol-based instant hand sanitizer use in military settings: a prospective cohort study of Army basic trainees. *Military Medicine*, **172**(11), 1170–1176.

Narula, V. K., & Narula, D. (2003). Waterless sanitizing hand cleanser. Retrieved from http://www.google.com/patents/US6617294 on 10/04/2017 at 7: 34: 02 PM

Nava, O. J., Soto-Robles, C. A., Gómez-Gutiérrez, C. M., Vilchis-Nestor, A. R., Castro-Beltrán, A., Olivas, A., & Luque, P. A. (2017). Fruit peel extract mediated green synthesis of zinc oxide nanoparticles. *Journal of Molecular Structure*, **1147**, 1–6.

Niraimathi, K. L., Sudha, V., Lavanya, R., & Brindha, P. (2013). Biosynthesis of silver nanoparticles using *Alternanthera sessilis* (Linn.) extract and their antimicrobial, antioxidant activities. *Colloids and Surfaces B: Biointerfaces*, **102**, 288–291.

Okafor, F., Janen, A., Kukhtareva, T., Edwards, V., & Curley, M. (2013). Green Synthesis of Silver Nanoparticles, Their Characterization, Application and

Antibacterial Activity. *International Journal of Environmental Research and Public Health*, **10**(10), 5221–5238.

Oke, M. A., Bello, A. B., Odebisi, M. B., El-Imam, A. A., & Kazeem, M. O. (2013). Evaluation of antibacterial efficacy of some alcohol-based hand sanitizers sold in Ilorin (North-central Nigeria). *Ife Journal of Science*, **15**(1), 111–117.

Okeke, I. N., & Sosa, A. (2003). Antibiotic Resistance in Africa–. Retrieved from http://emerald.tufts.edu/med/apua/about_issue/africahealth.pdf on 30/7/2017 at 5: 16: 18 PM

Oliveira, F. ., Andrade-Neto, V., Krettli, A. ., & Brandão, M. G. . (2004). New evidences of antimalarial activity of *Bidens pilosa* roots extract correlated with polyacetylene and flavonoids. *Journal of Ethnopharmacology*, **93**(1), 39–42.

Panáček, A., Kolář, M., Večeřová, R., Prucek, R., Soukupová, J., Kryštof, V., … Kvítek, L. (2009). Antifungal activity of silver nanoparticles against *Candida spp*. Biomaterials, **30**(31), 6333–6340.

Park, G. W., Barclay, L., Macinga, D., Charbonneau, D., Pettigrew, C. A., & Vinjé, J. (2010). Comparative efficacy of seven hand sanitizers against *Murine norovirus*, *Feline calicivirus*, and *GII. 4 norovirus*. *Journal of Food Protection*, **73**(12), 2232–2238.

Patil, R. S., Kokate, M. R., & Kolekar, S. S. (2012). Bioinspired synthesis of highly stabilized silver nanoparticles using *Ocimum tenuiflorum* leaf extract and their antibacterial activity. *Spectrochimica Acta Part A: Molecular and Biomolecular Spectroscopy*, **91**, 234–238.

Peters, M. W. (2008). Hand sanitizer and method of preparation. Retrieved from http://www.google.com/patents/US20090082472 on 15/3/2018 at 10: 12: 28 AM

Phaniendra, A., Jestadi, D. B., & Periyasamy, L. (2015). Free Radicals: Properties, Sources, Targets, and Their Implication in Various Diseases. *Indian Journal of Clinical Biochemistry*, **30**(1), 11–26.

Prabhu, S., & Poulose, E. K. (2012). Silver nanoparticles: mechanism of antimicrobial action, synthesis, medical applications, and toxicity effects. *International Nano Letters*, **2**(1), 32.

Prater, K. J., Fortuna, C. A., McGill, J. L., Brandeberry, M. S., Stone, A. R., & Lu, X. (2016). Poor hand hygiene by college students linked to more occurrences of infectious diseases, medical visits, and absence from classes. *American Journal of Infection Control*, **44**(1), 66–70.

Prüss, A., & Weltgesundheitsorganisation (Eds.). (1999). Safe management of wastes from health-care activities. Geneva: WHO.

Prüss-Üstün, A., Kay, D., Fewtrell, L., & Bartram, J. (2004). Unsafe water, sanitation and hygiene. Comparative Quantification of Health Risks: Global and Regional Burden of Disease due to Selected Major Risk Factors, 2. Retrieved from http://wwwlive.who.int/publications/cra/chapters/volume2/1321-1352.pdf on 12/2/2018 at 5: 56: 13 PM

Radzig, M. A., Nadtochenko, V. A., Koksharova, O. A., Kiwi, J., Lipasova, V. A., & Khmel, I. A. (2013). Antibacterial effects of silver nanoparticles on gram-negative bacteria: Influence on the growth and biofilms formation, mechanisms of action. *Colloids and Surfaces B: Biointerfaces*, **102**, 300–306.

Raghunath, A., & Perumal, E. (2017). Metal oxide nanoparticles as antimicrobial agents: a promise for the future. *International Journal of Antimicrobial Agents*, **49**(2), 137–152.

Raghupathi, K., T Koodali, R., & Manna, A. (2011). Size-Dependent Bacterial Growth Inhibition and Mechanism of Antibacterial Activity of Zinc Oxide Nanoparticles. *Langmuir*, **27**(7) 4020-8.

Rai, M., Yadav, A., & Gade, A. (2009). Silver nanoparticles as a new generation of antimicrobials. *Biotechnology Advances*, **27**(1), 76–83.

Raja, S., Ramesh, V., & Thivaharan, V. (2017). Green biosynthesis of silver nanoparticles using *Calliandra haematocephala* leaf extract, their antibacterial activity and hydrogen peroxide sensing capability. *Arabian Journal of Chemistry*, **10**(2), 253–261.

Rajiv, P., Rajeshwari, S., & Venckatesh, R. (2013). Bio-fabrication of zinc oxide nanoparticles using leaf extracts of *Parthenium hysterophorus* L. and its size

dependent antifungal activity against plant fungal pathogens. *Spectrchim Acta A Mol Biomol Spectrosc*, **112**, 384–387.

RAMAN, C. V., & KRISHNAN, K. S. (1928). A New Type of Secondary Radiation. *Nature*, **121**(3048), 501–502.

Rani, R., Kumar, H., Salar, R. K., & Purewal, S. S. (2014). Antibacterial Activity of Copper Oxide Nanoparticles Against gram-negative Bacterial Strain Synthesized By Reverse Micelle *Technique. Int. J. Pharm. Res. Dev*, **6**, 72–78.

Raut, S., Thorat, P. V., & Thakre, R. (2013). Green Synthesis of Zinc Oxide (ZnO) Nanoparticles Using *Ocimum Tenuiflorum* Leaves. *IJSR*, **4**(5), 1225–1226.

Ravichandran, V., Vasanthi, S., Shalini, S., Ali Shah, S. A., & Harish, R. (2016). Green synthesis of silver nanoparticles using *Atrocarpus altilis* leaf extract and the study of their antimicrobial and antioxidant activity. *Materials Letters*, **180**, 264–267.

Reimer, L. (1984). Transmission Electron Microscopy. In Springer Series in Optical Sciences: Vol. 36. Retrieved from http://link.springer.com/10.1007/978-3-662-13553-2 on 15/12/2017 at 2: 09: 32 PM

Ren, Y., Yang, H., Wang, T., & Wang, C. (2016). Green synthesis and antimicrobial activity of monodisperse silver nanoparticles synthesized using *Ginkgo Biloba* leaf extract. *Physics Letters A*, **380**(45), 3773–3777.

Roberts, I. S (1996). The biochemistry and genetics of capsula polysaccharide production in bacteria. *Annu Rev Microbiol*, **50**, 285–315.

Rodríguez-León, E., Iñiguez-Palomares, R., Navarro, R. E., Herrera-Urbina, R., Tánori, J., Iñiguez-Palomares, C., & Maldonado, A. (2013). Synthesis of silver nanoparticles using reducing agents obtained from natural sources (*Rumex hymenosepalus* extracts). *Nanoscale Research Letters*, **8**(1), 1-8.

Ruparelia, J. P., Chatterjee, A. K., Duttagupta, S. P., & Mukherji, S. (2008). Strain specificity in antimicrobial activity of silver and copper nanoparticles. *Acta Biomaterialia*, **4**(3), 707–716.

Sachan, A. K., & Gupta, A. (2015). A review on nanotized herbal drugs. *International Journal of Pharmaceutical Sciences and Research*, **6**(3), 961.

Salem, W., Leitner, D. R., Zingl, F. G., Schratter, G., Prassl, R., Goessler, W., … Schild, S. (2015). Antibacterial activity of silver and zinc nanoparticles against Vibrio cholerae and enterotoxic *Escherichia coli*. *International Journal of Medical Microbiology*, **305**(1), 85–95.

Santhoshkumar, J., Kumar, S. V., & Rajeshkumar, S. (2017). Synthesis of zinc oxide nanoparticles using plant leaf extract against urinary tract infection pathogen. *Resource-Efficient Technologies*, **3**(2017) 459-465.

Savithramma, N., Rao, M. L., Rukmini, K., & Devi, P. S. (2011). Antimicrobial activity of silver nanoparticles synthesized by using medicinal plants. *International Journal of ChemTech Research*, **3**(3), 1394–1402.

Scott, J. R & Barnett, T. C (2006). Surface proteins of gram-positve bacteria and how they get there. *Annu Rev Microbiol*, **60**, 397–423.

Selvarajan, E., & Mohanasrinivasan, V. (2013). Biosynthesis and Characterisation of ZnO nanoparticles using *Lactobacillus plantarum* VITES07. *Materials Letters* **112**, 180–182.

Shah, R. K., Boruah, F., & Parween, N. (2015). Synthesis and Characterization of ZnO Nanoparticles using Leaf Extract of *Camellia sinesis* and Evaluation of their Antimicrobial Efficacy. *Int. J. Curr. Microbiol. App. Sci*, **4**(8), 444–450.

Sharma, N., Kumar, J., Thakur, S., Sharma, S., & Shrivastava, V. (2013). Antibacterial study of silver doped zinc oxide nanoparticles against *Staphylococcus aureus* and *Bacillus subtilis*. *Drug Invention Today*, **5**(1), 50–54.

Sharma, V., Shukla, R. K., Saxena, N., Parmar, D., Das, M., & Dhawan, A. (2009). DNA damaging potential of zinc oxide nanoparticles in human epidermal cells. *Toxicology Letters*, **185**(3), 211–218.

Sheehy, K., Casey, A., Murphy, A., & Chambers, G. (2015). Antimicrobial properties of nano-silver: A cautionary approach to ionic interference. *Journal of Colloid and Interface Science*, **443**, 56–64.

Singhal, G., Bhavesh, R., Kasariya, K., Sharma, A., & Singh, R. P. (2011). Biosynthesis of silver nanoparticles using *Octinum sanctum* (Tulsi) leaf extract and screening its antimicrobial activity. *J Nanopart Res* **13**, 2981–2988.

Singleton, P (2004). Bacteria. In Biology, Biotechnology and Medicine (6th ed., p. 5770). West Sussex England: John Wiley & Sons.

Sintubin, L., Verstrate, W., & Boon, N. (2012). Biologically produced nanosilver: current state and future perspectives. *Biotechnol Bioeng* **10**(9), 2422–2436.

Smith, E., & Dent, G. (2005). Modern Raman spectroscopy: a practical approach. Hoboken, NJ: J. Wiley, 1-5.

Sondi, I & Salopek-Sondi, B (2004). Silver nanoparticles as antimicrobial agent: A case study on *E. coli* as a model for Gram-negative bacteria. *J. Colloid Interface Sci* **275**, 177–182.

Stephen, M. Morse. (1995). Emerging Infectious Diseases: Factors in the emergence of infectious diseases. *Emerg Infect Dis* **1**(1), 7–13.

Sun, Y., & Xia, Y. (2002). Shape-Controlled Synthesis of Gold and Silver Nanoparticles. *Science*, **298**(5601), 2176–2179.

Tanaka, N. (Ed.) (2014). Scanning transmission electron microscopy of nanomaterials: basics of imaging and analysis. Hackensack, NJ: Imperial College Press, 1-6.

Tao, A., Sinsermsuksakul, P., & Yang, P. (2007). Tunable plasmonic lattices of silver nanocrystals. *Nature Nanotechnology*, **2**(7), 435–440.

Taylor, L. (2000, October 13). Plant based drugs and medicines. Retrieved from http://www.rain-tree.com/plantdrugs.htm on 4/3/2017 at 7: 02: 27 PM

Thill, A., & et al. (2006). Cytotoxicity of CeO2 nanoparticles for *Escherichia coli*: Physiochemical insight of the cytotoxicity mechanism. *Environ Sci Technol*, **40**, 6151–6156.

Tien, D. C., Tseng, K. H., Liao, C. Y., Huang, J. C., & Tsung, T. T. (2008). Discovery of ionic silver in silver nanoparticle suspension fabricated by arc discharge method. *Journal of Nanomaterials* **463**(1–2), 408–411.

Tony Owen. (1996). Fundamentals of UV-visible Spectroscopy. Hewlett-Packard company, 1-4.

Tran, Q. H., Nguyen, V. Q., & Le, A.-T. (2013). Silver nanoparticles: synthesis, properties, toxicology, applications and perspectives. *Advances in Natural Sciences: Nanoscience and Nanotechnology*, **4**(3), 033001.

Tumwine, J. K., Thompson, J., Katua-Katua, M., Mujwajuzi, M., Johnstone, N., Wood, E., & Porras, I. (2002). Diarrhoea and effects of different water sources, sanitation and hygiene behaviour in East Africa. *Tropical Medicine & International Health*, **7**(9), 750–756.

Ubillas, R. P., Mendez, C. D & Jolad, S. D (2000). Antihyperglycemic acetylenic glucosides from *Bidens pilosa*. *Planta Med* **66**(1), 82–83.

Vaseem, M., Umar, A., & Han, Y. B. (2010). Metal oxide nanostructures and their applications. *American Scientific Publ*, **5**, 479-509

Verma, A., & Mehata, M. S. (2016). Controllable synthesis of silver nanoparticles using Neem leaves and their antimicrobial activity. *Journal of Radiation Research and Applied Sciences*, **9**(1), 109–115.

Vernon-Parry, K. D. (2000). Scanning electron microscopy: an introduction. *III-Vs Review*, **13**(4), 40–44.

Vijayakumar, M., Priya, K., Nancy, F. T., Noorlidah, A., & Ahmed, A. B. A. (2013). Biosynthesis, characterisation and anti-bacterial effect of plant-mediated silver nanoparticles using *Artemisia nilagirica*. *Industrial Crops and Products*, **41**, 235–240.

Virender, Sharma, K., Ria, Yngard, A., & Yekaterina, Lin. (2008). Silver nanoparticles: Green synthesis and their antimicrobial activities. *Adv Colloid Interface Sci* **145**(1–2), 83–96.

Vishwakarma, K. (2013). Green synthesis of ZnO nanoparticles using *Abrus precatorius* seeds extract and their characterization. Retrieved from http://ethesis.nitrkl.ac.in/5012/ on 19/3/2017 at 10: 12: 15 PM

Vivek, R. T., Muthuchelian, R., Gunasekaran, K., Kaveri, P., & Kannan, K. (2012). Green biosynthesis of silver nanoparticles from *Annona squamosa* leaf extract and its in-vitro cytotoxic effect on MCF-7 cells. *Process Biochemistry* **47**(12), 2405–2410.

Wamalwa, P., Omolo, J., & Makokha, A. (2013). Prevalence and risk factors for urinary tract infections among pregnant women. *Prime J Soc Sci*, **2**(12), 524–531.

Wang, J., Yang, H., Lin, Z. W & Sun, H. D (1997). Flavanoids from *Bidens pilosa* var. radiata. *Phytochemistry* **46**(7), 1275–1278.

Wang, R., Wu, Q. X & Shi, Y. P (2010). Polyacetylenes and flavanoids from the aerial parts of *Bidens pilosa*. *Planta Med*, **76**(9), 893–896.

Weber, D. J., Rutala, W. A., Fischer, W. A., Kanamori, H., & Sickbert-Bennett, E. E. (2016). Emerging infectious diseases: Focus on infection control issues for novel coronaviruses (Severe Acute Respiratory Syndrome-CoV and Middle East Respiratory Syndrome-CoV), hemorrhagic fever viruses (Lassa and Ebola), and highly pathogenic avian influenza viruses, A(H5N1) and A(H7N9). *American Journal of Infection Control*, **44**(5), e91–e100.

What is SEM? Scanning electron microscope technology explained. (2018). Retrieved from https://blog.phenom-world.com/what-is-sem on 12/4/2019, at 12:14:27 PM

Willard, D. M., Barraza, G., & Zook, J. D. (2005). Waterless hand cleaner containing plant derived natural essential oil. Retrieved from http://www.google.com/patents/US6884763 on 30/11/2017 at 12: 28: 24 PM

Withrock, I. C., Anderson, S. J., Jefferson, M. A., McCormack, G. R., Mlynarczyk, G. S. A., Nakama, A., … Carlson, S. A. (2015). Genetic diseases conferring resistance to infectious diseases. *Genes & Diseases*, **2**(3), 247–254.

World Health Organization. (2014). Antimicrobial resistance: global report on surveillance. Retrieved from https://www.who.int/drugresistance/documents/surveillancereport/en/ on 15/5/2018 at 10: 21: 47 AM

World Health Organization (2015). Worldwide country situation analysis: response to antimicrobial resistance. Retrieved from http://apps.who.int/iris/bitstream/10665/163468/1/9789241564946_eng.pdf?ua=1&ua=1 on 15/5/2018 at 11: 25: 03 AM

Wu, L. W., Chiang, Y. M & Chuang, H. C (2004). Polyacetylenes function as anti-angiogenic agents. *Pharm Res*, **21**(11), 2112–2119.

Wu, L. W., Chiang, Y. M & Chuang, H. C (2007). A novel polyacetylene significantly inhibits angiogenesis and promotes apoptosis in human endathelial cells through activation of the CDK inhibitors and caspase-7. *Planta Med*, **73**(7), 655–661.

Xia, Q., Liu, Y & Li, Y (2009b). Determination of hyperoside in different parts and different spieces of Herba Bidens by RP-HPLC. *Molecules* **50**, 48–53.

Xia, Q., Liu, Y& Li, Y (2009a). Determination of gallic acid from different spieces and different medical parts of Herba Bidens by RP-HPLC. *Molecules* **24**(3), 308–310.

Xie, Y., He, Y., Irwin, P. L., Jin, T., & Shi, X. (2011). Antibacterial Activity and Mechanism of Action of Zinc Oxide Nanoparticles against *Campylobacter jejuni*. *Appl. Environ. Microbiol*., **77**(7), 2325–2331.

Yang, H. L., Chen, S.-C., Chang, N.-W., Chang, J.-M., Lee, M.-L., Tsai, P.-C., … Hseu, Y.-C. (2006). Protection from oxidative damage using *Bidens pilosa* extracts in normal human erythrocytes. *Food and Chemical Toxicology*, **44**(9), 1513–1521.

Young, P. H., Hsu, Y. J., & Yang, W. C. (2010). *Bidens pilosa* L. and its medicinal use. In Awaad, A. S., V. K., & Govil, .J. N., Recent Progress in Medicinal Plants Drug Plant (2nd ed.). Stadium Press, Houston, Tex, USA.

Yu, Y., Yang, W., Sun, X., Zhu, W., Li, X.-Z., Sellmyer, D. J., & Sun, S. (2014). Monodisperse MPt (M = Fe, Co, Ni, Cu, Zn) Nanoparticles Prepared from a Facile Oleylamine Reduction of Metal Salts. *Nano Letters*, **14**(5), 2778–2782.

Yuan, L. P., Chen, F. H & Ling, L (2008). Protective effects of total flavanoids of *Bidens pilosa* L (TFB) on animal liver injury and liver fibrosis. *J Ethnopharmacol* **116**(3), 539–546.

Yuan, L.-P., Chen, F.-H., Ling, L., Dou, P.-F., Bo, H., Zhong, M.-M., & Xia, L.-J. (2008). Protective effects of total flavonoids of *Bidens pilosa* L. (TFB) on animal liver injury and liver fibrosis. *Journal of Ethnopharmacology*, **116**(3), 539–546.

Zarrindokht Emami-Karvani. (2012). Antibacterial activity of ZnO nanoparticle on Gram-positive and Gram-negative bacteria. *African Journal of Microbiology Research*, **5**(18), 1368-1373.

Zhang, B., Xie, M., Bruschweiler-Li, L., & Brüschweiler, R. (2018). *Nanoparticle-Assisted Metabolomics. Metabolites*, **8**(1), 21-35.

Zhao, A., Zhao, Q., Peng, L., Zhang, J., Lin, Z & Sun, H (2004). A new chalcone glycoside from *Bidens pilosa*. *Acta Botanica* **26**(1), 121–126.

Zulueta, M. C. A., Tada, M., & Ragasa, C. Y. (1995). A diterpene from *Bidens pilosa*. *Phytochemistry*, **38**(6), 1449–1450.